DEVELOPMENT OF HIGH-THROUGHPUT IMPEDANCE SPECTROSCOPY-BASED MICROFLUIDIC PLATFORM FOR DETECTING AND ANALYZING CELLS AND PARTICLES

A Dissertation

by

NEBRAS MOHAMMEDKAMAL A SOBAHI

Submitted to the Office of Graduate and Professional Studies of
Texas A&M University
in partial fulfillment of the requirements for the degree of

DOCTOR OF PHILOSOPHY

Chair of Committee,	Arum Han
Committee Members,	Won-Bo Shim
	Samuel Palermo
	Raffaella Righetti
Head of Department,	Miroslav M. Begovic

December 2017

Major Subject: Electrical Engineering

ABSTRACT

Impedance spectroscopy based microfluidics have the capability to characterize the dielectric properties of mediums, particles, cellular and sub-cellular contents in response to stimulating voltage signals over a frequency range. This label-free technology has broad ranges of applications in life sciences where there is a need for high-throughput, label-free, non-contact, and low-cost microsystems. To address these limitations, three innovative impedance spectroscopy microfluidic platforms have been developed and presented in this dissertation. The first platform was developed for detecting and characterizing the transverse position of a single cell flowing within a microfluidic channel using a single impedance spectroscopy electrode pair. Regardless of the cell separation methods used, identifying and quantifying the position of cells and particles within a microchannel are important, as these information indicate both the degree of separation as well as how many cells are separated into each position. Using a single pair of non-parallel surface microelectrodes, five different transverse positions of single cells flowing through a microfluidic channel were successfully identified at a throughput of more than 400 particles/s using the detected impedance peak height and width.

The second platform utilizes the above technology to count and quantify cells flowing through multiple outlets of microfluidic cell separation systems. A single pair of step-shaped electrodes was developed by integrating five different electrode-to-electrode gaps within a single pair of electrodes. Using this platform, an overall misclassification error rate of only 1.85% was achieved. The result shows the technology's capability in

achieving efficient on-chip cell counting and quantification, regardless of the cell separation methods used, making it a promising on-chip, low-cost and label-free quantification method for cell and particle sorting and separation applications.

The third platform was developed for counting cells and particles encapsulated in water-in-oil emulsion droplets using microfluidic based impedance spectroscopy systems. Impedance signal peak height and width were utilized to successfully quantify the number of cells encapsulated within a droplet, and was successfully applied for various cell types and growth media. In addition, the developed platform has been also successfully tested for identifying and discriminating filamentous fungal cell growth, where single fungal spores and filamentous fungi of different lengths could be discriminated inside droplets.

Overall in this research, several impedance spectroscopy based microfluidic systems have been successfully developed to solve current limitations in technologies that need high-throughput, low-cost and label-free detection and characterization method for a broad range of cell/particle screening applications.

To my dear father, mother, wife, kids, brother and sisters with great love and appreciation

ACKNOWLEDGEMENTS

First and foremost, all praises to Allah for the strengths and His blessing in completing this dissertation.

I am eternally grateful to my advisor and committee chair Dr. Arum Han, for his excellent guidance, caring, patience, and providing me his time to supervise my research work and study. I'm so glad and proud to work under his supervision during my graduate studies. This dissertation could not have been done in this excellent level without him.

Many thanks are extended to the examining committee members for their guidance and support during this research. Also I would like to thank all of our group members in the NanoBio Systems laboratory at Texas A&M University for their enormous help, support, and valuable feedbacks and discussions during my research. I have spent the greatest time in excellent atmosphere with these amazing friends.

Many thanks to King Abdulaziz University and Saudi Arabian Cultural Mission for their financially support during my graduate studies.

“My family” is my soul. My father and mother, who pray to Allah all time, and give me endless support, guidance and love to have all the best in my life. My wife, she is my love and the best and closest friend, she supports and encourages me all time, no matter what I choose to do. My brother and sisters, thanks a lot for all your supports. This study would have been impossible to be done without all of you.

CONTRIBUTORS AND FUNDING SOURCES

Contributors

This work was supervised by a dissertation committee consisting of Professor Arum Han (Advisor and committee chair) and Professors Samuel Palermo and Raffaella Righetti (Committee members) of the Department of Electrical and Computer Engineering and Professor Won-Bo Shim (Committee member) of the Department of Plant Pathology and Microbiology.

All work conducted for the dissertation was completed by the student independently.

Funding Sources

Graduate study was supported by a scholarship from the King Abdulaziz University and Saudi Arabian Cultural Mission. Also the dissertation research was supported by the National Science Foundation under grant numbers DBI-1353759 and EFRI-1240478.

Its contents are solely the responsibility of the authors and do not necessarily represent the official views of the King Abdulaziz University, Saudi Arabian Cultural Mission, and National Science Foundation.

TABLE OF CONTENTS

Page

ABSTRACT ii

DEDICATION iv

ACKNOWLEDGEMENTS v

CONTRIBUTORS AND FUNDING SOURCES vi

TABLE OF CONTENTS vii

LIST OF FIGURES ix

CHAPTER I INTRODUCTION AND LITERATURE REVIEW 1

1.1. Introduction 1
1.2. Impedance Spectroscopy 2
1.3. Microfluidic-Based Impedance Spectroscopy 5
1.4. Impedance Spectroscopy-Based Cell and Particle Position Detection in Microfluidic Systems 9
1.5. Quantifying Cells and Particles Microfluidic-Based for Sorting and Separation Applications 11
1.6. High-Throughput Cells in Droplets Characterization-Based Microfluidic Impedance Spectroscopy Systems 13
1.7. Objective and Chapter Outlines 14

CHAPTER II IMPEDANCE SPECTROSCOPY-BASED CELL/PARTICLE POSITION DETECTION IN MICROFLUIDIC SYSTEMS 16

2.1. Motivation 16
2.2. Principles of Impedance-Based Size and Position Detection 17
2.3. Design and Fabrication 19
2.4. Cell and Particle Position Detection 21
2.5. Conclusion 34

CHAPTER III HIGH-THROUGHPUT MULTI-OUTLET CELL COUNTING USING A SINGLE PAIR OF LABEL-FREE IMPEDANCE ELECTRODES 36

3.1. Motivation 36
3.2. Experimental Setups 37

3.3. Results and Discussion 42
3.4. Conclusion 59

CHAPTER IV DETECTION AND ANALYSIS OF CELLS ENCAPSULATED WITHIN A DROPLET USING IMPEDANCE SPECTROSCOPY MICROSYSTEMS 61

4.1. Motivation 61
4.2. Design Principle 61
4.3. Devices Fabrication 66
4.4. Detection and Characterization of Yeast Cells in Droplets 69
4.5. Discrimination of Droplets Containing a Single Cultured Filamentous Fungal Cell Using Impedance Spectroscopy 82
4.6. Conclusion 94

CHAPTER V CONCLUSIONS AND FUTURE WORKS 96

5.1. Conclusions 96
5.2. Future Works 98

REFERENCES 100

APPENDIX A MASK DESIGN 109

APPENDIX B MASTER AND ELECTRODE FABRICATION PROCEDURE 115

APPENDIX C PDMS DEVICE FABRICATION PROCEDURE 118

APPENDIX D IMPEDANCE ANALYZER EXPERIMENTAL PROCEDURE 120

APPENDIX E YEAST CELL AND YEPD MEDIUM PREPARATION 123

LIST OF FIGURES

Page

Figure 1. Electric field distributions of different electrode designs. 2

Figure 2. The circuit model of a single-cell in a medium 4

Figure 3. Principle of particle/cell position detection in the microchannel using non-parallel electrodes 18

Figure 4. Design of the impedance spectroscopy-based cell/particle position detection device with three electrode pairs having different tilting angles. 20

Figure 5. The detected position impedance signals for particles that pass through the non-parallel detection electrodes. 24

Figure 6. The data point of the detected peak amplitude impedance signals of particles passing through the three titled electrodes 25

Figure 7. Measured detected peak signal width (transit time) of the amplitude impedance signal 26

Figure 8. The detected impedance amplitude peak height of particles at five different positions 28

Figure 9. The detected impedance amplitude peak width of particles at five different positions 30

Figure 10. The detected impedance amplitude peak height at five different transverse positions using beads of 6 μm diameter 31

Figure 11. The detected impedance peak width at five different transverse positions using beads of 6 μm diameter 32

Figure 12. The comparison of normalized impedance signals of two different bead sizes (11 and 6 μm in diameter) at five different transverse positions (box plot). 33

Figure 13. Principle of multioutlet cell counting using a single impedance electrodes' pair 39

Figure 14. The electrode to electrode gap detection effects. 44

Figure 15. Effects of electrode-to-electrode gaps differences on the detected impedance signals of cell passing through. 46

Figure 16. The multioutlet microfluidic based impedance spectroscopy cell counting system. 49

Figure 17. The classification results of the detected impedance signals of cells passing by five different outlets at five different electrode to electrode gaps 52

Figure 18. The classification results of the detected impedance signals of cell passing by five different outlets at five different optimized electrode to electrode gaps. 55

Figure 19. The detection of multiple cells passing by the detection electrodes at different outlets simultaneously 58

Figure 20. Top view schematic of the developed high-throughput droplet microfluidic-based impedance spectroscopy platform components 62

Figure 21. The flow-focusing droplet generation region 64

Figure 22. Electrodes detection methods of flowed cells encapsulated in droplets. 65

Figure 23. The fabricated microfluidic impedance spectroscopy platform integrated with SMA connectors. 69

Figure 24. Yeast cell division using 100, 80, 50, and 10 % of YEPD mediums at 0 and 6 hr 71

Figure 25. Yeast cell division rate for yeast cell suspended in 10 different YEPD diluted mediums (10-100 %). 71

Figure 26. YEPD medium at 10 different dilutions (0-100) %. 73

Figure 27. Yeast cells encapsulated in droplet at different ratios 75

Figure 28. Detected electrical impedance of yeast cells in droplets using 100% YEPD medium 78

Figure 29. Detection of yeast cells encapsulated in droplets using 50 % YEPD medium. 79

Figure 30. Detection of yeast cells encapsulated in droplets using 10 % YEPD medium.....80

Figure 31. Comparison of average detected electrical impedance peaks of yeast cells encapsulated in droplets.....81

Figure 32. Detection of fungal cells encapsulated in droplets using impedance spectroscopy microsystem 85

Figure 33. Fungi cell growth differences between 100, 80, 50 and 10% YEPD 86

Figure 34. Preliminary results of detected fungal cell in 100 % YEPD medium at applied excitation signal of 4 V at 620 kHz 87

Figure 35. Detected fungal cells in 100 % YEPD medium at applied excitation signal of 4 V and 1.5 MHz.....88

Figure 36. Detected fungal cells in 100 % YEPD medium at applied excitation signal of 4 V and 2.5 MHz.....89

Figure 37. Impedance peak signals of flowed fungal cells in diluted medium.....90

Figure 38. Comparison between two different fungal lengths (11.62 and 75.55 µm) 91

Figure 39. Detected impedance signal of fungal cells in microchannels with two different heights (8.5 and 15µm).....92

Figure 40. Imaginary part of the impedance signal changed when droplets containing fungal cells in YEPD culture media and surrounded by the carrier oil pass through the detection electrodes. 93

Figure 41. Filamentous fungal cells of different growths were detected and characterized within droplet.....94

CHAPTER I

INTRODUCTION AND LITERATURE REVIEW

1.1. Introduction

Projected future growth influences how the industries and markets request the researchers and developers to have a robust identification and micro sensible systems for various range of biomedical application. Besides, due to these enormous growth rate in technologies, high-throughput is important to effectively characterize and study the substrate of the biological and biochemical components which have significant information that could accelerate understanding many different subjects. High-throughput screening of culture condition is one of the applications that have been significantly and widely developed for different aspects such as label free cells discriminating and identification. High-throughput is significantly beneficial in biological and biochemical applications if this type of sensors are sufficiently non-contact, non-invasive, label-free, low-cost, and highly sensitive. Therefore microfluidic-based systems have been developed and employed in broad range of applications such as cells and particles detection and characterization, drug and mutant library screening applications. Besides droplet based microsystems have been shown its capabilities of cells encapsulation and it can be effectively merged with other droplet for drug screening application using passive or active methods [1].

Thus there is an uncountable number of methods that have been developed and employed for characterizing different state of matter, however dielectric impedance

spectroscopy gives invaluable information for various biological and biochemical applications.

1.2. Impedance Spectroscopy

Dielectric impedance spectroscopy is a great tool for measuring the dielectric properties of any interested material by measuring the induced reduced electric field due to the dielectric properties of this material. This electric field cross over from a stimulating electrode to another detecting electrode based on its voltage strength and the medium properties as illustrated in Figure 1.

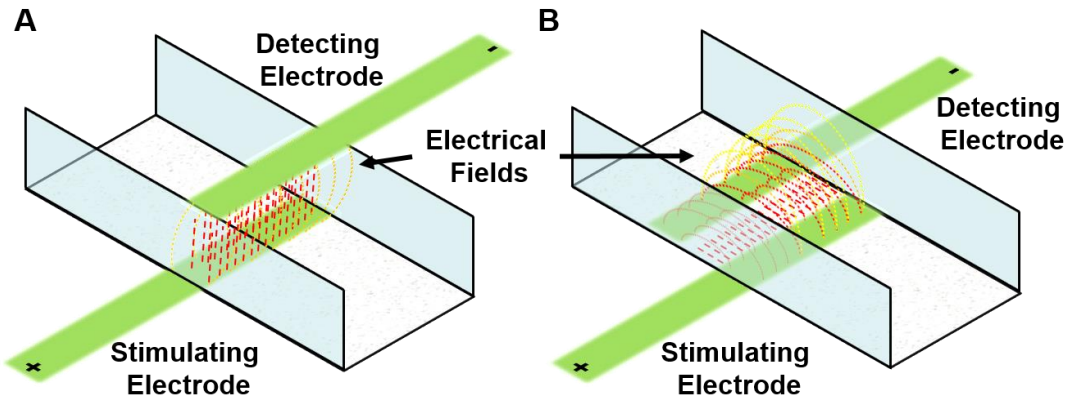

Figure 1. Electric field distributions of different electrode designs. (A) Illustration of electric fields distribution in a medium using parallel top/bottom electrodes, and (B) using planar electrodes.

However one of the main electrical parameter that distort this field is the permittivity of the materials. Permittivity is how much the change of the resistance when the medium influence by an electric field. Permittivity is represented the reduction in the electric field

due to the effect of the medium depolarization [2, 3]. Besides, the permittivity is formed as complex-valued that describes the phase difference between the applied electric field and the arising one. Therefore the dielectric spectroscope method is employed to measure the dielectric impedance with respect to spectrum frequency. The dielectric spectroscopy could be used with any materials under test such as solids, liquids, or gases [4-6]. To successfully identified and characterized the impedance measurements, the sample must be fully occupied the detection region. However, this type of technique has been greatly developed to successfully detect and characterize two different medium such as cells or DNA in liquids which has different permittivity comparing to liquid media [7].

The initial concept of impedance come out first from the electric resistance. The electric resistance is the ability of an electric component to resist the electric current that flow through this component. The electric resistance is the relation between the applied voltage and the current that flow through it as defined by Ohm's Law in Eq.1:

$$R = V/I \tag{1}$$

However this electric resistance measurement could not be applied or used in sophisticated behavior systems to study their electric resistivity due to other electric components that exhibit in a complex form. Therefore an electric impedance is used instead of resistance to characterize and measure the ratio of the applied voltage to the AC current that flow through a particular medium. This concept is widely used to characterize

the electrochemical properties of several number of mediums such as chemical solutions, cells, and many different biological tissues.

The impedance measurements response of a single-cell have been justified by developing an electric circuit model of a single-cell to interpret the impedance measurements of single-cell in a medium, such as Foster and Schwan's simplified circuit model as illustrated in Figure 2.

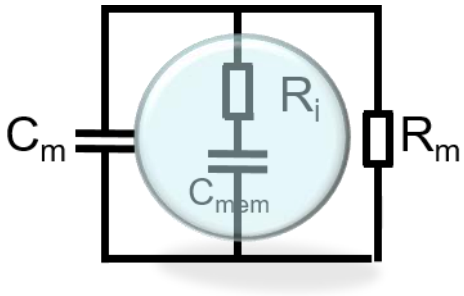

Figure 2. The circuit model of a single-cell in a medium.

As shown from this simplified model, the cell is located in suspended media that has two parallel electric components, a resistor R_m and capacitor C_m while the cell was modeled with a series of resistor and capacitor, R_i and C_{mem}. The resistor R_i is equivalent to the resistivity of the cytoplasm of the cell and C_{mem} to the capacitance of the cell membrane. This model has been widely used to agree with the cell impedance measurements [8-11]. This model can clearly interpret how the electric properties of the cell membrane and cytoplasm can be measured. Also, due to capacitance presence effect within the cell and the medium, using an AC signal to therefore result an impedance measurements that show valuable information of subcellular components of a single-cell.

However, the impedance measurement is a function of frequency whereas the amplitude and phase of the cell impedance measurements vary based on the frequency range that is used [12].

1.3. Microfluidic-Based Impedance Spectroscopy

Microfluidics is an abundant tool for purpose of studying the behavior of miniaturized flow at microscale dimensions. Confinement small volume of fluids at this scale can show different behaviors such as laminar flow, surface tension, and electrowetting [13]. Microfluidics is a method that can precisely manipulate fluids by using microscale devices that fabricate using technologies that developed from semiconductor industries. Using these novel devices, enormous influences that enable huge conurbations in many different fields of study, especially biology and medical research [14-18]. Therefore these miniaturized devices have been widely applied and used for various biological assays due to small sample volume requirements, which results in reducing the total cost of reagents and maximize the outcome invaluable information as consequences from that scale. Microfluidic devices are commonly fabricated using Poly (dimethylsiloxane) (PDMS) material due to, material and surface properties, low-cost, and easy fabrication process [19-21]. Using microfluidic technologies, cells analysis, discrimination, and sensing have been focused and demonstrated using different methods and technologies such as combing microfluidics with a variety of functional elements that can specifically manipulate and handle up to single cell. These analysis devices are commonly referred to as micro total analysis systems (μTAS) or lab-on-chip (LOC) [22-24].

Microfluidic-based impedance spectroscopy has been shown great potential due to its capabilities of detecting, sensing, and characterizing particles flow-through fluidic channels at microscale size. Microfluidic-based impedance spectroscopy systems for cell analysis have been developed at two different conditions: trapping and flow-through. Each of these conditions has its advantages and limitations. Impedance analysis of trapped cells is required for an application that need long culture monitoring by trapping the cell between two electrodes and characterize its impedance behavior, for example, capturing single-HeLa cells inside microchannels and performing electrical analysis as a result of impedance measurements [25]. Malleo et al. characterized single cell trapped hydro-dynamically and continuously performed differential impedance analysis [26]. Volume change of captured single cells in a microfluidic device was analyzed by measuring electrical impedance change [27]. A great potential was done by our group to minimize the leakage current besides increasing the trapping sites by fabricating an array of planar electrodes using micro-holes channels for cells trapping and then impedance measurements [28]. The throughput using this method is limited due to long time needed for each analysis for each cell. However, some researchers tried to increase the trapping site to a large number, but this result to increase the system complexity due to an enormous number of multiplexed impedance measurements [29-31]. Beside to the throughput limitation, the cell impedance measurements are affected by many factors such as cell sizes and trapping structure and dimensions.

In contrast flow-through condition is considered for high-throughput microfluidic-based impedance spectroscopy. Microfluidic based flow-through systems have been

broadly used for analyzing various types of cells [32-34]. Many different electrode designs have been reported for more accurate analysis, for example, an impedance of cells flow cytometry was developed using coplanar electrodes. These fabricated electrodes used to focus and electrically detect the flowing cells differentially by acquiring the impedance change [35]. Although they used focusing electrodes, vertically positional variations of cells could result deviation in the recording impedance. Two pair of electrodes were fabricated to be inside the microfluidic channels to reduce the cells position effect by stimulating using the outer pair and detecting using the two inner electrodes. This device was electrically discriminated between normal RBCs and glutaraldehyde-fixed RBCs [36]. Another method was used by fabricating 3D electrodes to have a uniform electric field that cross over the entire height of the channel and to overcome the vertical position issue that is in the planar electrodes [37]. Also, differentiating between living and dead cells using liquid electrodes was demonstrated [38], as well as discriminating between undifferentiated human induced pluripotent stem cells (iPSC) and iPSC derived cardiomyocyte (iPSC) cells [39]. Also, integration impedance detection and electrical sorting for living and dead cells were demonstrated [40]. In addition, high speed single cell analysis using impedance spectroscopy technique was used to differentiate between two different sizes of polystyrene bead particles using maximum length sequence analysis (MLS) [41]. Another microfluidic differential-based impedance cytometer device was developed for discriminating between small polystyrene beads (1μm and 2 μm diameters) as well as between yeast cells and beads [42]. For further analysis, integration of vision system with differential impedance spectroscopy for direct comparison analysis of yeast

cells and polystyrene beads [43], also another integrated system for size, shape, and position determination of cells using impedance measurements were shown [44]. Another integrated complex device was fabricated by combing single-ended and differential electrical electrodes as well as combing trapping sites and flow-through channels to completeness analysis [45].

Many other recent researchers have been focused on discriminating between cells type and size such as using contactless disposable microfluidic impedance cytometer [46], using an external Wheatstone bridge for more sensitivity and differentially measured the electrical impedance response for passing cells, and characterizing of subcellular components of cells using high excitation frequency range up to 500 MHz [47, 48]. Using their top/bottom parallel electrodes design can help the detection sensitivity since the electric fields cross over the microchannel; conversely, the planar bottom electrodes can be varied its sensitivity based on the applied signal. However, using microfluidic sandwiched parallel electrodes could make the fabrication process more difficult and add more complexity for the whole integrated device as depicted in Figure 1(B) comparing to planar electrode design as shown in Figure 1(A).

For additional cells analysis, some researchers have been focused on combining electrical and mechanical measurements by continuously aspiring cells through a construction channel and comparing the transit time and impedance amplitude of different cells [49, 50]. Another group used a tapered microfluidic channel to maximize the impedance sensitivity [51]. Many other researchers have shown their interests for

classifying of cells based on the mechanical microfluidic structure and their electrical impedance response [52].

Most of the previous microfluidics flow-through impedance analysis works, they have tried to have small volume at the detection region to realize high sensitivity. However this could lead to fabrication limitation and channel clogging issues. To overcome this issue, a hydrodynamically focusing the suspended particles in electrolyte using high dielectric insulated fluid could be used. Regardless the channel width and by using this focusing technique, discriminating between 1 μm and 2 μm beads as well as Escherichia Bacteria were demonstrated [53]. A wide microfluidic based differential impedance cytometer for platelet analysis was used by using dielectric sheath to focus the particles within conductive liquid core [54].

1.4. Impedance Spectroscopy-Based Cell and Particle Position Detection in Microfluidic Systems

Microfluidic particle/cell sorting and separation systems allow identification and selection of cells or particles of interest from a heterogeneous mixture [55-60]. Regardless of the methods used for sorting and separation, a common requirement is to be able to identify the transverse positions of cells and particles within a microfluidic channel, as such positions are directly related to the degree of separation in a particular separation scheme. Thus the transverse positions can directly indicate the property of the target cells under a specific applied force. In addition quantifying the separation event or counting the number of cells/particles passing through multiple separation outlets simultaneously are

highly desirable instead of having to do an off-chip quantification of the collected samples. Therefore methods that can quickly and accurately do so at high speed and low-cost is in great need.

Traditionally the positions of suspended particles/cells in microchannels are examined using optical instruments such as microscopes equipped with cameras. Though convenient and easy to use, this usually requires expensive high-speed cameras and intensive image processing, which not only makes the relevant microfluidic systems difficult to be widely utilized but also hinders the development of low-cost instruments that can be broadly utilized. It is typically challenging to achieve real-time analysis at high throughput due to limitations of expensive high-speed camera, complex real time image processing and computing power. Photodiodes (PDs) and photomultiplier tubes (PMTs) can improve the throughput and reduce cost as compared to microscopic imaging, and are also compact for development of portable systems, however such systems are typically limited to fluorescent samples as well as do not provide position information. In addition, although monitoring multiple fluidic outlets using PD/PMTs is possible, it is technically challenging to implement due to difficulties in integrating multiple optical channels within a small footprint [61-64].

Impedance spectroscopy is a versatile and label-free tool to study dielectric characteristics of particles and cells. In continuous flow, impedance spectroscopy is not only widely adopted for high-throughput cell counting and size quantification, but also used for cell type classification [34, 65, 66]. Based on the principle Coulter explored, impedance spectroscopy has been successfully utilized for high-throughput detection of

human blood cells, bacteria cells, and circulating tumor cells, as well as classification of subgroups of human blood cells. However to the best of our knowledge, there is no report so far on impedance spectroscopy-based method to detect transverse positions of passing cells/particles inside a microchannel [33, 35, 46, 67, 68].

1.5. Quantifying Cells and Particles Microfluidic-Based for Sorting and Separation Applications

Microfluidic cell sorting and separation systems have been widely utilized for identifying and selecting cells of interest from heterogeneous mixture of samples [69-71]. Microfluidic based cell sorting and separation have been developed and increasingly implemented by integrating range of passive or active sorting and separation methods such as inertial forces [72], gravity [73], biomimetic [74], deterministic lateral displacement [75], hydrodynamics [76], acoustophoresis [77], dielectrophoresis [78], magnetophoresis [79], or optical forces [80-82]. For quantifying the sorting and separation events and examining the performance of the sorting or separation method, it is commonly conducted by counting the number of cells passing through multiple outlet channels, typically located downstream of the sorting/separation region. Doing so on-chip in real time is much more beneficial compared to off-chip quantification of collected samples, in terms of being able to provide real-time quantification, improved throughput, less sample handling steps, and no loss in samples during the off-chip collection process. Up to date, the most traditional quantification technique is collecting the sorted/separated cells from each outlet and counting them off-chip [83], however this common technique suffers from high samples

loss especially when dealing with a small amount of rare collected samples. However there are different on-chip cell detection methods have been developed and used for cell counting and characterization such as using high-speed cameras [84] or integrating optical detection systems [85]. These methods could be integrated and utilized to overcome the cell losses during the collecting and handling process for off-chip cell counting and analysis, however these methods are limited in monitoring multiple outlets simultaneously due to the difficulty and complexity of integrating multiple optical detectors such as photodiodes (PDs) or photomultiplier tubes (PMTs) to one microsystem, also these detection methods require significant image processing steps, and are often expensive when high-speed cameras are utilized [59]. Furthermore label-based cell detection method requires an integration of complex fluorescent based system that could need specific markers, which they could be unknown in some types of infected or healthy cells. An impedance spectroscopy is a label-free and low-cost method that has been intensively used for characterizing the dielectric properties of particles and cells. The impedance spectroscopy-based microfluidic systems have been broadly utilized in high-throughput cell counting and size quantification [35, 44, 86], as well as cellular and subcellular characterizations [12, 48]. Therefore the impedance spectroscopy-based microsystem can be broadly utilized in detecting and counting of separated and sorted cells flowing through multiple outlets simultaneously by integrating multiple pair of electrodes to each outlet, however this requires an impedance analyzer of multiple detection channels, whereas it is currently limited to maximum 4 channels in the available commercial instruments.

1.6. High-Throughput Cells in Droplets Characterization-Based Microfluidic Impedance Spectroscopy Systems

Droplets-based microfluidic systems have been widely used for cells manipulations, handling, and analysis at high-throughput rates [87, 88], such as particles synthesis [89-91] and chemical screening and analysis [92-95]. Using microfluidic devices, microdroplets can be generated at different sizes, manipulated (merging and sorting), and encapsulated with cells for cells and drug effect screening [96, 97]. Furthermore droplet-based microfluidic system can successfully achieve high-throughput of kHz rates. However high-throughput and label-free detection and characterization of cells encapsulated within droplets has been rarely developed, whereas a droplets-based systems for cells electrically sensing had not been developed until Kemna et al. developed a first droplet-based microfluidic electrical impedance device that can discriminate between viable and nonviable cells within droplets at throughput of 100Hz [98]. However they have adjusted and significantly reduced the medium conductivity to 0.0009 S m^{-1} to can detect the encapsulated cells in droplet which it could be suitable for range of biological samples. Also the generated droplet size was very small comparing to the encapsulated cell, which it was occupied 25% of the droplet size as depicted in their work which it could be not practical for many droplet based culturing and screening applications. Moreover adjusting the medium conductivity to this very low level could not be met in many different application and might affect the cell growth. Therefore developing impedance spectroscopy based microfluidic system is potentially desirable since it can significantly detect and characterize the droplet contents within a microfluidic systems as well as

discriminate up to single cell encapsulated in droplet using an integrated label-free and non-contact impedance spectroscopy microsystems.

1.7. Objective and Chapter Outlines

The objective of this work is to develop a microfluidic-based systems for high-throughput, label-free and low-cost on-chip cells and particles screening applications. This work focuses initially on developing a unique high-throughput microfluidic based impedance spectroscopy systems for detecting and precisely locating cells and particle position within microchannel as discussed in Chapter II. In this chapter a high-throughput and low-cost impedance spectroscopy-based particle position detection method is discussed. Three designs of non-parallel electrode pairs with different tilting angles are evaluated using different particle sizes.

Chapter III shows a developed label-free and on-chip detection technique using single impedance spectroscopy-based electrodes that is used for monitoring and quantifying sorted and separated cells that pass through multiple outlet microfluidic channels. Therefore different single pair of electrodes designs are developed and discussed. Three different statistical classification methods are utilized for quantifying the detected impedance signals.

Chapter IV shows a novel label-free method for detecting, counting, and characterizing cells encapsulating within droplets using impedance spectroscopy-based microsystems. Detection characterization of yeast cells encapsulated in droplets using different diluted medium are compared and explained. furthermore the developed

microsystem are utilized to study and discriminate among different fungal cells growth based on their size and length of single cell encapsulated in droplet.

The conclusion of this work is briefly summarized and discussed the results and the proposed future work as shown in last chapter.

CHAPTER II

IMPEDANCE SPECTROSCOPY-BASED CELL/PARTICLE POSITION DETECTION IN MICROFLUIDIC SYSTEMS*

2.1. Motivation

In majority of the impedance detection systems developed so far, a single pair of parallel electrodes (or two pairs for differential measurement) are utilized, and passing particles/cells are detected by the change in impedance between the electrodes. However to use the above approach for cell/particle position detection or counting from multiple positions will require one electrode pair for each position of interest, thus multiple pairs of electrodes are required by placing multiple parallel electrode pairs at different transverse positions. Particles/cells passing by a particular position would induce impedance signal at the corresponding electrode pair. However such an approach is limited in the resolution of detected positions it can achieve due to constraints in electrode footprint, as well as due to number of available detection channels in most impedance analysis instruments (only up to 4 channels are available in commercial impedance analyzer models). Therefore, an approach where a single-channel impedance analyzer can be used to detect multiple positions of cells with simple configuration is desirable.

---

* [H. Wang‡, N. Sobahi‡, and A. Han, "Impedance spectroscopy-based cell/particle position detection in microfluidic systems", Lab on a Chip, 17, 1264–1269, 2017] – Reproduced by permission of The Royal Society of Chemistry (http://pubs.rsc.org/en/Content/ArticleLanding/2017/LC/C6LC01223J).

Therefore, here we present for the first time a cell/particle position detection technology using a single-channel impedance spectroscopy device that is low-cost and high-throughput.

2.2. Principles of Impedance-Based Size and Position Detection

The developed position detection system uses a pair of non-parallel electrodes that generate gradually changing electric field along the transverse direction in a microfluidic channel, causing varied impedance change when cells/particles pass through at different transverse positions. As shown in Figure 3, particles/cells passing through the electrode pair with varying electric field at different transverse positions would induce different impedance signals (both in terms of amplitude and width) even when the size and properties are identical, thus the crossing positions could be determined by evaluating the measured impedance signal.

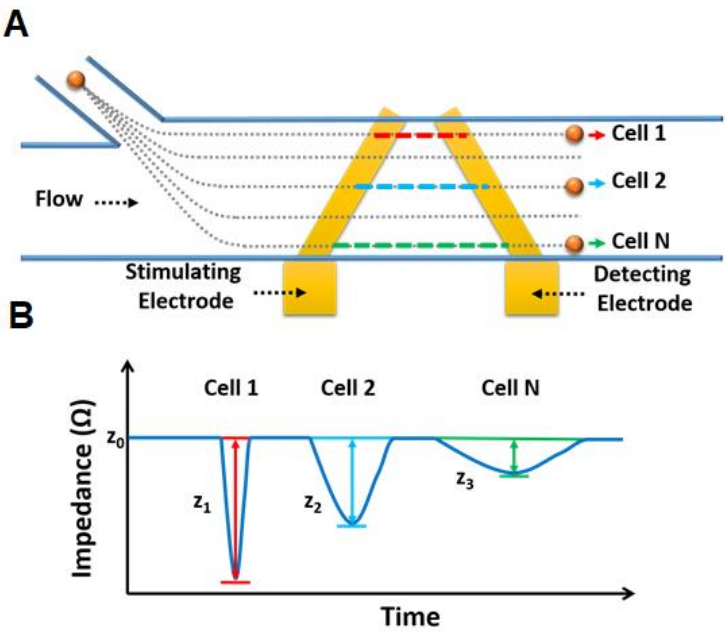

Figure 3. Principle of particle/cell position detection in the microchannel using non-parallel electrodes. (A) Showing a pair of non-parallel electrodes is placed in the microchannel in the direction perpendicular to the fluid flow (top view). (B) Illustrating a results of cells or particles (of the same dielectric property) flowing through the electrode pair at different transverse positions, which experience different electric field strength and duration, and thus show different impedance signals (amplitude and width).

Two types of signals can be obtained in this measurement, the amplitude of detected impedance peaks, and the width of the peaks that reflects the transit time of cells/particles passing through the electrodes. Particles/cells passing through the top part (short electrode-to-electrode distance side) of the electrode pair will show larger amplitude and smaller width, as the electric field is denser at the top and the transit time across the electrode pair is shorter. In contrast, particles/cells passing through the bottom part of the channel (long electrode-to-electrode distance side) will show smaller amplitude and larger width, as the electric field is sparser and the transit time is longer. Using this configuration,

a single channel of an impedance analyzer with a single pair of non-parallel electrodes can provide quantitative information about the transverse positions of particles/cells passing through. Therefore, this principle offers a simple and low-cost method for evaluating the transverse position of particle and cells, and can also be readily integrated with other microfluidic systems.

2.3. Design and Fabrication

2.3.1. Design

A microchip with three pairs of non-parallel electrodes having different angles was designed (Figure 4A and B, designs E1 – E3). A pair of parallel electrodes was included (design E4) as a reference for validation of the detected signal of passing particles. To characterize the performance of each of the electrode pair design, a flow-focusing scheme with two independent sheath flows was used to manipulate the transverse positions of cells and particles by tuning the flow rates of each of the three inlets respectively.

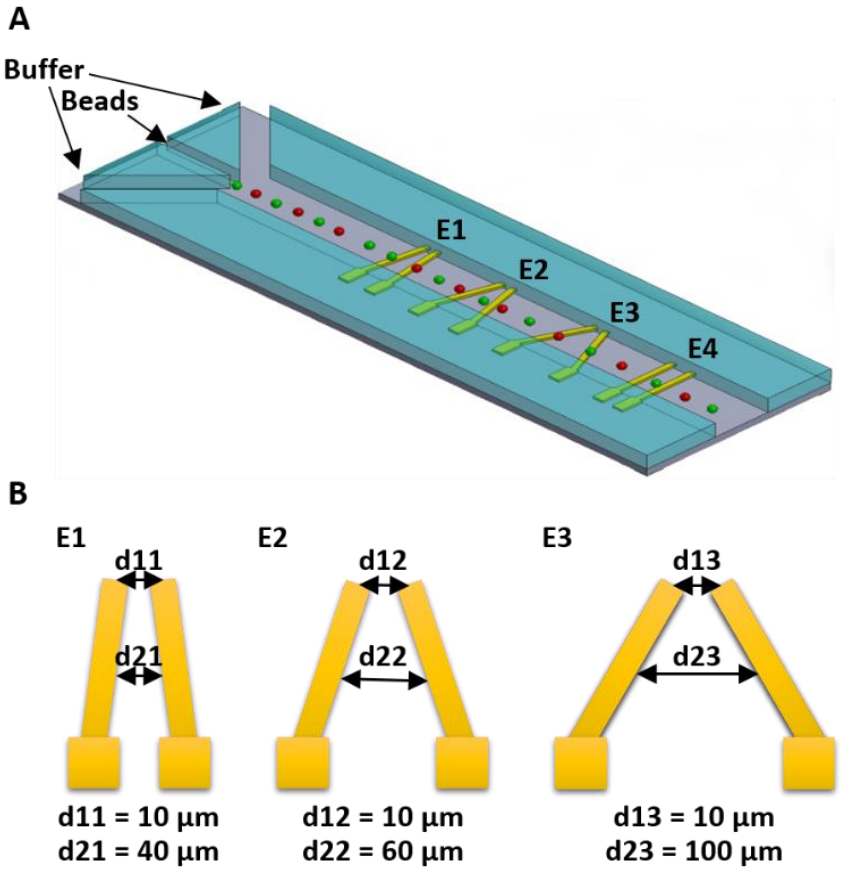

Figure 4. Design of the impedance spectroscopy-based cell/particle position detection device with three electrode pairs having different tilting angles. Designs E1 – E3 have 18.2°, 29.8°, and 51.3° tilting angles. The microfluidic has a three-channel flow-focusing inlet to change the transverse position of the cells and particles. The design E4 is a pair of reference parallel electrodes (zero tilting angle) to validate the signal of passing particles. The width of the electrodes is 15 µm in all cases. The design E4 is a pair of reference parallel electrodes (zero tilting angle) to validate the signal of passing particles. The width of the electrodes is 15 µm in all cases.

2.3.2. Microchip Fabrication

The electrodes were fabricated by depositing chrome and gold on the glass substrate, followed by etching of gold and chrome using lithographically patterned positive photoresist (Shipley® S1818) as an etch mask. The microchannel was fabricated by soft lithography, where poly(dimethylsiloxane) (PDMS, Sylgard 184, Dow Corning) channels were replica-molded using patterned negative photoresist (MicroChem SU-8 2015) with a channel height of 17 μm and channel width of 188 μm [99]. The channel height of 17 μm was selected to be slightly larger than the particle sizes of 6 and 11 μm used here, which represents a typical size of cells (5 – 15 μm), while minimizing the distance between the surface electrode and the cell passing through the detection zone for maximum detection sensitivity. The channel width of 188 μm was selected to simulate the scenario where a common cell is being separated based on their phenotypes into multiple different outlets. The PDMS block and glass substrate were aligned and bonded using oxygen plasma.

2.4. Cell and Particle Position Detection

2.4.1. Experimental

For device characterization, polystyrene beads (Polysciences, 6 and 11 μm in diameter) suspended in water were used. By tuning the flow rates of the three inlets, five positions in the transverse direction that are evenly spaced where particles passed by were verified by microscopy. Particle position detection was performed by applying a peak excitation signal of 3 V at 12 MHz and measuring the output signal using a commercial

2-channel impedance analyzer with a current amplifier (HF2IS and HF2TA, Zurich instruments AG, Switzerland). This optimal voltage and frequency condition was identified by scanning a broad voltage (0.5 - 5 V) and frequency (0.02 - 50 MHz) range, and selecting the one having the best signal-to-noise ratio of the detected signal. The particles were introduced at a combined flow rate of 120 µl/hr (corresponding to ~10.5 mm/s at the middle position). Data analysis was performed for the detected signal using MATLAB® (MathWorks, Inc.). A post-processing algorithm that performs baseline correction of the detected time-domain impedance signal, peak amplitude detection of corrected impedance signal, as well as peak width calculation was used. The measured peak amplitude and width were compared for each pair of non-parallel electrodes and evaluated.

To also demonstrate the ability of the developed cell/particle position detection microsystem to detect smaller polystyrene beads having diameter of 6 µm, as well as to test whether the positions can be discrimination when heterogeneous mixtures of cells/particles with different sizes that pass through, the detected impedance amplitude and width signals of both particle sizes (6 and 11 µm) were compared to that from the neighboring positions.

2.4.2. Results

As shown in Figure 5, it illustrated the peak amplitude signals for particles passing through the non-parallel electrodes at five different positions. The amplitude signals gradually decreased when the particles passed through transverse positions with wider

distances between the two electrodes, since the electric field is greatest at locations where the two electrodes are closest. The signal amplitude decreases as the two electrodes have larger distances. Also, the detected peak signals showed different peak width that reflect the required transit-time for particles that pass through the non-parallel electrodes at different positions. The peak width of the detected signals gradually increased from top to bottom (form position 1 to 5) since the electrode-to-electrode distances increase proportionally.

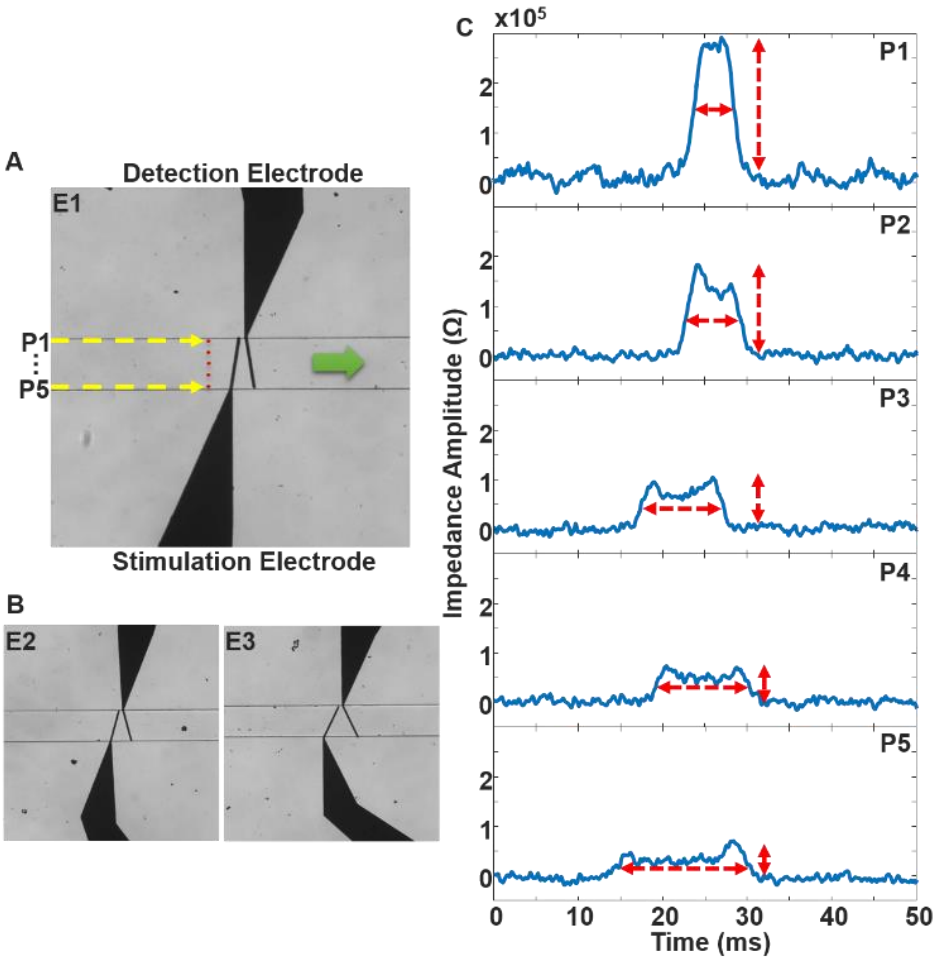

Figure 5. The detected position impedance signals for particles that pass through the non-parallel detection electrodes. The peak amplitude and width of the detected signals were different with respect to their positions between the two non-parallel electrodes.

Based on these preliminary experiment that shows clear changing in the detected impedance amplitude peak heights and widths of cells that passed through different position. Therefore the novel developed microsystem has also shown great discriminated detected position results as shown Figure 6 and Figure 7. The detected amplitude impedance peaks for particle passed the non-parallel electrodes were characterized at five different position equally distributed. For each pair of electrodes, clear difference can be realized for both detected peak amplitude electrical impedance signal and peak width.

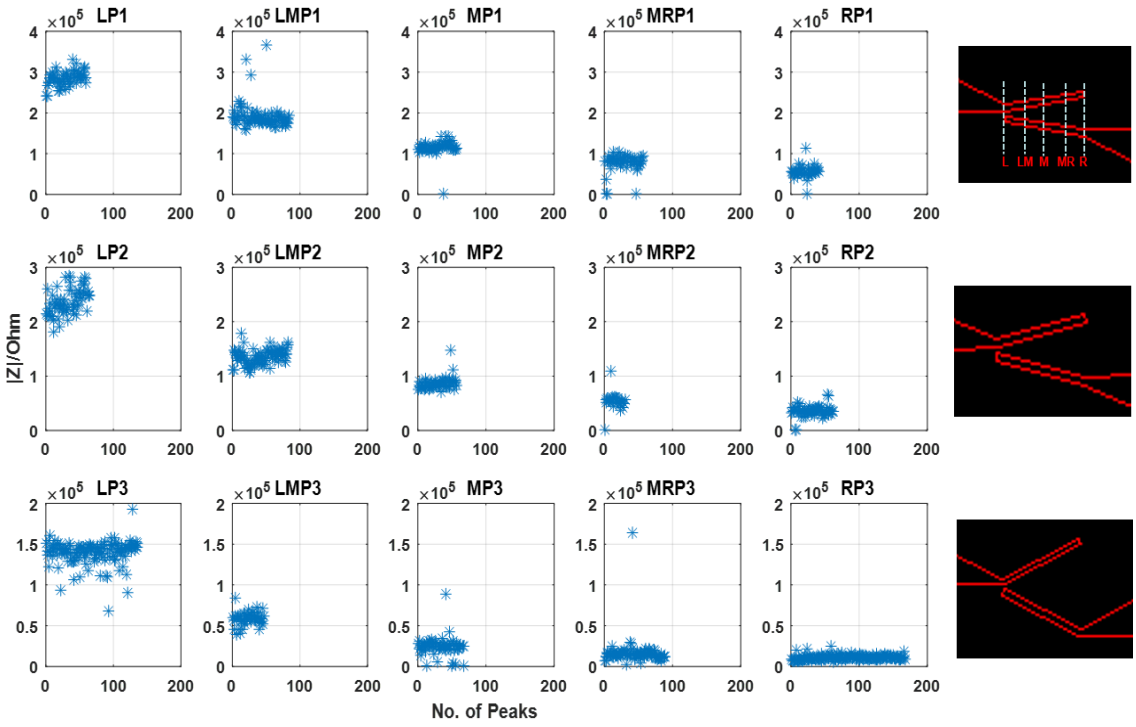

Figure 6. The data point of the detected peak amplitude impedance signals of particles passing through the three titled electrodes. For each designs, five positions were tested.

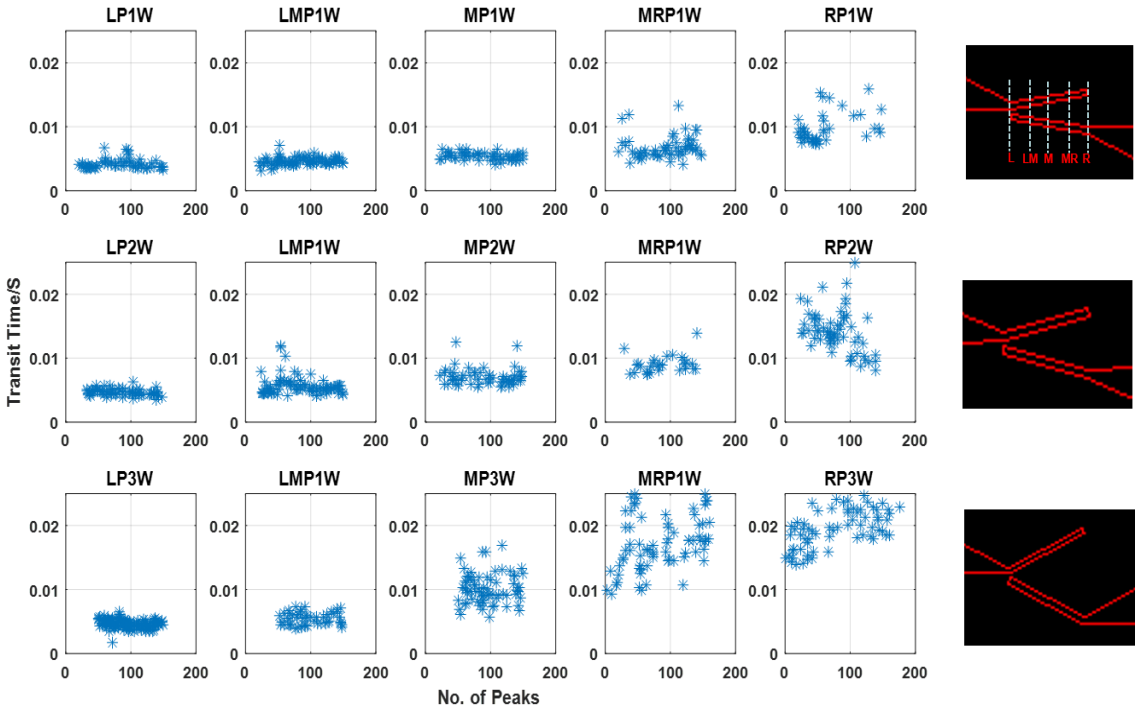

Figure 7. Measured detected peak signal width (transit time) of the amplitude impedance signal.

The developed microchip showed a significant position discrimination results as shown in Figure 8A. The figure shows the measured peak amplitude when particles of 11 µm passed through different transverse positions across the three non-parallel electrode pairs with different tilting angles. For all three designs, the measured peak amplitude gradually decreased as the particle positions moved from top to bottom. From the measured impedance peak results, all three designs could successfully differentiate the five transverse positions within the microchannel ($p<0.05$).

Electrode pair E3 has the largest change in electrode-to-electrode distance from top to bottom of the channel, however it showed the smallest percentage change in measured impedance peak amplitudes, while both E1 and E2 designs had relatively higher

percentage change in measured impedance peaks as particle passed through different locations between the two titled electrodes. Also, design E3 showed largest standard error in peak amplitudes, while E1 and E2 both showed lower level of standard error (Figure 8B). Therefore, for impedance peak-based position detection, both designs E1 and E2 could be utilized.

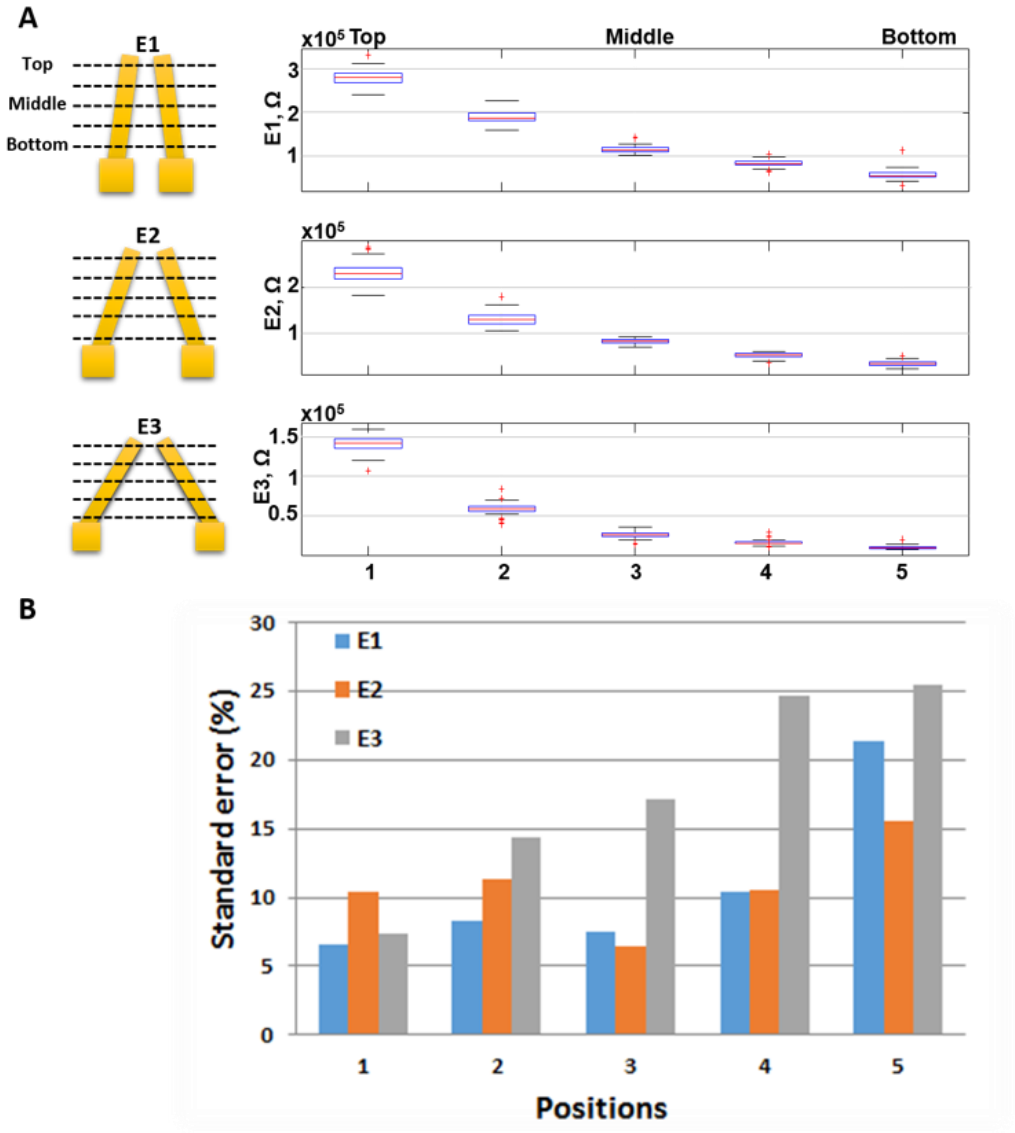

Figure 8. The detected impedance amplitude peak height of particles at five different positions. (A) Measured impedance peak amplitude for each electrode pair at five different transverse positions within a microchannel. For each electrode pair, the peak amplitude of neighboring positions all satisfied $p<0.05$. (B) Standard error for peak amplitude of each electrode pair at the five different positions. The third design (E3) showed highest standard error.

Figure 9A shows the measured peak width of the impedance signals when 11 μm beads passed through the five different positions. In the design E1, the peak widths of the first two positions were not statistically different. In E3, the standard error was highest among the three designs, suggesting that there is a large variation in the measured peak width, making it unsuitable for position detection. E2 showed the smallest standard error and also clearly distinguishable peak width signals depending on the transverse positions. Overall, design E2 was determined to be most suitable to quantify the transverse positions of particles in microchannels, and both peak amplitude and peak width can be used to obtain sufficient position sensitivity and resolution (33 μm particle position difference in the 188 μm wide channel used, corresponding to the average distances between the 5 different positions tested).

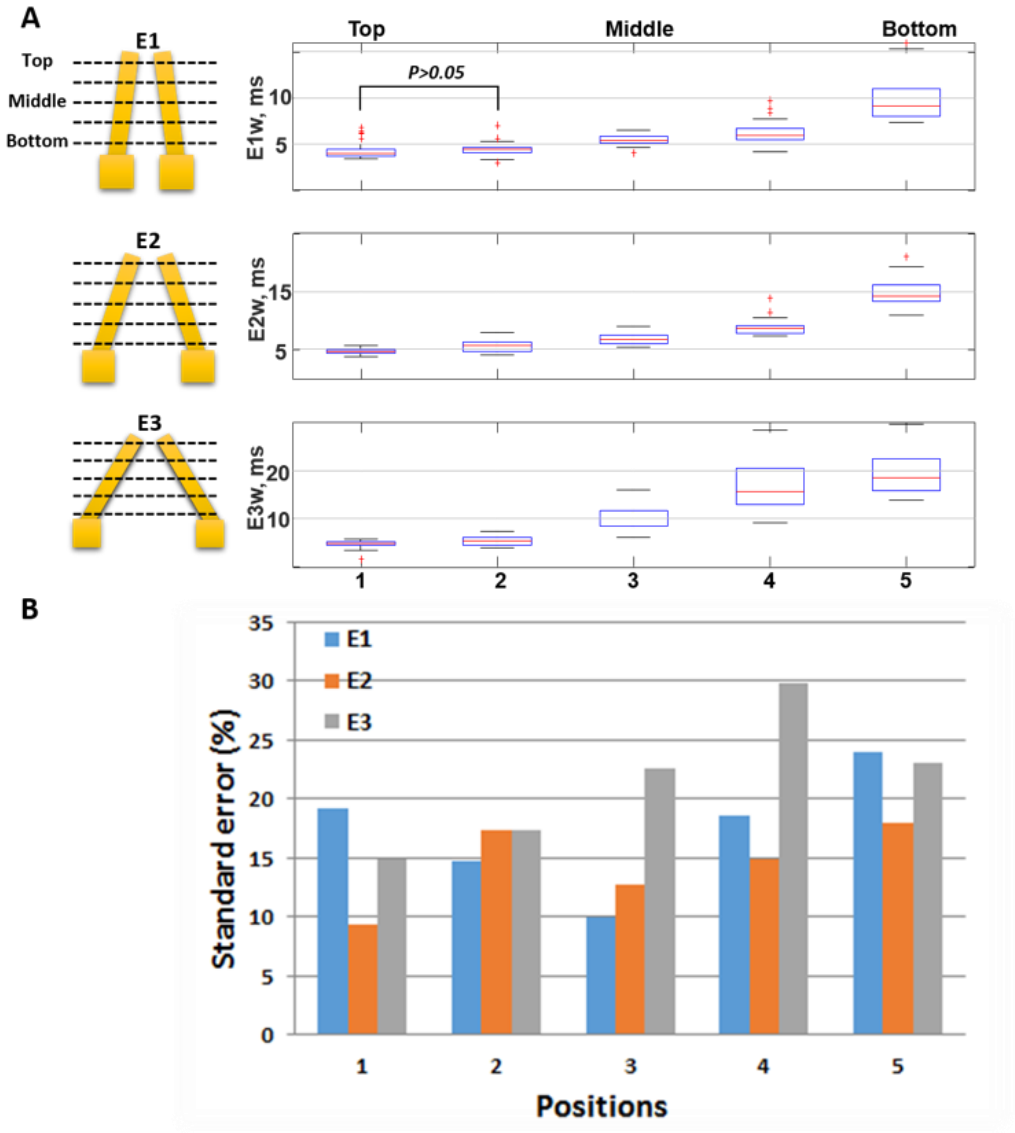

Figure 9. The detected impedance amplitude peak width of particles at five different positions. (A) Measured impedance peak width for each electrode pair at five different transverse positions. (B) Standard error for peak width of each electrode pair at the five different positions. For E1, the peak width of first two positions showed $p>0.05$. For E2 and E3, the peak width of neighboring positions all satisfied $p<0.05$.

In addition 6 µm diameter particles were also tested using the electrode design E2 that showed the best result from the 11 µm diameter particle testing. The detected peak amplitude signals as the particles passed through the 5 transverse positions gradually decreased as shown in Figure 10. Significant position discrimination of $p<0.005$ has been obtained for particles passed though the five different positions. The measured peak width signals of the five transverse positions gradually increased and also showed significant differences ($p<0.001$) (Figure 11), demonstrating that the five different positions can be distinguished using either impedance width or peak signals, similar to the case for the 11 µm diameter particles.

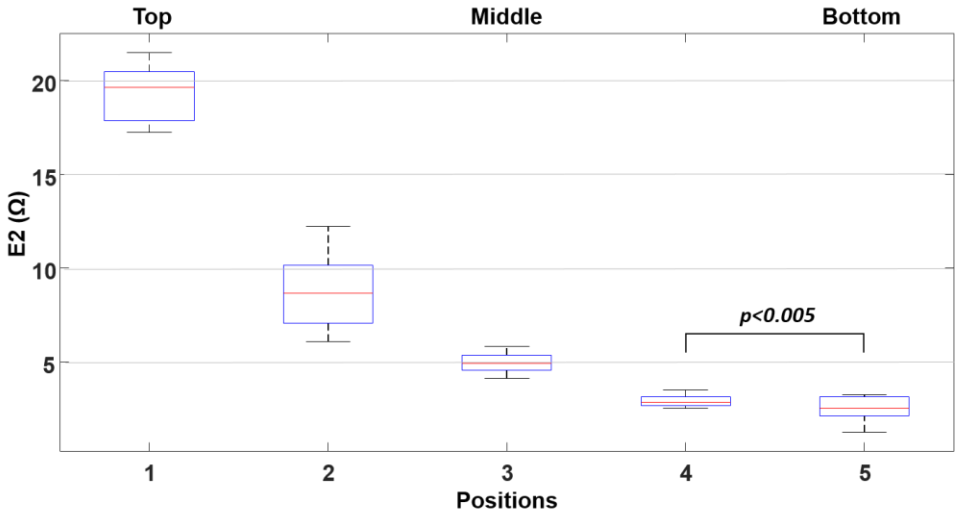

Figure 10. The detected impedance amplitude peak height at five different transverse positions using beads of 6 µm diameter. The peak amplitude signals are significantly different from position to position. The applied excitation signal condition was 3 V at 27 MHz.

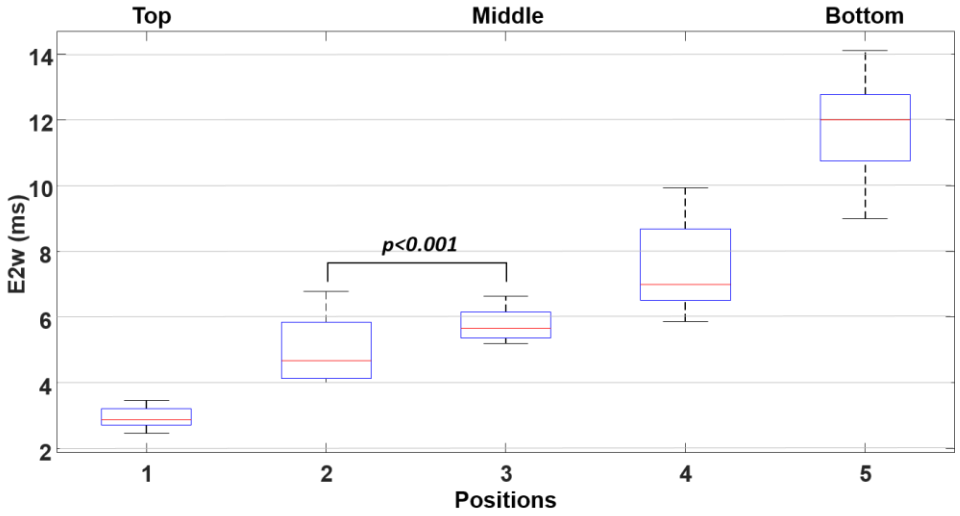

Figure 11. The detected impedance peak width at five different transverse positions using beads of 6 µm diameter. The peak width signals are significantly different from position to position.

To test how the presented position detection method will perform when using heterogeneous populations of particles/cells having different sizes, the impedance amplitude peak and the impedance peak width of the 6 and 11 µm particles from each position were compared to that from the neighboring positions. In all position cases, the differences between the impedance signals (amplitude and width) between the two particles were smaller than that from the impedance signals coming from the neighboring positions ($p<0.05$ when comparing impedance amplitude signals and $p<0.001$ when comparing impedance width signals in all five transverse positions). As shown in Figure 12A and Figure 12B, the normalized impedance signals (amplitude and width) from the two particle sizes have similar range of signals within the same position, and showed significant differences compared to the ones from the next position. This results clearly show that cell/particle position detection and discrimination of five different transverse

positions can be successful achieved even if cells/particles having different sizes in the range of 6-11 µm in diameter flows through.

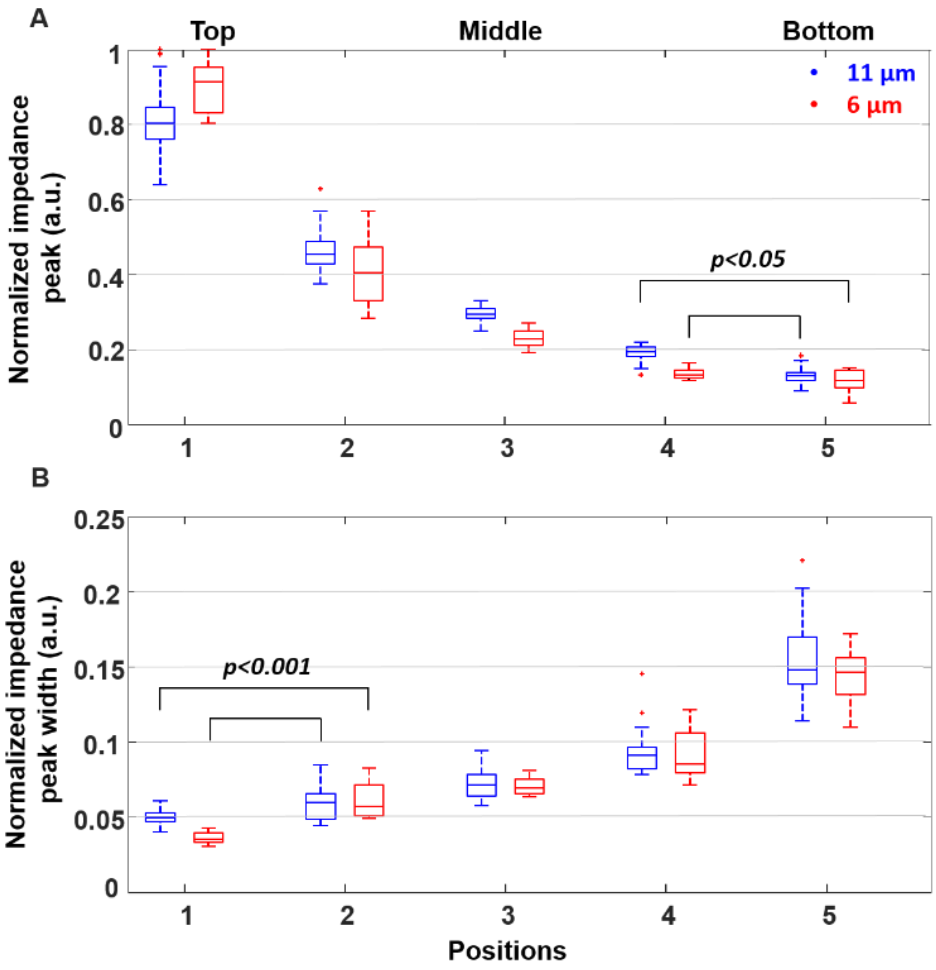

Figure 12. The comparison of normalized impedance signals of two different bead sizes (11 and 6 µm in diameter) at five different transverse positions (box plot). (A) Normalized impedance peak amplitude of different particle sizes (Impedance peak amplitude / maximum impedance peak amplitude). (B) The detected impedance peak width of both particle sizes normalized by the flow speed (Impedance peak width x flow speed).

This microsystem has achieved particle detection at a speed of up to 400 particle/s (corresponding to a flow rate of 480 µl/hr, highest flow rate attempted so far). Considering the cell separation rates from few to few thousand cells/sec in most microfluidic cell separation systems, this throughput covers quite a broad range of cell separation microfluidic devices. We expect that even a higher detection rate at higher flow rates can be achieved through further electrode design optimization, which is part of our future work.

2.5. Conclusion

In this work, a high-throughput and low-cost impedance spectroscopy-based particle position detection method was developed and successfully demonstrated in determining the transverse positions of particles within a microfluidic channel and achieving a detection rate of more than 400 particles/sec. Three designs of non-parallel electrode pairs with different tilting angles were tested, with the design that has medium tilting angle (design E2, 29.8°) showing the best quantifiable measured signal and smallest standard error in both impedance peak amplitude and peak width measurement when 11 µm diameter beads were used. The system was also tested using 6 µm diameter beads and showed the same capability in distinguishing five different transverse positions. For the 11 µm diameter beads, this results in position resolution of 33 µm, and for the 6 µm diameter beads, this results in position resolution of 40 µm. Also, to test the feasibility of the developed position detection microsystem in case of heterogeneous populations of particles/cells having different sizes, the measured peak amplitude and width signals were

compared to those of 11 μm diameter beads, and clearly showed that regardless of the different bead sizes of 6 and 11 μm, they showed significant differences between that from the neighboring positions when using either the impedance peak amplitude or width signals. After initial calibration, this method could be readily used to quantify multiple transverse positions using single-channel impedance detection. Although differential impedance measurement in general provides higher sensitivity, it requires equipment capable of two-channel impedance detection, increasing the cost and complexity. Even though the presented work used only a single electrode pair, the peak amplitude results of neighboring positions showed significant difference ($p<0.05$) and achieved our goal in discriminating the particle positions without having to use a two-channel differential measurement. Based on the need, the exact configuration of the presented system can be easily modified for different application scenarios, adding more versatility and flexibility to the presented method. This method offers a simple, fast and low-cost approach for quantification of particle/cell positions inside a microchannel without complex optical setup. Also this method can be readily integrated with most microfluidic systems and impedance spectroscopy systems with minimum effort, greatly enabling the capability of the techniques in which particle position is of interest such as flow cytometry and particle/cell sorting/separation applications.

CHAPTER III

HIGH-THROUGHPUT MULTI-OUTLET CELL COUNTING USING A SINGLE PAIR OF LABEL-FREE IMPEDANCE ELECTRODES

3.1. Motivation

Microfluidic-based cell sorting and separation systems have been successfully developed and widely utilized for identifying and selecting cells of interest from heterogeneous mixture of samples. However quantification and counting of sorted and separated cells and particles have been suffered from high samples loss during handling collection process for off-chip cell counting and analysis, especially when dealing with a small amount of rare collected samples.

Recently we have developed as shown in Chapter II, a high-throughput and low-cost impedance spectroscopy-based cell/particle position detection method using a pair of non-parallel (tilted) electrodes that could detect the transverse positions of particles flowing within a wide single microchannel [100]. Using this concept, we present an integrated on-chip, low-cost and label-free cell detection and counting microsystem capable of monitoring multioutlet simultaneously by integrating and utilizing only a single pair of impedance spectroscopy-based electrodes to multiple microfluidic outlet channels that has the ability to detect, count and quantify the sorted/separated particles and cells.

3.2. Experimental Setups

3.2.1. Cell Counting Method Using a Single Pair of Electrodes

The developed multioutlet cell counting microsystem consists of 5-outlets microfluidic channels integrated with a single pair of electrodes that has a step-shaped design. The electrodes' design has five different parallel electrode-to-electrode gaps and been aligned and positioned at each outlet vertically to the direction of cell flow and microchannel direction. These electrodes were connected to each other's to form a single pair of electrodes (Figure 13A). The electrode to electrode gap differences have been carefully designed to have higher detection sensitivity and significant signal differences from each outlet to all other outlets. Applying an AC voltage to this pair of electrodes, it will generate a non-uniform distributed electric field between this pair of electrodes due to non-equal gaps between this pair of electrodes at each outlet. The induced electric field can be disturbed when the medium in between the two electrodes is changed to different medium such as flowing cell or particles through a liquid medium. However, since the electric field strength is inversely proportional to the distance between the stimulation electrode and detection electrode, thus varying the gap in between two electrodes can be an importance role in the electric field distribution and strength in between different electrode to electrode gaps. Therefore different electrode to electrode gaps can be utilized at each outlet to induce different electric field across each outlet; resulting in different electric impedance signal in between each electrodes' gap (Figure 13B). Furthermore, as successfully presented in our previous work [100], two types of signal properties were extracted and used; the impedance amplitude peak height and the impedance amplitude

peak width (peak transit-time). When a cell or particle passes through the detection region, it will cause a change in the dielectric properties of the whole surrounded medium. This limited time varying in the dielectric properties of the surrounded medium will cause a change in the total detected impedance signal; resulting in a peak signal that has different height and width. For instance, particles passing O_1 will result in higher and narrower impedance amplitude peak signals, in contrast particles that flow-through O_5 will show lower and wider impedance amplitude peak signals. This impedance amplitude peak height is calculated as a difference between the highest impedance peak height value acquired when cells flow through the detection region and the baseline impedance amplitude value without cells, while the impedance peak width is measured by calculating the transit-time of the detected impedance peak signal for cells passing through the stimulation electrode to the detection electrode.

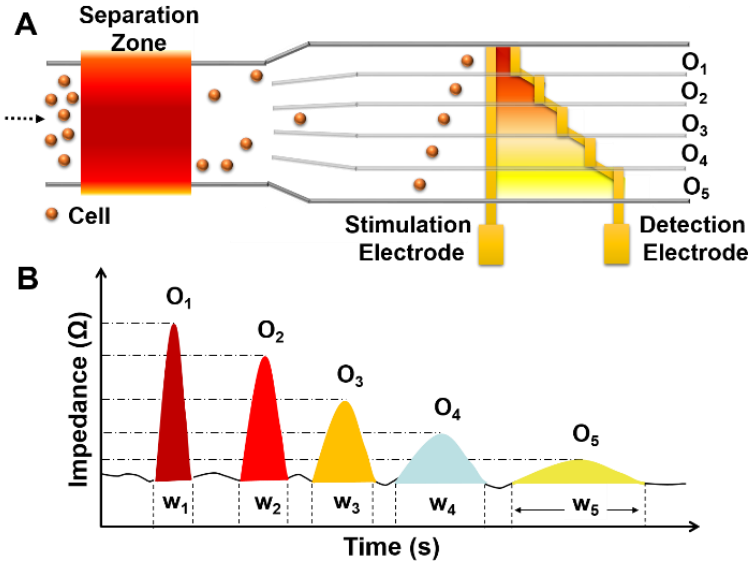

Figure 13. Principle of multioutlet cell counting using a single impedance electrodes' pair. (A) A single impedance electrode pair having different electrode-to-electrode gaps for each outlet channel. Smaller gap results in higher electric field compared to larger gap between electrodes, and thus cells passing through the different outlet channels (O_1 to O_5) are exposed to different electric field strength. (B) Illustration of the predicted impedance signal peak height and width of cells passing through different outlets.

The electrode to electrode gap difference effect to the acquired impedance signal was initially simulated, followed by detecting and characterizing microbeads flowed within a single channel integrated with 7 pairs of electrodes that has different electrode to electrode gap. Thereafter the developed single pair of step-shaped electrodes that has 5 different electrode to electrode gaps was tested at five parallel microfluidic outlet channels using yeast cell. Further optimizations for the previous electrode to electrode gaps were performed and tested to not only demonstrate higher discriminated signals of the detected cells from each outlet to other outlets but also to have significant lower misclassification error between each other's.

3.2.2. Chip Fabrication

The microsystem was fabricated by integrating two layers; a PDMS microfluidic channel and deposited electrodes on a glass substrate. The microfluidic channel was fabricated by soft lithography, where poly(dimethylsiloxane) (PDMS, Sylgard 184, Dow Corning) channels were replica-molded using patterned negative photoresist (MicroChem SU-8 2015). The electrodes were deposited on a glass substrate (20 nm titanium/200 nm gold) and fabricated using the standard lithography process using positive photoresist (Shipley® S1818). The developed 5-multioutlet microfluidic device has outlet channels' width of 20 µm, with a 25 µm wide walls of PDMS positioned in between the outlets. The main microfluidic channel width and height were 200 and 16 µm, respectively.

3.2.3. Cell Counting Measurement and Analysis

For electrode to electrode gap effect characterization, a preliminary single microfluidic channel device that has 50 µm width and 16 µm height integrated with 7 pair of electrodes of non-equal gaps. This preliminary characterization microsystem has been tested using polystyrene microbeads (11 µm in diameter, Polysciences) suspended in water to validate the electrode to electrode gap difference effect in the detected impedance signals (height and width) of flowing homogenous particles.

Thereafter yeast cells suspended in Yeast extract peptone dextrose (YEPD) medium were introduced to five multioutlet microfluidic device using a flow-focusing scheme to characterize and validate the performance of the developed single pair of the step-shaped electrodes that has five different electrode to electrode gaps. Therefore the yeast cells have been suspended and sorted to each outlet separately to can thereafter evaluate the

functionality of the developed method. The flow-focusing of three inlets has been utilized to mimic the separation and sorting methods, whereas the inlets of flow-focusing were precisely tuned and controlled to manipulate the cells flow at each outlet. The applied excitation signal was selected based on the highest impedance peak signal to baseline noise ratio by testing cells flowing through a pre-optimized microfluidic channel width and height at ranges of frequencies (0.1-50 MHz) and voltages (0.1-5 V). However the applied voltage and frequency were optimized and selected based on the highest impedance peak signal to baseline noise ratio at the largest selected electrode to electrode gap (O_5), and thus the detected signals of cells that passing through other outlets will gradually increase due to higher electric field strength in smaller electrode to electrode gaps located in the other outlets. Therefore an optimal excitation signal of 3 V AC signal at 1.2 MHz were chosen and applied to the developed step-shaped electrodes. Signal excitation and output measurement were performed using single-ended measurement mode provided by 2-channel impedance spectroscope (HF2IS). Data processing of the detected signals was accomplished using MATLAB for further analysis such as baseline correction of the detected time-domain impedance signal as well as peaks properties (height and width) extraction of the detected impedance peaks.

To quantify the discrimination performance of the detected signals of cells flowed through the five different outlets, three different classification methods using different approaches were performed and compared since there is no one classification method will lead to the best results in all situations. First method was realized by implementing a manual linear threshold that is selected to maximize the distance in between each subset

of data from each outlet to the neighboring subsets from the other outlets. Therefore, for *k* subsets of data, *k-1 is* the number of the selected threshold lines, which these lines locate in between the subsets of data. The second classification method is Linear Discriminant Analysis (LDA). LDA is very common statistical algorithm for data classification, which it picks a new dimension that maximizes the separation distance in between the means of the projected classes (subsets of data) and minimizes the variance within each projected class. For k^{th} subsets of data, LDA classifier provides *k-1* linear decision boundaries in between subsets of data by calculating the linear relation of the feature in the subsets of data. LDA method assumes that each subset of data has different mean but the covariance matrix is identical for all k^{th} subsets of data [101, 102]. The third classification method is Quadratic Discriminant Analysis (QDA), which it is an alternative algorithm to LDA. QDA classifier is similar to LDA classifier in assuming each subset of data has different mean, however quadratic discriminant analysis classifier is assumed that each subset of data has different covariance matrix for each subset of data; leading to non-linear decision discriminating boundaries in between subsets of data [103].

3.3. Results and Discussion

3.3.1. Electrode to Electrode Gap Detection Effect

Preliminary simulations were performed for assessing and evaluating the detection effect of a microfluidic channel that has different pairs of electrodes of different electrode to electrode gaps. Therefore different electrode to electrode gaps were designed and simulated using the AC/DC module of COMSOL Multiphysics 5.3 (COMSOL AB, Sweden). The electric field norm has been simulated at seven different electrode to

electrode gaps starting from 20 µm to 140 µm with fixed increment of 20 µm as shown in Figure 14. It demonstrated that there was a nonlinear drop in the calculated electric field strength as shown in Figure 14C and D from 87.7 x 10^3 V m^{-1} at 20 µm to 19.5 V m^{-1} at 140 µm electrode to electrode gap. Moreover there was a high electric field strength difference between 20 µm and 40 µm of 31.92 x 10^3 V m^{-1} while a very small electric field strength difference in between larger electrode to electrode gaps such as 120 µm and 140 µm of 2.92 V m^{-1}. Therefore the electric field intense can be potentially affected by varying the electrode to electrode gaps in between the stimulation electrode and the detection electrode.

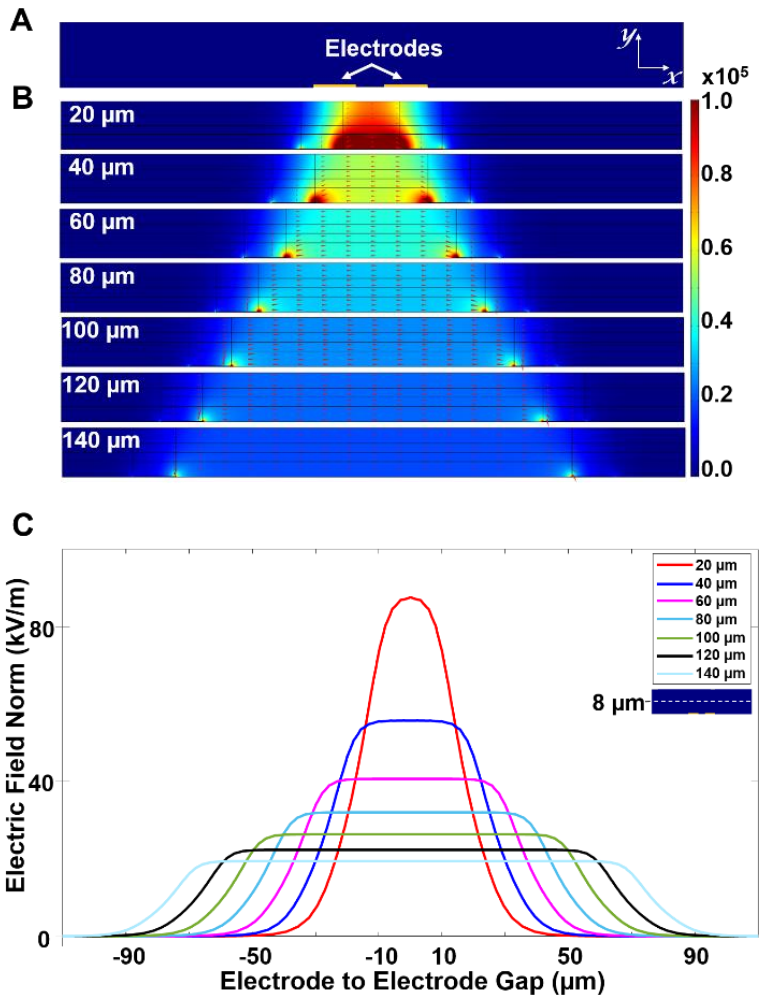

Figure 14. The electrode to electrode gap detection effects. (A) Side-view of a pair of electrodes integrated in a microfluidic channel. (B) Simulation of electric field norm of seven different electrode-to-electrode gaps within the microfluidic channel. (C) Simulated electrical field norm distributions between pair of electrodes at seven different electrodes' gaps in between. The width of the electrodes was 15 µm. The simulated electric field has been performed at 8 µm height from the electrodes to show the electric field strengths and distributions. A 3 V AC signal was applied to stimulation electrode, and the detection electrode was grounded. A YEPD medium was considered as liquid (σ = 0.3 S m^{-1}, ε_r = 80). (D) The histogram shows and compares the maximum electric field strength in between seven pair of electrodes, resulting in gradually decrement in the calculated electric filed strength while the gaps were increased.

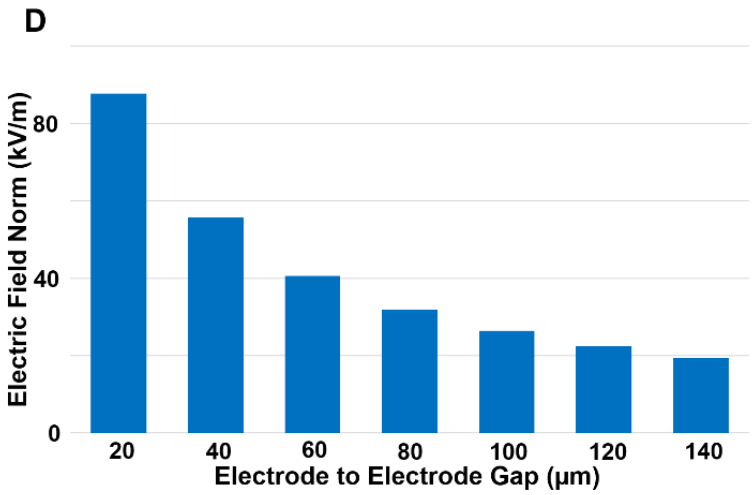

Figure 14. Continued.

Figure 15A shows a microscopic image of seven pair of electrodes with 7 different pairs of electrodes integrated to a single microfluidic channel. When PS particles flowed through the seven pair of electrodes, different impedance peak signals have been detected. Examples of 4 different impedance amplitude peak signals have been demonstrated as shown in Figure 15B of particles flowed through different pairs of electrodes. As shown, the peak height of the detected impedance signal decreased when the particles passed through larger electrode to electrode gaps, while the impedance peak width increased since the gaps were increased. When the PS particles flowed through the smaller gaps such as 20 µm, it resulted in sharper impedance peak signal of around 30 kΩ, while the detected impedance amplitude peak height was small at gap of 140 µm of lower than 2 kΩ (Figure 15C). In contrast the detected impedance amplitude peak width were gradually increased from 1.17 to 8.36 ms when PS particles flowed through 20 to 140 µm electrode to electrode gaps, respectively, since the electrode to electrode gaps were gradually increased by 20 µm in between each pair of electrodes. The detected impedance peak signals of the beads

flowed through these seven pair of electrodes showed a small standard deviation as high as 1.6% in the detected impedance amplitude peak signals due to their monodisperse properties as well as their similar dielectric properties.

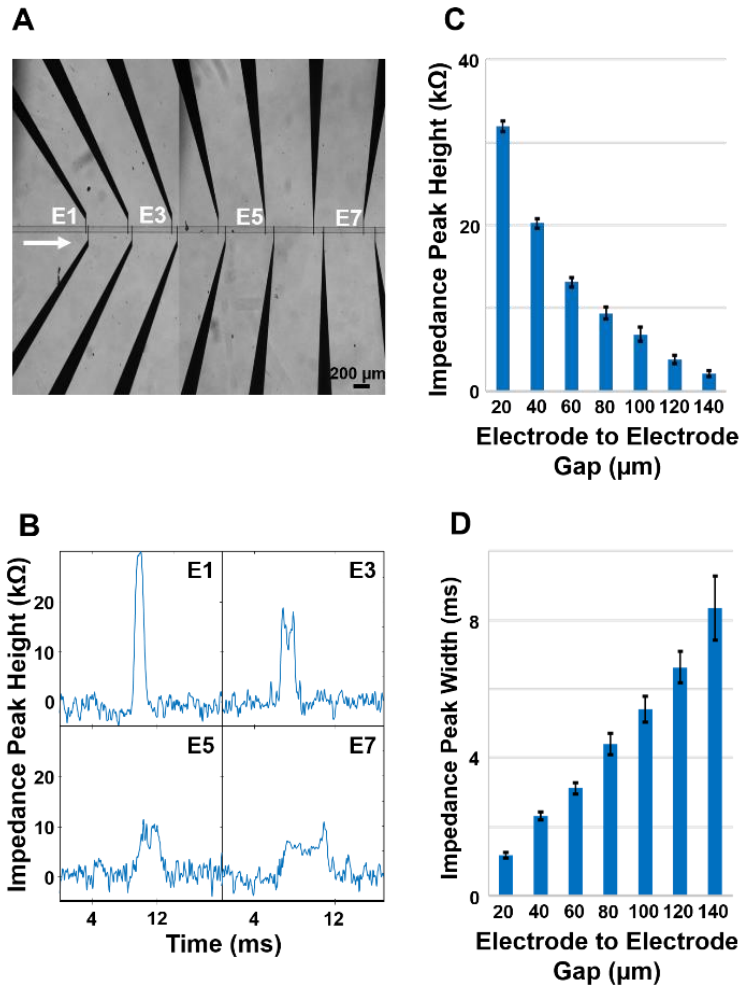

Figure 15. Effects of electrode-to-electrode gaps differences on the detected impedance signals of cell passing through. (A) Image of microfluidic channel integrated with gold based electrodes with seven different electrode-to-electrode gap pairs. (B) Acquired impedance peak height signals from microbeads passing through four different detection electrodes pairs. (C) and (D) showing the average of the detected impedance signal peak height and width, respectively.

3.3.2. Cell Counting at 5-Outlets Microchannels Using a Single Pair of Electrodes

Upon the previous preliminary simulations and experiments of using different pairs of electrodes that have different gaps, they showed clear differences in the calculated electric field strength as well as the acquired impedance amplitude peak height and width. However, in the case of cells, the detected impedance signals could be varied in each pair of electrodes and resulted in a broad range of impedance peak height signals due to their non-uniform cell sizes, therefore considerable difference in the detected peak signals for either homogeneous or non- homogeneous particles and cells was needed. In addition, when single pair of electrodes is considered to be used to detect and discriminate cells that flow through multiple outlet channels, higher leakage current through the carrier medium could be occurred since the total cross-section area of the detection region will be larger; resulting in lower detection sensitivity. Thus a single pair of electrode that has five parallel integrated electrode to electrode gaps (10, 50, 90, 130, 170 µm) of 40 µm increment were developed, utilized and integrated to 5 parallel outlet microfluidic channels (Figure 16A). In order to enhance the detection sensitivity, further optimization for the microfluidic channel was done by decreasing the microfluidic channel width from 50 µm to 20 µm not only to lower the current leakage through the carrier media but also to increase the detection sensitivity by decreasing the cross-section detection area to 60% lower comparing to the cross-section detection area of the previous device that have been used to characterize the effect of different electrode to electrode gaps on the detected impedance signals. The detected impedance amplitude peak signals of yeast cells passing through the five different outlets as shown in Figure 16B were clearly showed differences in both

impedance amplitude peak height and width from outlet to outlet. Since the fractions of the cell volume to the total media volume in between the two electrodes in each outlet were different, the flowing cells in each outlet that has different electrode to electrode gap have exposed to different level of electric fields; resulted in different electric impedance peak signals. Therefore, by increasing the electrode-to-electrode gap in each outlet from 10 to 170 µm, the acquired impedance amplitude peak height gradually decreased when the cells passed-through the larger electrode to electrode gaps in each outlet, in contrast the impedance amplitude peak width was gradually increased from O_1 to O_5 since the electrode-to-electrode gap gradually increased in each outlet resulting in more transit time was needed for each cell to pass through the detection region at each outlet. Furthermore, Figure 16C shows the simulated electric field norm distribution in between each pair of electrodes of the selected five different gaps, which demonstrated a maximum electric field norm as high as 114.08 x 10^3 V m^{-1} at 10 µm electrode to electrode gap, while at 170 µm, 16.32 x 10^3 V m^{-1} of maximum electric field strength was induced and demonstrated (Figure 16D). Besides high difference was shown and demonstrated in both the detected impedance peak signals and the simulated electric field strengths in between 10 µm and 50 µm electrode to electrode gaps of outlets 1 and 2 of ~650 Ω and 67.05 x 10^3 V m^{-1} respectively. However gradually decreased in the differences of the detected impedance peak heights as low as ~20 Ω and the simulated electric field norms of 4.54 x 10^3 V m^{-1} as shown in between outlets 4 and 5.

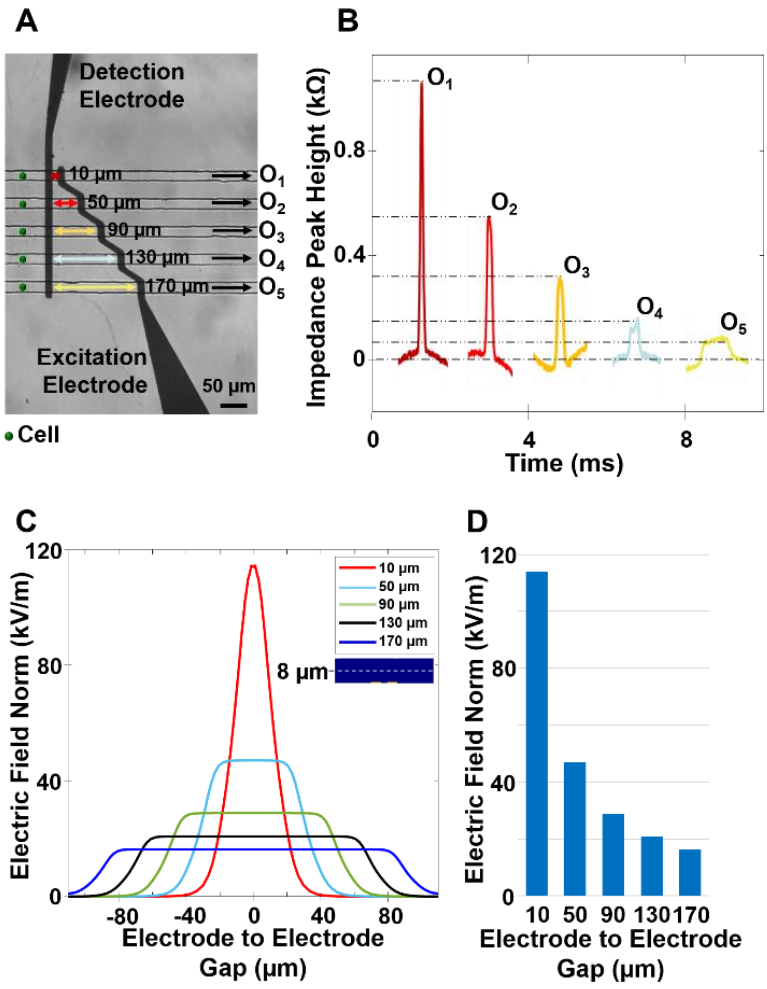

Figure 16. The multioutlet microfluidic based impedance spectroscopy cell counting system. (A) Image of the multioutlet microfluidic system having a single pair of step-shaped electrodes integrated to five microfluidic outlets. (B) Measured impedance signals of cells passing through different five detection regions of the five different outlets. (C) Simulated electrical field norm distributions between pair of electrodes at five different electrodes' gaps in between. (D) The bar graph shows the maximum electric field norm strength at five different electrode to electrode gaps. The simulated electric field has been performed at 8 µm height from the electrodes to show the electric field strengths and distributions. The width of the electrodes was 15 µm.

Figure 17A showed a scatter plot of the detected impedance amplitude peak height versus the impedance amplitude peak width categorized at five different colors corresponding to yeast cells flown through five different electrode to electrode gaps at five parallel microfluidic outlet channels. To quantify the performance of the detected training data that has five different subsets of data, three different classification methods were used: manual linear threshold, LDA, and QDA. For the manual linear threshold, four vertical linear threshold lines were selected manually at 600, 148.4, 51, and 34.5 Ω, whereas each threshold line was selected to maximize the distance in between each subset of data to the neighboring subset and minimize the misclassified cells at each outlet (Figure 17A). For the first two linear threshold lines that classified outlets 1, 2, and 3, 600 Ω and 148.4 Ω were selected to classify subsets of data from O_1, O_2 and O_3 from each other and to find the missed classified data points from the detected cells from each outlet. Based on these thresholds, the detected cells from outlet 1 and outlet 2 were 100% successfully classified as outlet 1 and outlet 2, respectively. However the cells detected at outlet 4, 7.6% (19 cells) misclassified as outlet 3 and 1.2% (3 cells) misclassified as outlet 5. The largest error of 10.85% (42 cells) misclassification was from the detected cells at outlet 5, whereas they misclassified as outlet 4 as shown in Figure 17B. Of the overall training data points (the five subset of data), 3.33% or 109 cells were misclassified as different outlets out of all detected training data points of 3272 when the manual linear threshold method.

By using LDA method, each two subsets of data detected from two neighboring outlets (O_{12}, O_{23}, O_{34}, and O_{45}) were consecutively classified and quantified to examine how well

is the performance of the developed single pair of electrodes that has different electrode to electrode gaps on the detected training data that have been collected from five different outlets. Therefore the decision boundaries as shown in Figure 17C have been obtained by LDA method and used to find the misclassified error in between each subset of data to the neighboring subset. For the first two subsets of data of the detected cells from outlets 1 and 2 (O_{12}), the calculated decision boundary discriminated each two subsets of data to two regions and resulted in a small misclassification error of 1.035% of total 1449 detected cells (detected cells from outlets 1 and 2). However, when LDA was performed in between outlets 2 and 3 (O_{23}), 3 and 4 (O_{34}), as well as 4 and 5 (O_{45}), it showed high misclassification error as maximum as 9.37% (1922 detected cells) in between data subsets of outlets 2 and 3. Furthermore LDA was implemented to classify the overall training data of five subsets; showing high classification error of 32.89% or 1076 misclassified cells.

QDA classifier as mentioned before can give alternative approach, which it could provide more accurate non-linear classification decision boundaries between different subsets of data. Therefore since there are five different subsets of data, QDA classifier was applied by considering both methods; in between each two subsets of data consecutively (O_{12}, O_{23}, O_{34}, and O_{45}) as well as to the overall five subsets of data. In case of in between each two subsets of data, O_{12} showed very low classification error of 0.35% of the total number of detected cells from outlets 1 and 2, in contrast high classification error of 8.5% was shown in between data detected from outlet 4 and 5 (O_{45}). However the total number of misclassified cells from all five subsets of data was 3.76% or 123 cells when QDA

classifier was applied using the approach of classifying in between each two subsets of data (Figure 17D). Furthermore QDA classifier was utilized using the approach of assessing the overall five subsets of data together; resulting in similar number of missed classified number of cells of 3.76% as the QDA classifier when it was applied in between each two subsets of data.

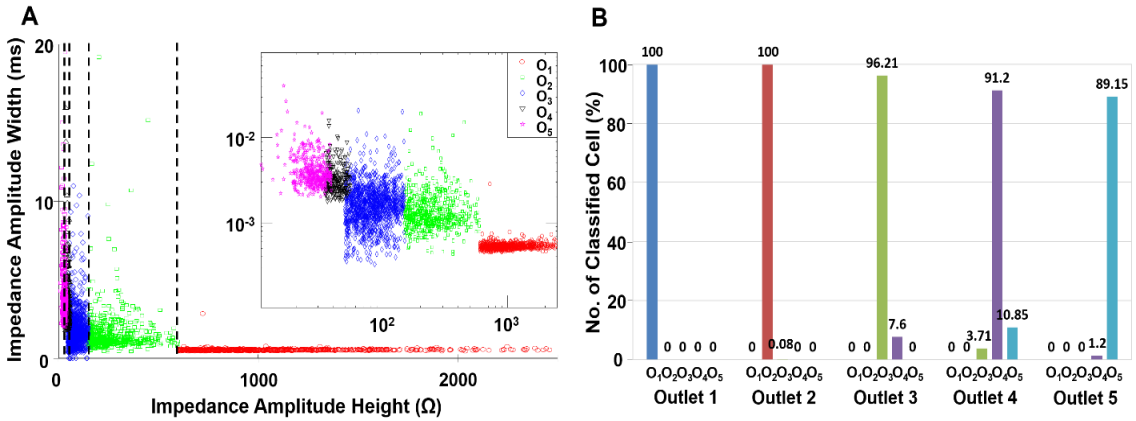

Figure 17. The classification results of the detected impedance signals of cells passing by five different outlets at five different electrode to electrode gaps. (A) An impedance scatter plot for yeast cells flowing through five different outlets and showing the measured impedance peak amplitude height and width using the single pair of step-shaped electrodes that has five different electrode to electrode gaps (10, 50, 90, 130, and 170 µm). From outlet 1 (O_1) to outlet 5 (O_5), the detection electrode to electrode gap were increased resulting in increasing in the impedance peak width and decreasing in the impedance peak height. The annotated four different straight line thresholds classify the detected events to 5 different colored groups. (B) The bar graph that shows the percentages of detected cells at each outlet were represented based on the selected manual linear thresholds that used to discriminate between the outlets. (C) and (D) showing the scatter plot of the measured impedance amplitude peak height and width that include the decision threshold boundaries for both Linear Discriminant Analysis and Quadratic Discriminant Analysis, respectively. Also the misclassification results using LDA and QDA by considering both methods have been calculated and tabulated.

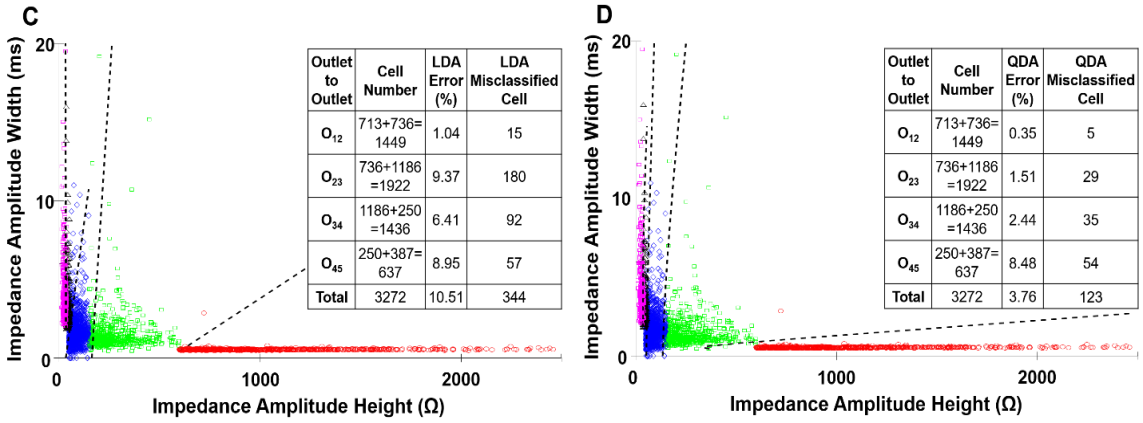

Figure 17. Continued.

As shown from the previous three classification methods, manual linear threshold method gave the lowest overall classification error of 3.33% of the detected training data. By using this method, it showed that the highest classification errors were from the detected cells from outlet 4 of 8.8% as they misclassified as outlets 3 and 5 as well as the detected cells from outlet 5 of 10.85% misclassified cells were considered as outlet 4. In contrast, misclassification errors of 0% in between subsets of data from outlets 1 and 2 (10 µm and 50 µm electrode to electrode gaps) as well as from outlet 3 and 5 (90 µm and 170 µm electrode to electrode gaps) were successfully obtained, respectively. From the previous results, it was more important to understand and assess each subset of data from each outlet to other outlets to improve the discrimination in between each outlet to other outlets, consequently decrease the overall classification error. Thus optimizing the detection impedance signals differences in between the outlets were needed. To do that, the electrode to electrode gaps' differences were optimized to have higher discrimination from each outlet to other outlets by reconsidering the electric field differences in between

each electrode to electrode gap to the neighboring gap. Since the highest classification errors were in between outlets 3 and 4 and outlets 4 and 5 as successfully examined and shown in both manual linear threshold and QDA methods, the electric field norm difference in between electrode to electrode gaps of 130 µm (O_4) to 90 µm (O_3) as well as 130 µm (O_4) to 170 µm (O_5) were 8.04 x 10^3 V m^{-1} and 4.54 x 10^3 V m^{-1}, respectively (Figure 16D). As mentioned before, the classification error in between the two subsets of data from outlets 3 and 5 was 0% and has the electric field difference of 12.58 x 10^3 V m^{-1}, therefore the gaps of the single pair of step-shaped electrodes were redesigned to have as minimum as 12.58 x 10^3 V m^{-1} electric field difference in between each electrode to electrode gap to all other gaps. Thus the single pair of step-shaped electrodes was modified to have optimized electrode to electrode gaps of 10, 30, 50, 90, and 170 µm by adding 30 µm electrode to electrode gap in between 10 and 50 µm electrode to electrode gaps instead of the 130 µm electrode to electrode gap that it was in outlet 4. The 30 µm electrode to electrode gap was selected and added since the simulated electric field strength difference between 10 and 50 µm was 67.05 x 10^3 V m^{-1}, therefore adding one more electrode to electrode gap of 30 µm that has electric field differences of 45.75 x 10^3 and 21.31 x 10^3 m^{-1} to electrode to electrode gaps of 10 and 50 µm, respectively, it could be sufficient to have higher discrimination results and lower the overall classification error.

In this optimization process, different parameters were kept fixed, namely the microfluidic channel height and width, the YEPD medium conductivity, and the applied signal. Consequently, yeast cell suspended in YEPD medium have been retested and detected using the modified single pair of impedance electrodes that has five different

electrode to electrode gaps (10, 30, 50, 90, and 170 µm). Figure 18A shows a scatter plot of the detected impedance amplitude peak height and width using the modified single pair of electrodes.

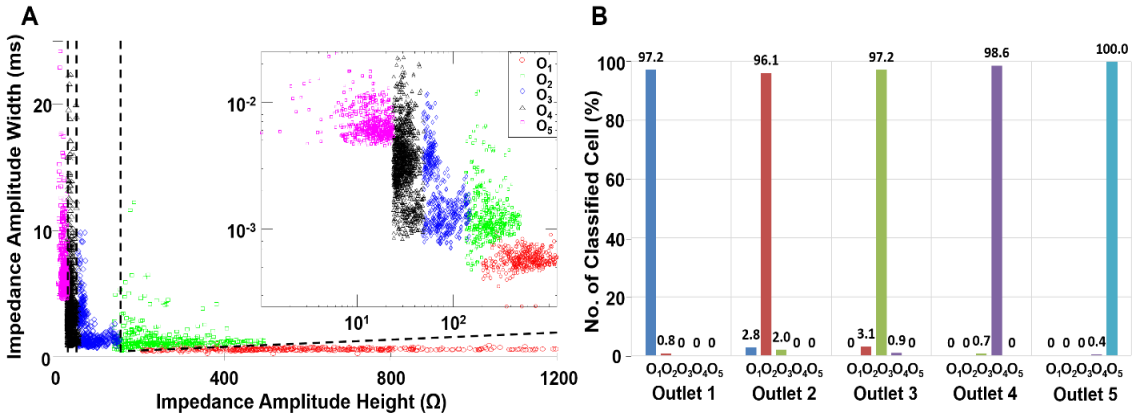

Figure 18. The classification results of the detected impedance signals of cells passing by five different outlets at five different optimized electrode to electrode gaps. (A) An impedance scatter plot for yeast cells flowing through five different outlets and showing the measured impedance peak amplitude height and width using a single pair of step-shaped electrodes that has five different optimized electrode to electrode gaps (10, 30, 50, 90, and 170 µm). From outlet 1 (O_1) to outlet 5 (O_5), the detection electrode to electrode gap were increased resulting in increasing in the impedance peak width and decreasing in the impedance peak height. The annotated four different straight line thresholds classify the detected events to 5 different colored groups. (B) The bar graph that shows the percentages of detected cells at each outlet were represented based on the selected manual linear thresholds that used to discriminate between the outlets. (C) and (D) showing the scatter plot of the measured impedance amplitude peak height and width that include the decision threshold boundaries for both Linear Discriminant Analysis and Quadratic Discriminant Analysis, respectively. Also the misclassification results using LDA and QDA by considering both methods have been calculated and tabulated.

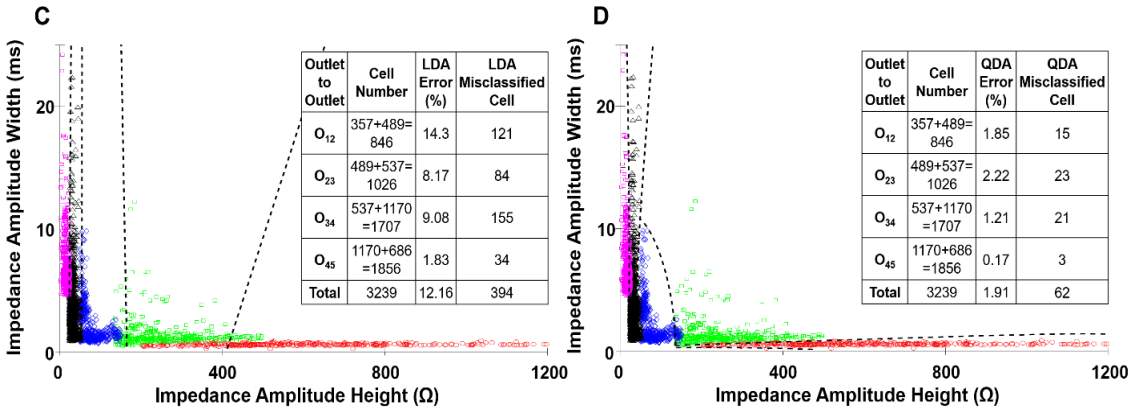

Figure 18. Continued.

For quantification, the three different classification methods were reutilized on the new detected data. By using manual linear threshold method, the decision boundaries were selected as mentioned before to maximize the classification in between each subset of data from each outlet to other subsets of data from other outlets (Figure 18A). Based on these selected threshold lines, 96.1% of cells were correctly classified as outlet 2 that has electrode to electrode gap of 30 µm, also all others outlets showed higher classification results, resulting in an overall classification error of 1.85% or 60 misclassified cells of total 3239 detected cells (Figure 18B). Furthermore LDA and QDA methods using the two previously mentioned approaches were performed. When LDA method was applied using two subsets of data approach, it showed low misclassification error of 1.83% in between outlets 4 and 5 (O_{45}) that have 90 and 170 µm electrode to electrode gaps, respectively, showing higher performance in the classification results in between outlets 4 and 5 in comparison to the previous experiment results of O_{45} as shown in Figure 18C and Figure 17C. However high misclassification errors in between outlets 1 and 2 (O_{12}),

2 and 3 (O_{23}), as well as 3 and 4 (O_{34}) were observed of more than 8.17% classification error. In contrast, when QDA method was applied using two subsets of data approach, 2.22% is the highest classification error in between outlets 2 and 3 (O_{23}) was successfully obtained, showing significant classification results of total 1.91% or 62 misclassified cells from the overall training data (Figure 18D). In addition LDA method was implemented using all five subsets of data approach; presenting high overall classification error of 41.34%, however much lower overall classification error of 1.98% when QDA method was utilized.

Multiple classification methods were compared using different approaches since there is no one classification method will lead to the best results in all situations. Also it was important to improve the precision of the developed detection electrodes by understanding the detection sensitivities and differences in between each outlet to other outlets when a single pair of impedance electrodes was used. Therefore, when the optimized single pair of step-shaped electrodes of 10, 30, 50, 90, and 170 μm electrode to electrode gaps was compared to the previous single pair of electrodes that has 10, 50, 90, 130, and 170 μm electrode to electrode gaps, higher classification precision in between each outlet to other outlets have been successfully obtained when manual linear threshold and QDA classification methods were used.

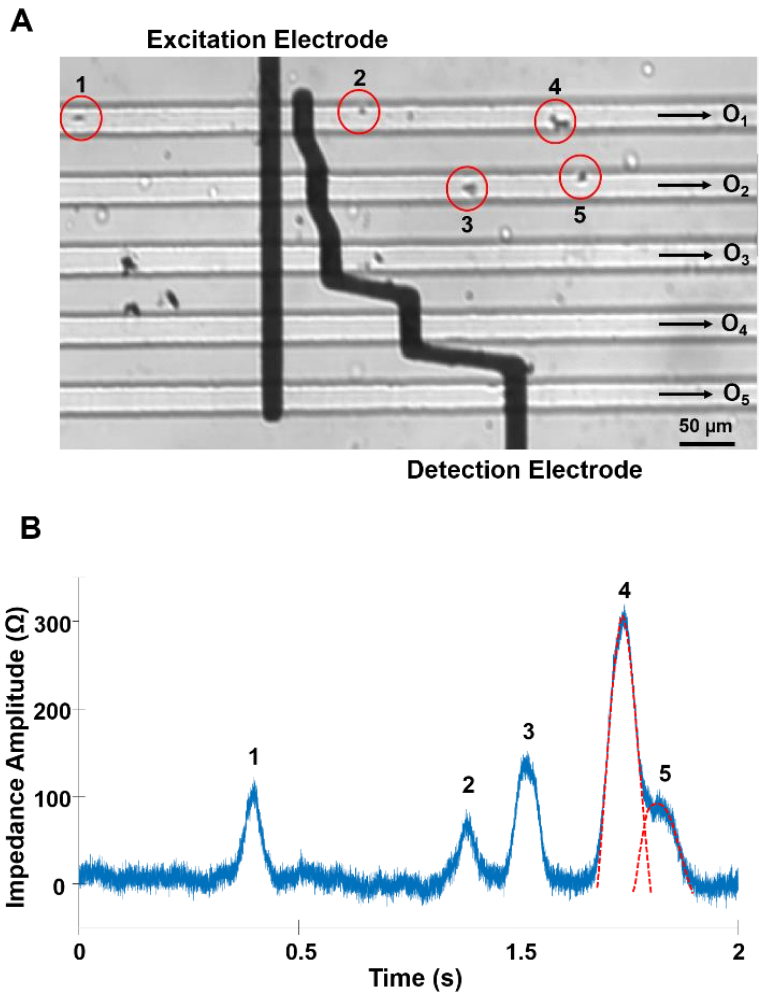

Figure 19. The detection of multiple cells passing by the detection electrodes at different outlets simultaneously. (A) Image of multiple cells passing through different detection regions within different outlets simultaneously. (B) Measured impedance signal of multiple cells passing through outlets 1 and 2 at the same time.

More characterizations were performed to show the capabilities of the developed multioutlet microsystem using a single pair of impedance electrodes in detecting and discriminating multiple cells passing through different detection regions at different outlets simultaneously (Figure 19A). Therefore yeast cells of non-homogenous sizes flowed through different outlets simultaneously, resulting in overlap impedance peak

signals as clearly illustrated in peaks 4 and 5 (Figure 19B). Therefore overlap peak signals were distinguished and discriminated from each other's using straightforward signal processing techniques, consequently the overall throughput could be dramatically increased even though different sorted cells passed through the detection electrodes at different outlets at the same time. This shows the effeteness of the developed microsystem as well as the perfectness of using both height and width parameters of the detected impedance peak signals for not only cell counting at each microfluidic outlet channel, but also for classifying and discriminating between the overlap peak signals of multiple sorted/separated cells and particles that flow-through the detection channels at different outlets simultaneously.

3.4. Conclusion

To conclude, we have developed a novel label-free and low-cost cells separation and sorting quantification technique using a single pair of step-shaped impedance electrodes that has the capabilities for detecting, discriminating and quantifying the separated/sorted cells that flow through multiple microfluidic outlet channels. Using the acquired impedance amplitude peak signal properties (height and width), a suspension containing polystyrene particles were initially assessed to evaluate the detection signals of different electrode to electrode gaps, confirming that different electrode to electrode gaps successfully resulted in different impedance amplitude peak heights and widths. We found that the simulated electric field strength and the detected impedance amplitude peak height and width were proportional to the increment of the electrode to electrode gap. Therefore two different pairs of impedance electrodes that have two different five electrode to

electrode gaps were tested and compared to detect suspended yeast cells flowed through five different outlet microchannels. To quantify the performance of the cells detection and counting using a single pair of electrodes, three different classification methods were utilized, showing that the lowest overall misclassification error of 1.85% can be successfully achieved when the electrode to electrode gaps in the developed single pair of electrodes were optimized to have 10, 30, 50, 90, and 170 μm electrode to electrode gaps. The future work can successfully involves in integrating our cell/particle counting detection scheme to range of passive or active sorting and separation methods, which could overcome the traditional techniques that have been suffered from either cell losses during the collecting and handling process for off-chip cell counting and analysis, unknown markers, or expensive instruments. Furthermore since the largest electrode to electrode gap of 170 μm has been demonstrated a maximum of 16.3 x 10^3 V m^{-1} electric field strength and has been successfully utilized for cell detecting and counting, and the minimum electrode to electrode gap of 10 μm showed high electric field strength of 114.08 x 10^3 V m^{-1}, five more other electrode to electrode gaps can be used that could have more than 15 x 10^3 V m^{-1} electric field strength difference, which will allow the sorting and separation microsystems to have up to seven microfluidic outlet channels enabling successful on-chip cell counting and quantification using a single pair of impedance electrodes.

CHAPTER IV

DETECTION AND ANALYSIS OF CELLS ENCAPSULATED WITHIN A DROPLET USING IMPEDANCE SPECTROSCOPY MICROSYSTEMS

4.1. Motivation

A high-throughput impedance detection spectroscopy system has been developed and fabricated to detect and discriminate droplet content either for discriminating different medium or detecting the characterizing the cell concentration within droplet. The developed device integrates single-ended connection based electrodes which was developed with a gradually reduced in the geometry of the detection region as well as the electrodes dimensions and gaps in order to realize high sensitive sensing that could discriminate and distinguish between different cell concentrations encapsulated in droplet. Therefore, an impedance spectroscopy-based microfluidic system was developed to detect and distinguish up to a single cell encapsulated in droplet. Also, this developed microsystem can detect and discriminate among different cells within a single droplet as well as different size of cells within droplets.

4.2. Design Principle

A high-throughput cells encapsulated in droplet based impedance spectroscopy microsystem was designed based on a single-ended electrode measurement. The platform is consisting of two main parts: a) the microfluidic channel and b) the sensing electrodes patterned on glass slides as illustrated in Figure 20.

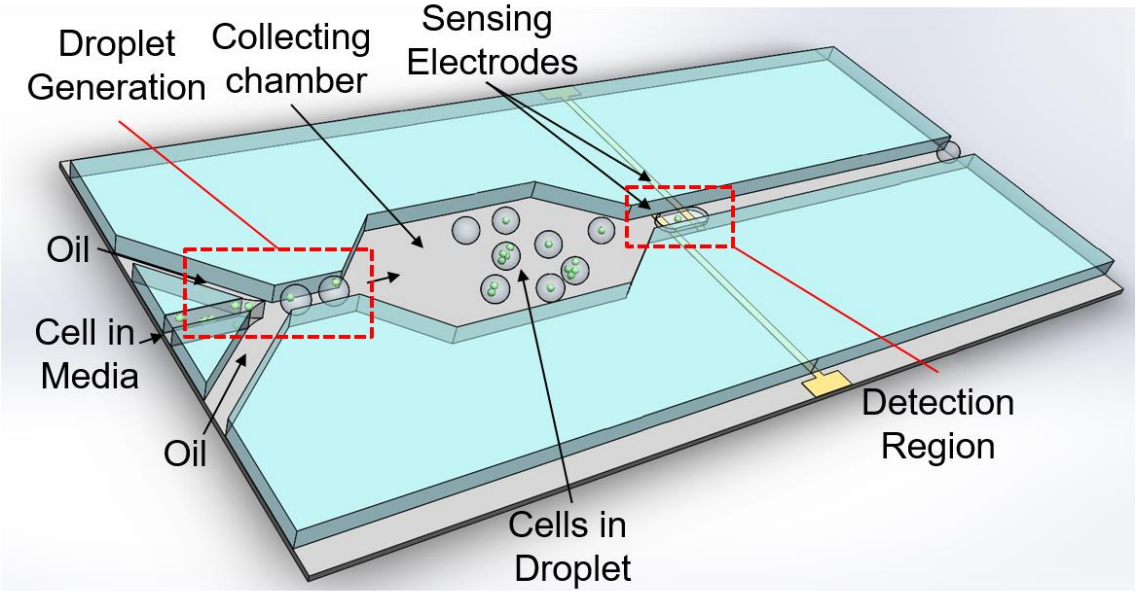

Figure 20. Top view schematic of the developed high-throughput droplet microfluidic-based impedance spectroscopy platform components. In this illustration, droplet generation, collecting chamber, and detection region are presented.

The PDMS microfluidic channel layer involves of two main sections: a flow-focusing droplet generation and droplets detection sections. Each of these section are explained in further details in the following sections. Micro-electrodes were patterned on (2 X 3 in) glass slide to perform as an electrical stimulating and sensing of the developed platform. The design of each of these parts are explained in more details in the following sections.

4.2.1. Droplets-Based Microfluidics Generation

The microdroplets are generated using a flow-focusing droplet generator with three inlet channels as illustrated in Figure 21. One inlet was split to two continuous-flow channels with 45 µm width are used to precisely control and focus the generated droplets. Another microchannel is added with 30 µm is used to carry the target fluid such as deionized water to form water droplets in oil. The flow-focusing microfluidics generator has orifice with 50 µm and 15 µm width and height, respectively. The two continuous flow channels are tilted with 120º to help reducing the effect of the back pressure at low flow rates as well as more focusing capability and droplets stability. Also, by using this developed design, diffusion between the carrier oil will reduce and consequently prevent droplets breaking effects at high flow rates for successful high-throughput experiments. The fluids are driven using syringe pumps whereas two syringe pump are used to generate stable micro-sized droplets ranging from 25 µm up 150 µm in diameter. In the detection channel, the microfluidic width was designed to be 60 µm. Therefore, the microfluidic channel height is 15 µm to therefore have detection channel dimensions of (15 µm × 60 µm).

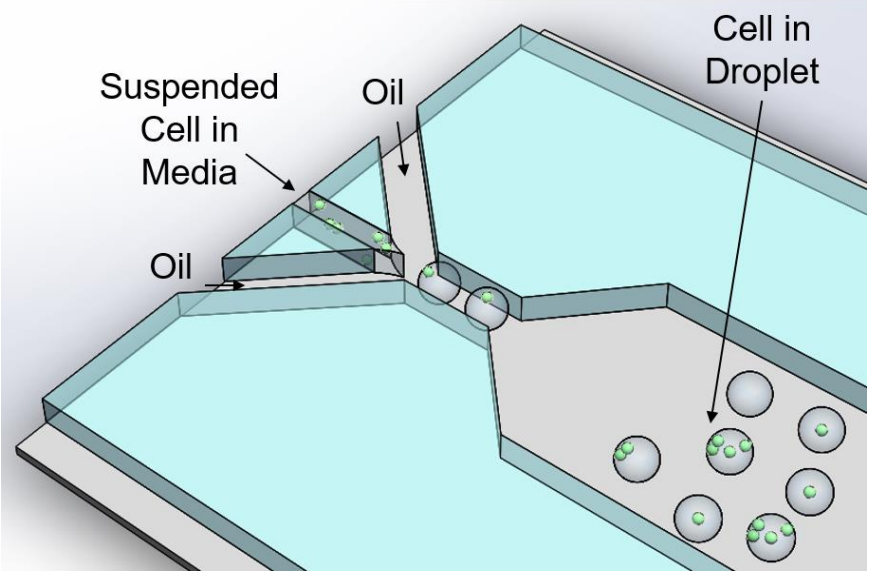

Figure 21. The flow-focusing droplet generation region.

4.2.2. Planar Electrodes Detection

Planar detector using gold patterned electrodes are employed to detect and characterize the droplets passing a pair of electrodes. The electrodes were gradually optimized in order to get more sensitivity and accuracy. The gold plated electrodes pattern use to measure the impedance change when any droplet passing by the two electrodes. The width and gap between the electrodes are precisely designed to easily detect and discriminate between the droplets contents after designing and experimentally testing different widths and gaps. The planar electrodes at the bottom of the microfluidic channels as shown in Figure 22 generate electric fields based on the applied excitation AC voltage.

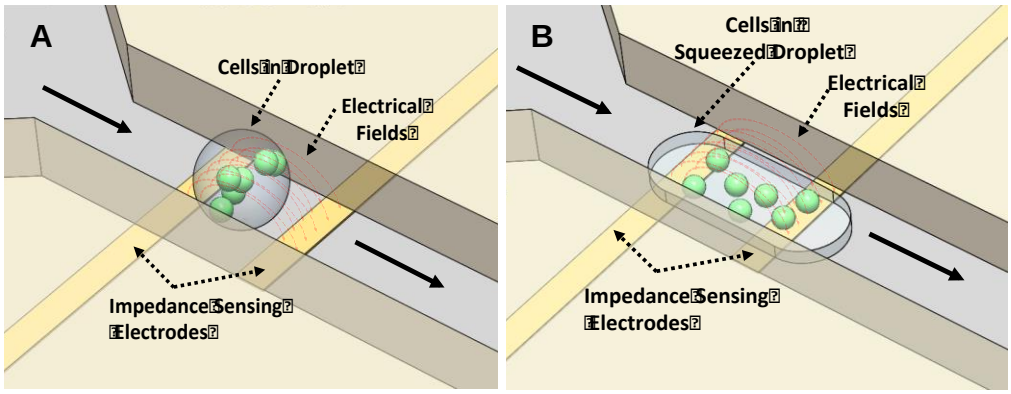

Figure 22. Electrodes detection methods of flowed cells encapsulated in droplets. (A) Illustration of cell encapsulated in small droplet passing the sensing region of the developed impedance spectroscopy platform, and (B) represent cell in squeezed droplet as an alternative impedance detection method for potentially higher sensitivity. Both representations illustrate the electric field lines between the pair of electrodes.

This opposing electrodes design as shown in Figure 22 reduces the electric field crosstalk effects that could by using the parallel electrodes. Therefore, the opposing electrodes design is used and precisely aligned inside the microfluidic channel to highly confine the electric field within the detection region; thus, the dielectric measurements are expected to show more sensitivity and accuracy as a result of this accurate design. The gold patterned electrodes with 10 µm width and 15 µm gap are selected for this conducting research, so the total volume for this detection region is $35 \times 15 \times 60\ \mu m^3$ or more based on the intensity of the applied AC voltage. This planar electrodes design was developed to overcome repeatability and complexity of fabrication techniques to assemble very thin microfluidic channel in between top and bottom patterned electrodes slides. This type of fabrications need more methanol bonding procedures for each electrodes layer for electrodes alignments. The thickness of the glass slide comparing to the microfluidic

channel thickness is massive and significantly generate poor bonding after the second glass slide bonding.

4.3. Devices Fabrication

The developed cell concentration in droplet-based impedance spectroscopy platform is composed of two layers, a single microfluidic channel layer and a glass slide that comprises of gold patterned electrodes. By using soft lithography, the microfluidic channel layer was fabricated using polymimethylsiloxane (PDMS, Sylgard 184, Dow Corning). Initially the master mold was fabricated with the standard photolithography techniques starting from piranha cleaning the silicon wafer. Piranha cleaning is a mixture of sulfuric acid and hydrogen peroxide. The hydrogen peroxide must be added to the acid slowly, while that time the temperature of this mixture will be increased; therefore, they should be carefully handled and used. Thereafter, the loaded wafers on the Teflon boat will be immerse after wearing the complete protective clothing in the piranha solution for 10 min, then the boat will be immersed in the preheated DI water at 95 ºC for 3 min or more. After that, the room temperature DI water will be used as the last wet cleaning step to double check of removing any remaining acids on the wafers before touch them for another 3 min or more. During these three immersion steps, the boat should be agitated slowly. Then the silicon wafers were dried using nitrogen gun to remove any remaining liquid on the wafers. This step must be done to remove any contamination that is on the wafers.

Thereafter, the target height of the microfluidic channel was 15 µm; therefore, to achieve that, the negative photoresist (SU-8 2015) was spin coated at two different speed, 500 rpm for 10 s to uniform the photoresist on the wafer, then 2800 rpm for 30 s to exactly yield 15 µm photoresist thickness. This height was realized after performing and comparing three different speed, 2700, 2800, and 2900 rpm. Then, the wafer was soft baked using a hotplate for 30 min at 60 ºC and 4 min at 90 ºC. Then, the wafer was exposed to UV light (Karl Suss MA6 Mask Aligner) using dark field mask at dosage of 180 mJ/cm^2 due to this selected 15 µm photoresist thickness.

A hard baking step was immediately performed to cross link the exposed photoresist by baking the wafers at 90 ºC for 4 min. The dark field mask with negative photoresist makes the non-exposed area be soluble during the development process. Microposit EBR 10-A remover is used to remove the non-exposed photoresist and therefore the microfluidic patterned channels were realized by immersing the wafer inside the developer until the non-exposed photoresist completely removed, after that it rinsed with IPA and dried with nitrogen. Thereafter microfluidic PDMS layer was prepared by mixing pre-polymer and curing agent at weight ratio of 10:1, respectively and degassed using a vacuum chamber for 30 min. then the microfluidic channel layer was casted to form 0.5 cm height by mixing 20 mg pre-polymer and 2 mg curing agent. Finally, the PDMS mold was cured for 2 hr at 80 ºC.

The electrodes were fabricated using standard photolithography techniques. At first, glass slides were cleaned using the piranha cleaning process. A uniform of gold (Au) layer was deposited on a glass slide substrates using one of evaporation method of thickness

2000 Å. Before that, another layer of titanium (Ti) was deposited as an adhesion layer of thickness 200 Å. Gold metal is widely used in biomedical application due to its nontoxic properties and high electrical conductivity comparing to many other metals. Au/Ti films were deposited using E-beam evaporation equipment (Lesker PVD 75 Ebeam Evaporator). Then, a positive photoresist, S1818, was spin coated at 3500 rpm for 30 s onto a gold coated slide, soft baked at 95 ºC for 10min, exposed at 85.25 mJ/cm^2, hard baked at 110 ºC for 2 min, and developed for 30 s using MF319 to remove the exposed area by using a clear field mask. Thereafter, the glass slides were immersed in gold Au etchant (Type TFA, Transene Company Inc.) to remove the exposed area, then the Ti was etched using Ti etchant (HF:H2O at 1:300). After that, the remaining photoresist was removed using acetone. Finally, the gold patterned glass slides were cleaned using DI water and dried by N2 gas.

Before bonding the microfluidic channel to the patterned glass slide, a passivation layer is employed to prevent any reaction could happen between the electrodes and samples. Therefore, a silicon oxide thin film layer was deposited using Plasma-enhanced chemical vapor deposition (PECVD). Then, the PDMS microfluidic channel casting mold was aligned and bonded on glass slide after treating the two parts with oxygen plasma chamber (100 mTorr at 100 W) for 1.5 min. The resulted fabricated device as shown in Figure 23. However, due to hydrophobicity and droplet hanging issue, 200 ºC hotplate for 4 hour was used to solve this issue after bonding the microfluidic layer to the patterned electrode. Finally SMA connectors were soldered using flux to enhance the soldering efficiency.

Figure 23. The fabricated microfluidic impedance spectroscopy platform integrated with SMA connectors.

4.4. Detection and Characterization of Yeast Cells in Droplets

4.4.1. YEPD Dilution Detection Sensitivity Effect

Microfluidic based impedance spectroscopy microsystems have been wildly used to detect and characterize different types of cell in different medium, and it can shows very successful and significant results. However, for cell encapsulated in droplet, the resulted detected electrical impedance for cell encapsulated in droplet surrounded by carrier (oil) will be more complex and resulted more noise. Therefore, different research works represented how changing the medium conductivity can help the impedance spectroscopy detection and sensitivity [98, 104]. As mentioned before, for cell in droplet surrounded by oil which results three different mediums that the impedance spectroscopy microsystem will measure (cell, medium, and oil); therefore, this will result more complex electrical impedance signal that might can hardly detect the encapsulated cells. Moreover, lower the conductivity by adjusting the medium might not be suitable for all different cells and applications. Therefore cell culture experiments using the adjusted medium should be considered and need to be evaluated.

4.4.2. Yeast Cell Division in Different YEPD Medium Dilutions

Yeast cell division cycle experiment was conducted and performed at different YEPD dilutions. The YEPD medium was diluted to result 10 different YEPD concentrations (100-10 %) by diluting the original YEPD with DI water. Yeast cell was prepared and loaded to these 10 YEPD mediums and cultured for 18 hr using 24 well plate. A picture for each well was taken using Zeiss microscope and set to 15 min capture interval time.

As shown in Figure 24 shows successful cell division number comparing among 100, 80, 50, and 10 % of YEPD medium between 0 and 6 hr. After 18 hr of culture, a huge number of yeast cell was shown in all YEPD dilutions which could not be used to visually discriminate among the 10 different cases.

Therefore a hemocytometer for cell counting was used before and after the yeast cell culture for all 10 YEPD medium dilutions. As shown in Figure 25, yeast cell division cycle for 10 different YEPD dilutions (10-100 %) after 18 hr was different. Using 10 % of YEPD, 156 yeast cell division cycles was shown; however, 10 times higher yeast cell division cycles of 1580 was shown when using 90 % of YEPD medium.

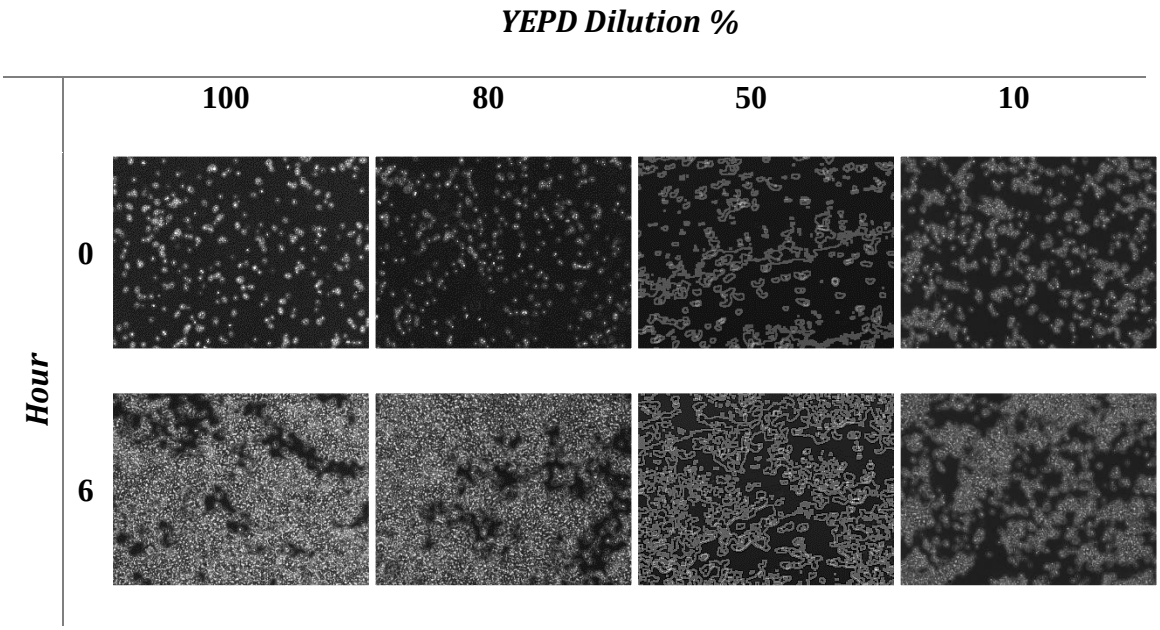

Figure 24. Yeast cell division using 100, 80, 50, and 10 % of YEPD mediums at 0 and 6 hr.

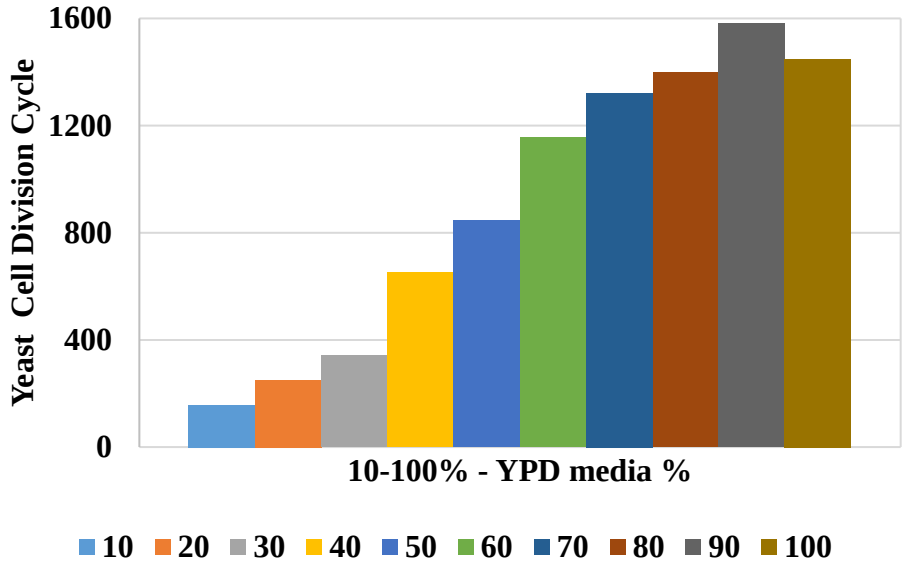

Figure 25. Yeast cell division rate for yeast cell suspended in 10 different YEPD diluted mediums (10-100 %).

Also, around 40% difference between 50 and 100 % YEPD medium in yeast cell division cycles was apparent. Overall yeast cell division cycle was gradually increased from 10 to 100 % of YEPD medium.

4.4.3. YEPD Medium Conductivity Measurements

Dilution of YEPD medium using DI water will reduce the electrical conductivity to different level which it can improve the detection sensitivity for cell encapsulated in droplet. The original YEPD medium has electrical conductivity of 0.1916 S m^{-1} as shown in Figure 26B, while at 10 % of YEPD medium is 0.0231 S m^{-1}. Also the YEPD medium gradually change their medium color as represented in Figure 26A.

The lower YEPD medium (10 % dilution) is still higher than the low conductivity medium (LC media of conductivity: 0.009 S m^{-1}) that commonly used in other impedance detection microsystems [98].

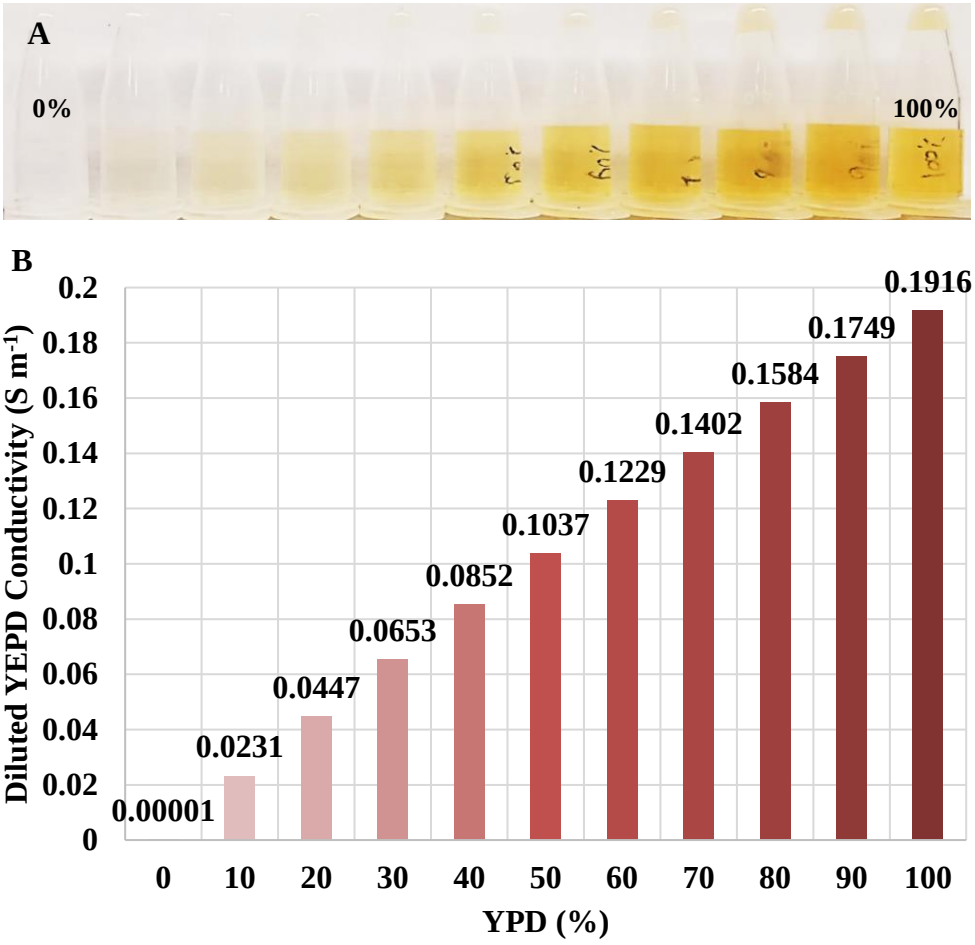

Figure 26. YEPD medium at 10 different dilutions (0-100) %. (A) Shows the gradient of YEPD medium color, and (B) shows the measured electrical conductivity of YEPD diluted mediums from 0 to 100%.

4.4.4. Experimental Setups

For device characterization, yeast cell was selected due to their most commonly size and division cycle. Yeast cells were suspended in different YEPD dilution and experimentally tested using the developed microsystem. By tuning the flow rates of the two inlets between the oil and suspended cell in medium, different droplet size were generated. Due to the channel height, the droplet were squeezed and elongated. Therefore,

all encapsulated cell will be distributed within the microdroplet, thus the distance between the surface electrodes and encapsulated yeast cells will be minimized. Therefore, the detection sensitivity will be increased.

Yeast cell encapsulated in droplet detection was performed by applying a peak excitation signal of 7 V at 7 MHz and measuring the output signal using a commercial 2-channel impedance analyzer with a current amplifier (HF2IS and HF2TA). This optimal voltage and frequency condition was identified by scanning a broad voltage (2 - 8 V) and frequency (10 kHz - 50 MHz) range, and selecting the one having the best signal-to-noise ratio of the detected signal. The cell in medium were introduced to the flow focusing microfluidic channel to generate cell encapsulated in droplet as shown in Figure 27(A-E) as they are passing the detection channel. Due to the droplet size and channel height, the droplets are squeezed within the detection channel for higher detection sensitivity.

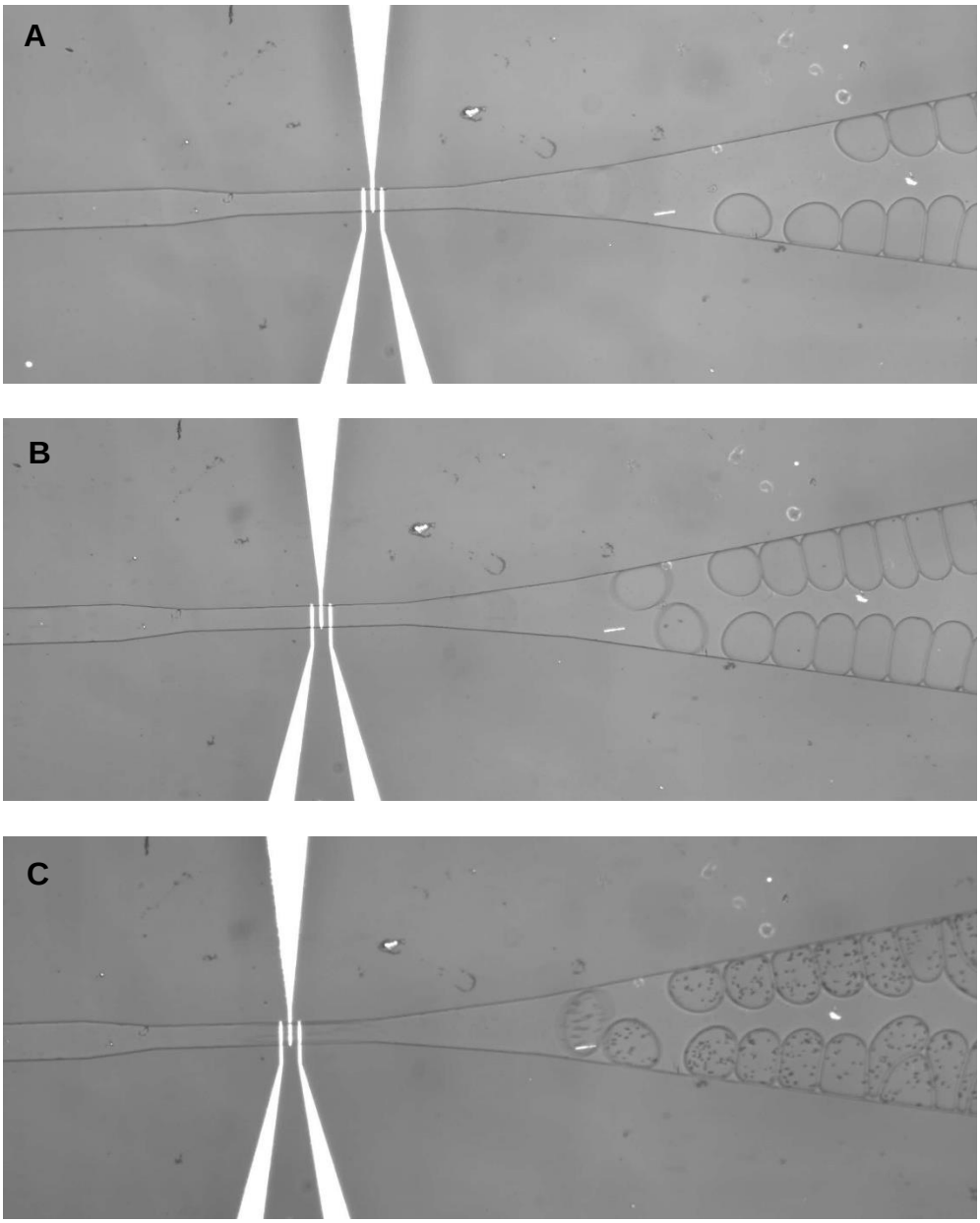

Figure 27. Yeast cells encapsulated in droplet at different ratios. (A-E) show successful encapsulation different number of cells in droplet.

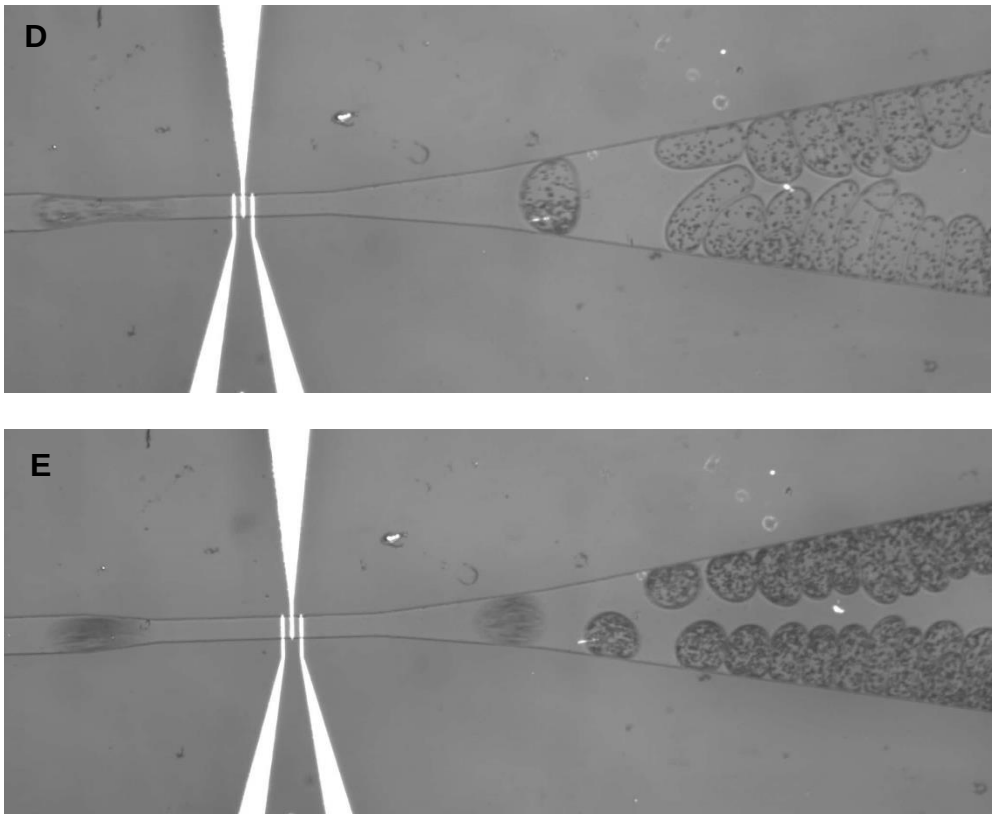

Figure 27. Continued.

The average droplet diameter was 80 µm based on adjusting the oil and YEPD medium flow rates to 15 and 1 µL/hr, respectively.

Data analysis was performed for the detected electrical impedance signal using MATLAB. A post-processing algorithm that performs baseline correction of the detected time-domain impedance signal for each of peak amplitude, phase, real, and imaginary impedance signal as well as peak height calculation were successfully performed.

4.4.5. Results and Discussion

We have characterized yeast cell encapsulated in droplet using the developed microsystem at height of 15 µm. At this height higher flow resistance can been shown due to back pressure effect within the microchannel. However, shallower channel can provide higher detection sensitivity due to close cell to detection electrodes can be observed from the detected impedance signal. Yeast cell cannot be vertically overlap more than two cells due to channel height due to the average yeast cell size of 8 µm. Yeast cells in droplets have been successfully tested and compared for three different YEPD diluted medium (100, 50, and 10 %).

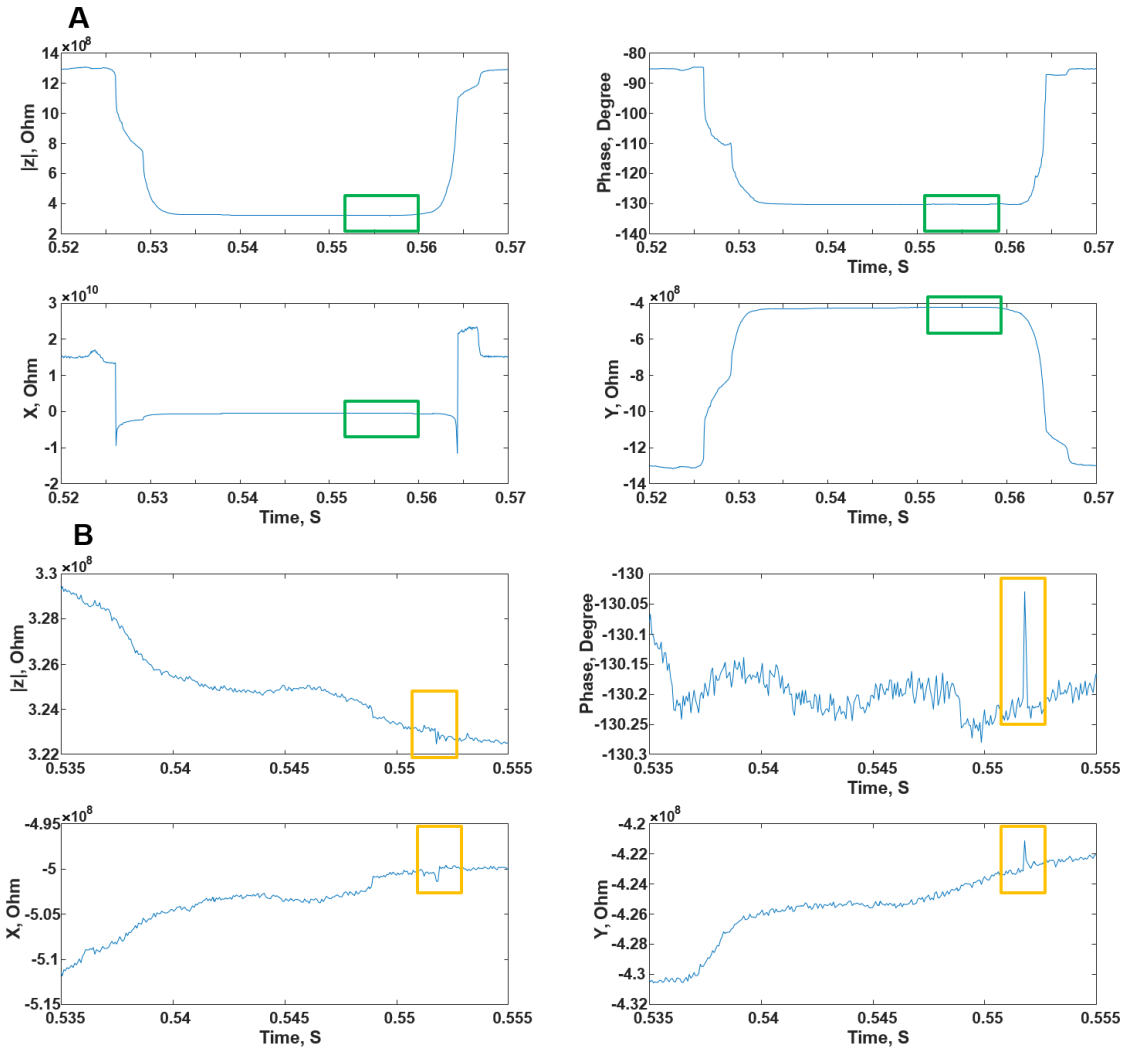

Figure 28. Detected electrical impedance of yeast cells in droplet using 100% YEPD medium. (A) Shows the one complete impedance signal drop once the YEPD medium droplet passes the detecting electrodes, and (B) Shows a zoom in of detected yeast cell encapsulate in droplet. Amplitude, phase, real, and imaginary electrical impedance were analyzed.

From the detected electrical impedance signals, four different output signal were analyzed and used for this comparison. From the initial result as shown in Figure 28-Figure 30, the showed that clearly the detected peak impedance signal increases for the detected peak impedance signal by decreasing the YEPD medium ratio. However, the peak signal direction of detected yeast cell in droplet using 100 % YEPD medium were flipped over the another direction when 50 and 10 % YEPD mediums used for all four resulted data. Also, as shown in Figure 29 and Figure 30, the detected impedance signal was significantly improved comparing to cell in droplet using 100 % YEPD medium. The sensitivity of the detected peak of the amplitude impedance signal in all three dilutions were successfully detected and clearly shown potential increase in their peak values comparing to baseline noise when the YEPD medium dilutions decrease as depicted in Figure 29 and Figure 30, respectively.

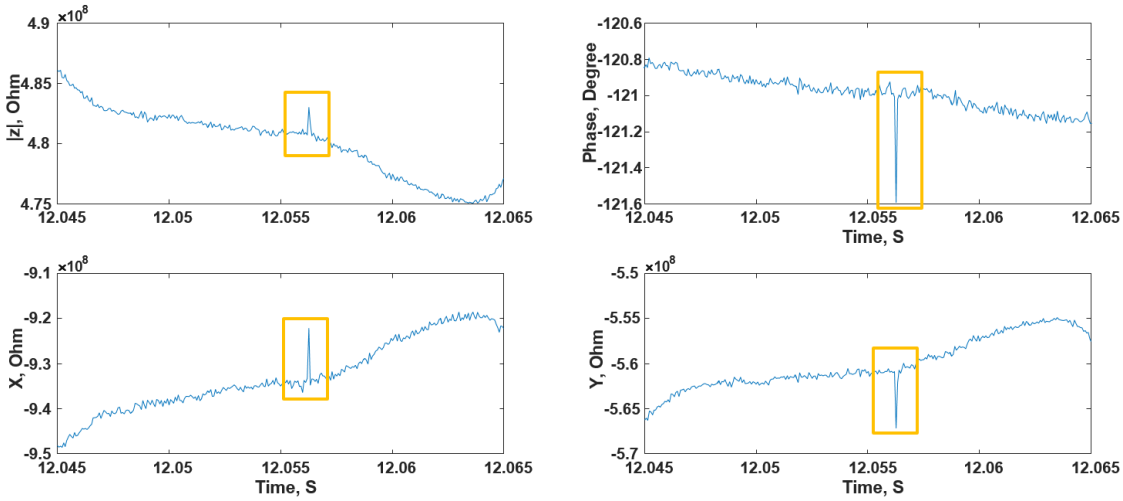

Figure 29. Detection of yeast cells encapsulated in droplets using 50 % YEPD medium.

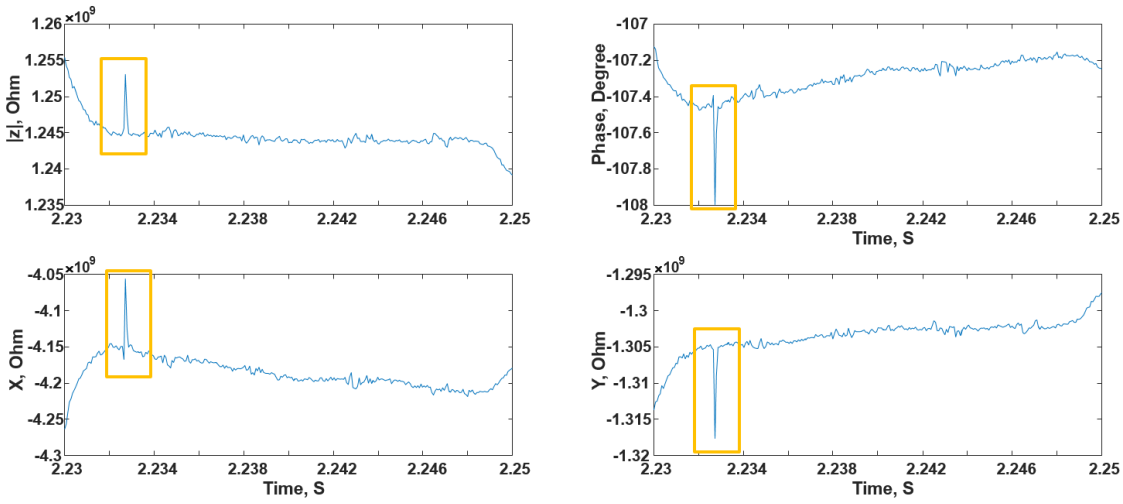

Figure 30. Detection of yeast cells encapsulated in droplets using 10 % YEPD medium.

As mentioned before, significant change in the detected peak of cell in droplet using different YEPD medium dilutions were tested and compared. The average amplitude, real, and imaginary parts of the detected impedance signals in Figure 31 shown significant gradually decreasing when the YEPD medium percentages increase. However, the average imaginary impedance signal (Y) for all three dilutions shown high standard deviations comparing to the average amplitude (|Z|) and real (X) parts of the impedance signal. From another side, higher average detected peaks were shown in the detected phase of the impedance signal when the 100 % YEPD medium was used comparing to 50 % YEPD medium.

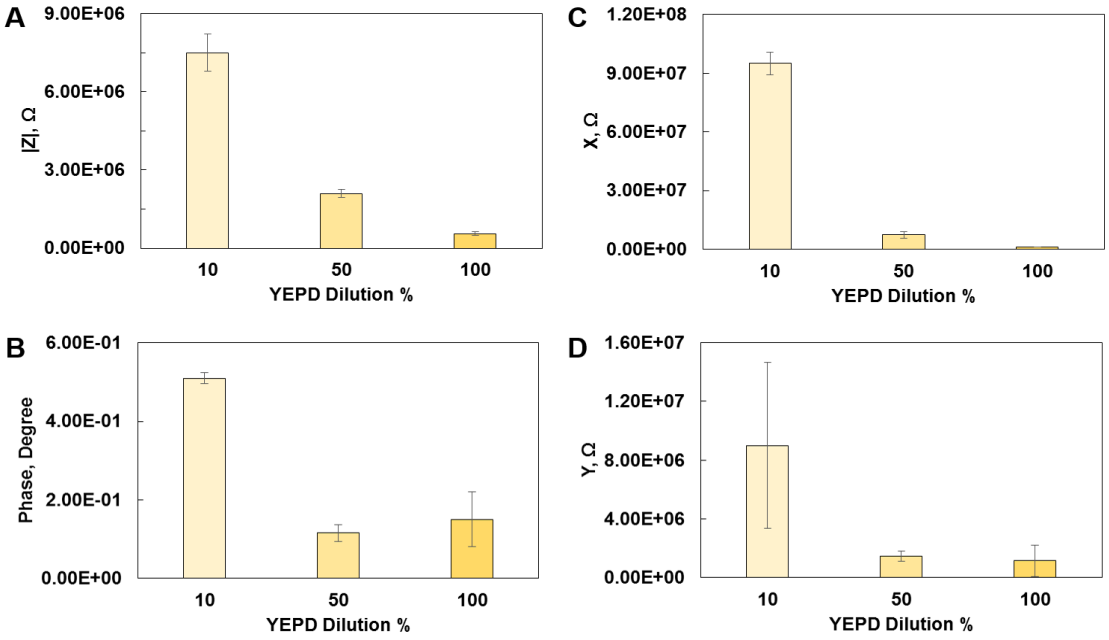

Figure 31. Comparison of average detected electrical impedance peaks of yeast cells encapsulated in droplets. At three different diluted YEPD mediums, the acquired electrical impedance signal as shown in (A) Amplitude, (B) Phase, (C) Real, and (D) Imaginary electrical impedance.

Overall significant results were shown when the detected impedance signals were analyzed using the four different parameters that mentioned before. Amplitude and real parts of the detected electrical impedance signal were shown higher sensitivity and lower standard deviations, which they can more useful tools for many cells screening applications.

4.5. Discrimination of Droplets Containing a Single Cultured Filamentous Fungal Cell Using Impedance Spectroscopy

4.5.1. Motivation

Fungi are eukaryotic organisms that can cause diseases to plants, animals and humans. To characterize the function of a gene of interest in fungi, gene knockout mutants are most commonly used to provide comparative phenotypic analyses against the wild-type progenitor [105]. The identification of a 'true' gene knockout mutant requires screening of a large number of transformants. In the presence of selective pressure (e.g. antifungal drugs), non-transformed fungal spores will not survive and stall at single-spore stage, while only successfully transformed spores will rapidly grow into filamentous hyphae. Thus, by discriminating fungal growth phenotype, the identification of fungal knockout mutants can be achieved. Microdroplet-based screening systems have been developed to perform high-throughput screening using fluorescent reporters [106]; however, fluorescent reporters for the fungi of interest do not always exist. Recently, label-free impedance based identification of cells in droplets has been demonstrated [98]. However, at present, no attempts have been made to detect and identify filamentous fungal cells in droplets label-free. Here, for the first time, we used impedance spectroscopy to detect and distinguish fungal filaments cultured from single fungal spores inside droplets.

4.5.2. Designs and Experimental Setups

The developed droplet microfluidics impedance spectroscopy-based system that has been used to successfully used to characterize the yeast cells concentration within droplets

was reutilized to characterize and discriminate the single fungi cell encapsulated in droplet. Also the developed droplet microfluidic impedance spectroscopy-based system was refabricated with height of 8.5 μm. This device was compared to the previous developed device of 15 μm height to evaluate the detection sensitivity improvement when all fungal spores were enforced to be more close to the sensing electrodes, assuming that the shallow channel can minimizing the distance between the surface electrodes and encapsulated fungal cells when the droplet will be more squeezed, resulting in increasing in the sensitivity.

As mentioned in the previous yeast cells culturing experiments at different diluted YEPD medium, the detection sensitivity can be affected the medium conductivity, therefore four different YEPD dilution medium (100, 80, 50 and 10 %) were tested and compared to validate the fungal spores growth rate in these four dilutions. Fungal spores were suspended in these four dilutions and cultured for 26 hr. Using Zeiss microscope (40x), images were taken for each well at different locations to insure that they have similar growth at each interval time.

Also initial characterization of fungal spores and fungal hyphae with different length detection using the developed platform (15 μm height) was performed to characterize the best applied AC voltage and frequency that could be used to discriminate among different lengths and shapes of cultured fungi cells in the flowing 100% YEPD media. Therefore different level of AC voltage (1-4 V) and frequencies (0.62, 1.5, 2.5, 25, and 29 MHz) were tested and compared to show how these two factors can dramatically affect the detection sensitivity.

Moreover, fungal spores and fungal hyphae of different lengths were suspended in 50% YEPD medium to test and compare the electrical impedance signal differences and how it can enhance the detection sensitivity comparing to 100% YEPD medium. Besides the two different microchannel height were tested and compared to find and use the best signal to noise ratio that could be utilized for this study. This experiment was conducted by applying 4 V AC excitation signal at 2.5 MHz using single-ended experimental mode.

Furthermore, using developed microsystem of 15 µm height, the optimal AC voltage and frequency for detecting and discriminating fungi cell within droplet were performed by scanning both of them to find the best signal to noise ratio that can use to discriminate between fungal spores and fungal hyphae. Due to multiple level of impedance change among fungal cell, YEPD medium, and oil, a change in the optimal frequency and AC voltage need to be slightly change. Therefore, the optimal voltage and frequency were 3 V AC and 29 MHz, which they were used in this experiment to detect and discriminate among various length of fungal cell. For this experiment, fungal spores were cultured in 14 hr and suspended in 50% YEPD medium (conductivity: 0.1037 S m^{-1}) for higher detection sensitivity and more significant discrimination. In this experiment, YEPD culture media was used and utilized instead of low-conductivity media (conductivity: 0.009 S m^{-1}) commonly used in other droplet-based impedance detection microsystems [98], as the droplet microfluidic system needs to support standard fungal cell culture within droplets for 10-24 hours

The excitation and detected signals were generated and recorded using the HF2IS impedance analyzer to detect the electrical impedance change of single spore/fungal

hyphae within a droplet, as demonstrated in Figure 32. As illustrated, different fungal cell's length or growth could show different peak signal with each droplet.

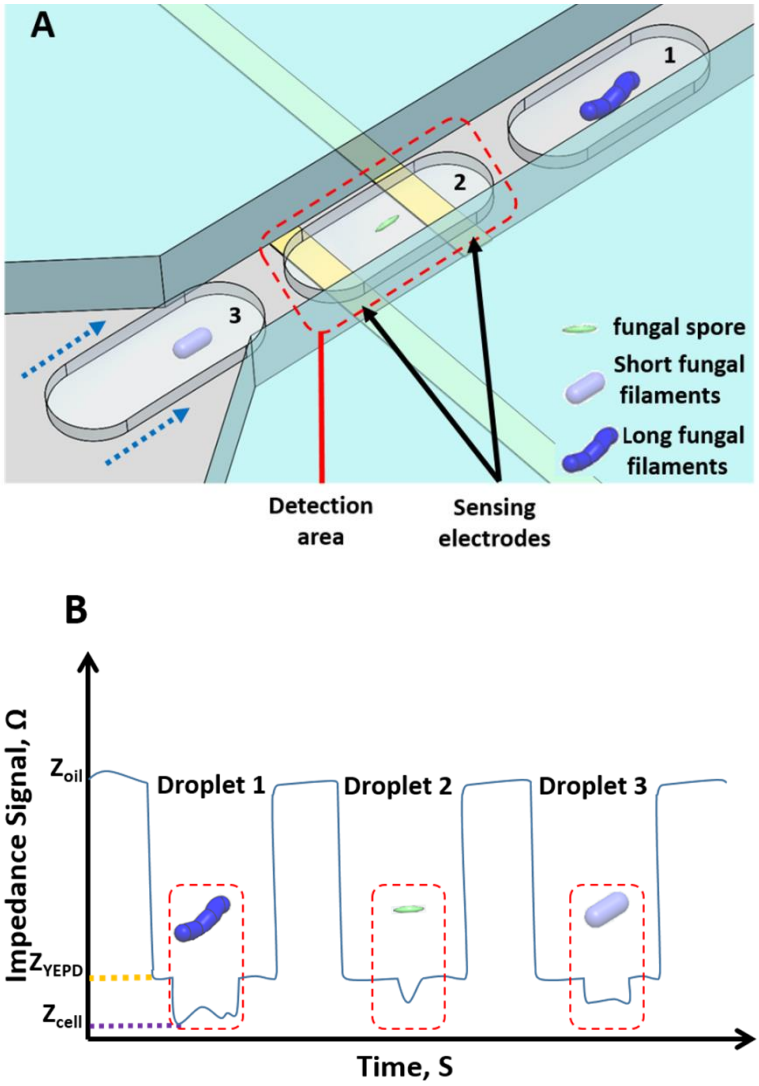

Figure 32. Detection of fungal cells encapsulated in droplets using impedance spectroscopy microsystem. (A) Illustration of the impedance detection system where droplets containing single fungal spore and fungal hyphae with different lengths pass through the impedance electrode pair. (B) Theoretical representation of impedance signal change.

4.5.3. Results and Discussion

Single fungal spores were cultured in 24 well plate and compared at 4 different YEPD dilution mediums as shown in Figure 33. After 5 hr culturing, the cells were started showing nonlinear growth, resulting in almost equal growth in all four medium condition. In all conditions, an average of 100 μm cell length were measured at different cells in between 5 to 10 hr culturing time. These results show that using diluted YEPD mediums could be used for fungal cell growth, which these diluted medium could help dramatically in enhancing the detection sensitivity for either detecting single fungal spores flowing in media or encapsulated in droplet as shown before in the yeast cell experiment.

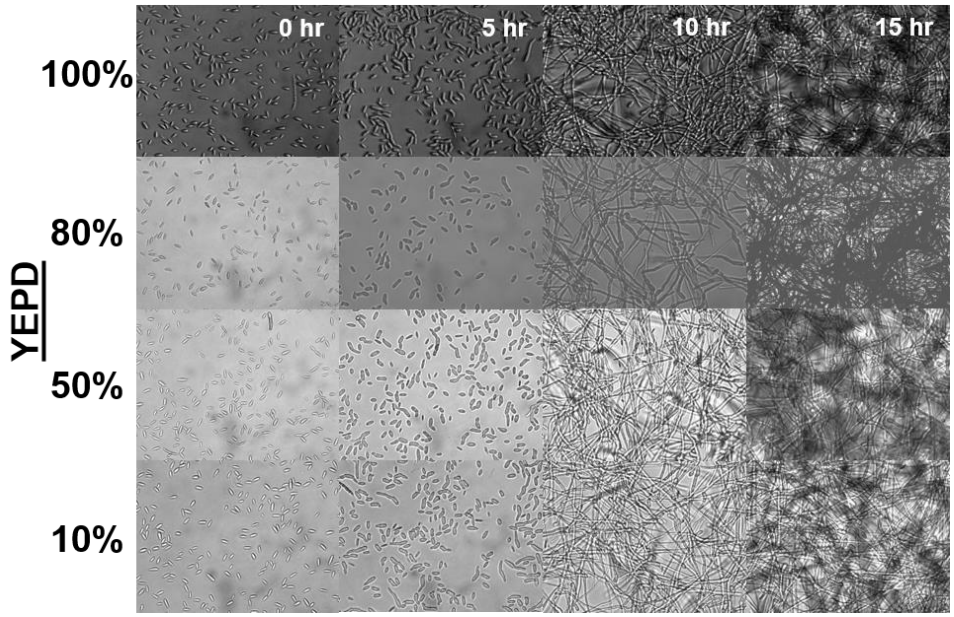

Figure 33. Fungi cell growth differences between 100, 80, 50 and 10% YEPD. Using Zeiss microscope at 40 x, images were captured at 15 min time interval, whereas 16 images were presented at 4 different time intervals (0, 5, 10, and 15 hr) at the four diluted mediums.

Characterizing fungal cells in medium only using the original YEPD dilution (100%), it showed that there was significant improvement in the detected impedance signal cell by changing the frequency level and fixing the applied excitation AC voltage to 4 V. As shown in Figure 34 to Figure 36, the detected amplitude impedance (|Z|) significantly improve their signal to noise ratio when the applied frequency was increased. However, the real impedance signal showed that the noise level was increased which result less signal to noise ratio comparing to lower applied frequencies.

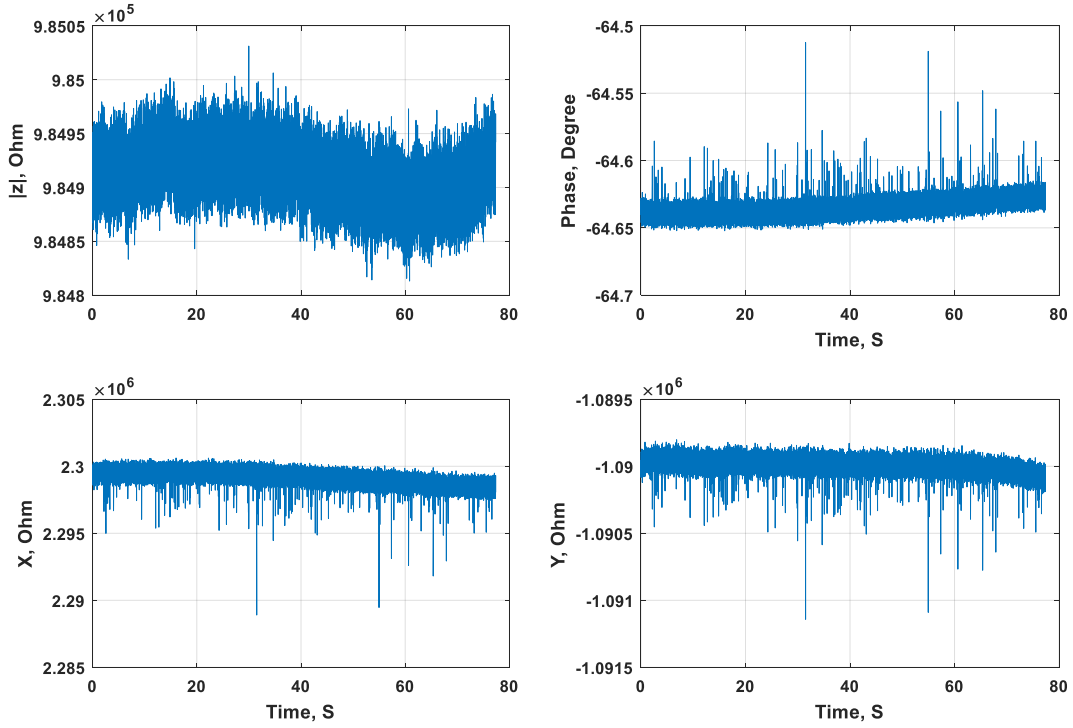

Figure 34. Preliminary results of detected fungal cell in 100 % YEPD medium at applied excitation signal of 4 V at 620 kHz.

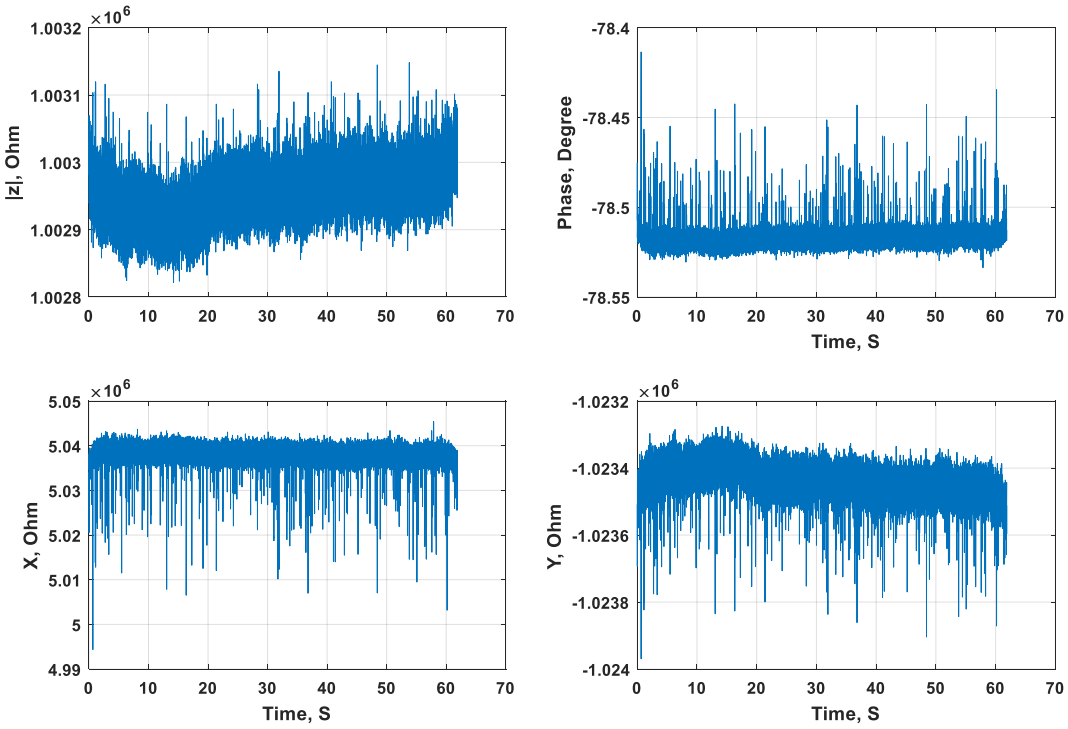

Figure 35. Detected fungal cells in 100 % YEPD medium at applied excitation signal of 4 V and 1.5 MHz.

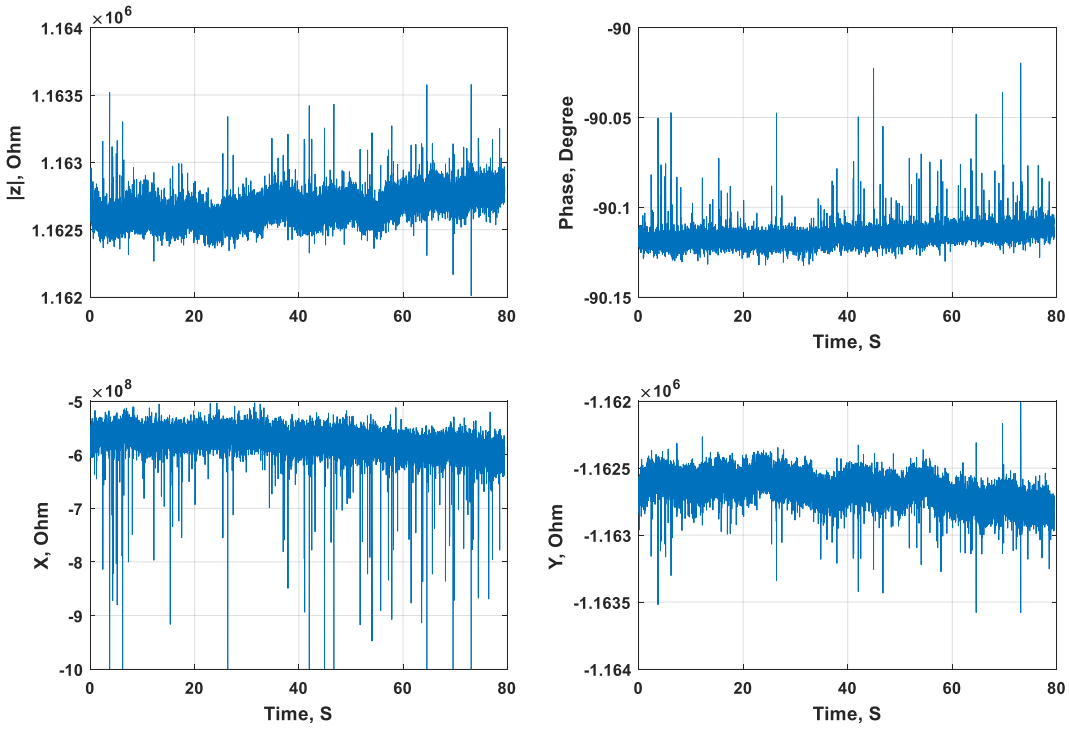

Figure 36. Detected fungal cells in 100 % YEPD medium at applied excitation signal of 4 V and 2.5 MHz.

Moreover, based on the previous successful results of the fungal cell growth at different diluted mediums, fungal spores were tested at 50% YEPD medium at higher frequency (25 MHz) as shown in Figure 37. The detected impedance amplitude peak signals of the fungal spores were positive in the previous lower applied frequencies in comparison to 25 MHz, which means the electric fields start to pass through the fungal spores and results lower total impedance signal than the surrounded medium. Also the detected impedance amplitude peak signal showed higher peak height comparing to the previous condition.

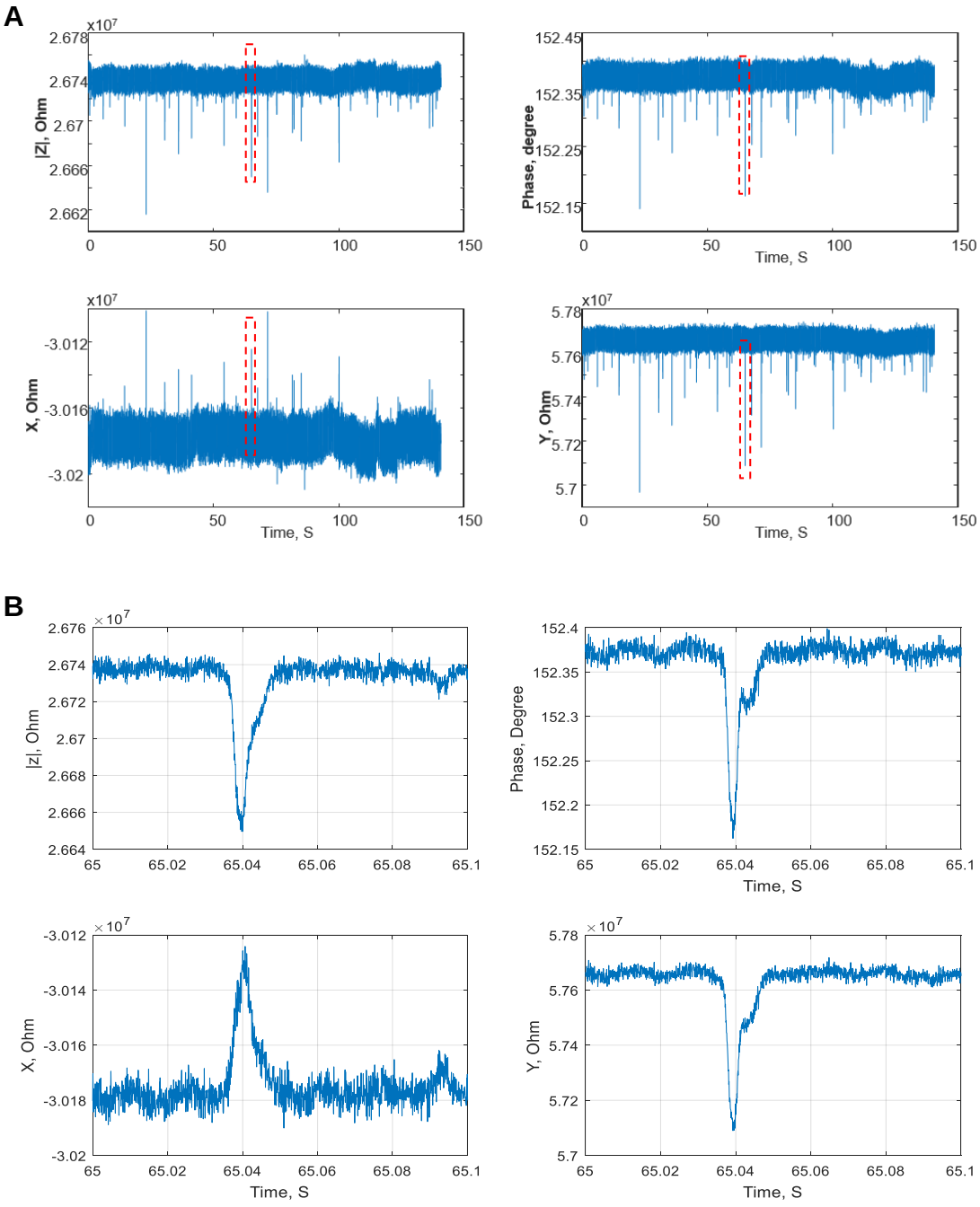

Figure 37. Impedance peak signals of flowed fungal cells in diluted medium. (A) Detected cultured fungal cells of different lengths suspended in 50 % YEPD medium at applied excitation AC signal of 4 V and 25 MHz, and (B) single peak impedance signal of fungal cell passing by the sensing electrodes. It can show that higher signal to noise ration can be realized at this condition.

Therefore, based on the previous high detection sensitivity, different fungal hyphae that have different lengths were detected and compared. Clear difference in the detected electrical impedance signals has been shown between different lengths of fungal hyphae as shown in Figure 38. The amplitude of the impedance signal for cell length of 75.55 µm is 5.7-fold increased comparing to 11.62 µm.

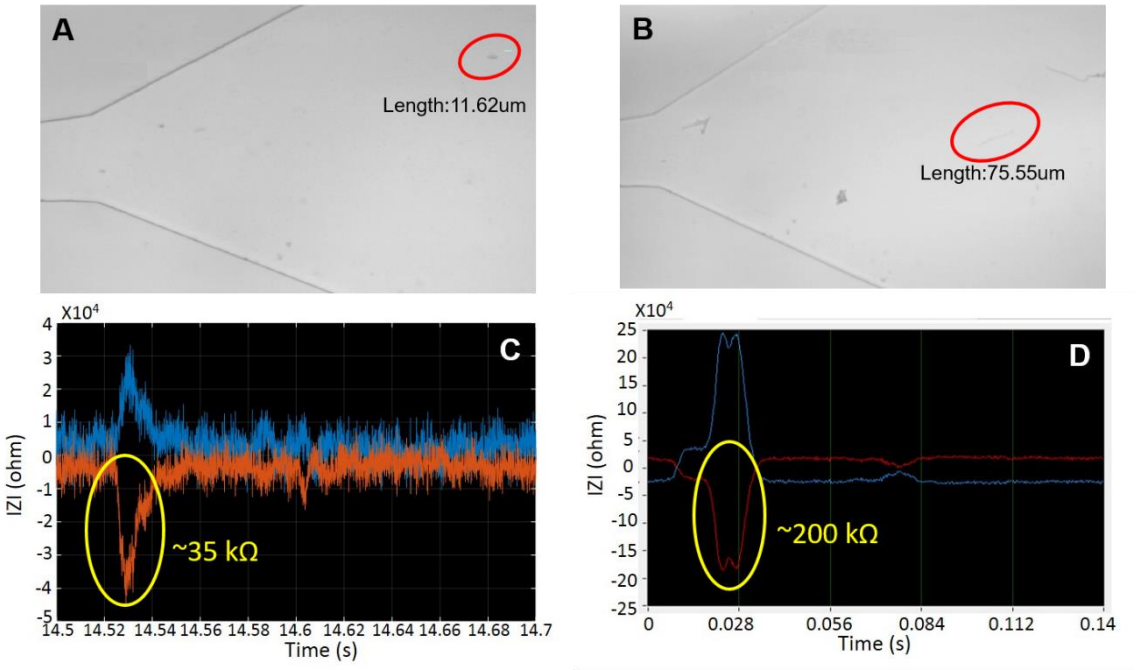

Figure 38. Comparison between two different fungal lengths (11.62 and 75.55 µm). (A) and (B) show two different fungal lengths that passed the detection regions, and (C) and (D) shows significant difference in the detected peak amplitude impedance signal.

Furthermore, since the cell detection could be improved by decreasing the cross-section detection area, 8.5 µm microfluidic channel height was tested and compared to the developed device of 15 µm. Fungal spores were compared at these two different microfluidic channel heights and showed that higher detected impedance amplitude peak

signal when using 8.5 µm microfluidic channel height was successfully achieved as shown in Figure 39. However, at this height more cell can easily block the microfluidic channel and more back pressure can be seen. Furthermore, for droplet-based applications, at 8.5 µm channel height, unstable droplet generation was observed when more than 80 µm droplet diameter was required.

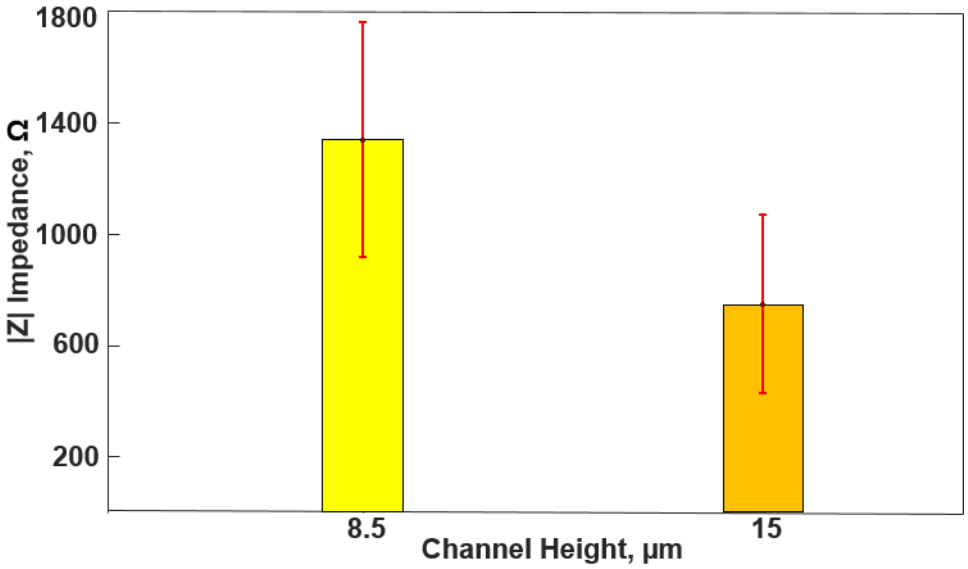

Figure 39. Detected impedance signal of fungal cells in microchannels with two different heights (8.5 and 15µm).

Based on the previous intensive characterization for selecting the optimal medium condition, device height, applied signal, a single fungal cell encapsulated in different droplets were tested and compared. A discrimination of different impedance peak signals for different cell lengths in different droplets were performed. They have demonstrated that there were clear differences in between single fungal spores and fungal hyphae with different lengths for cells encapsulated in droplets as shown in Figure 40.

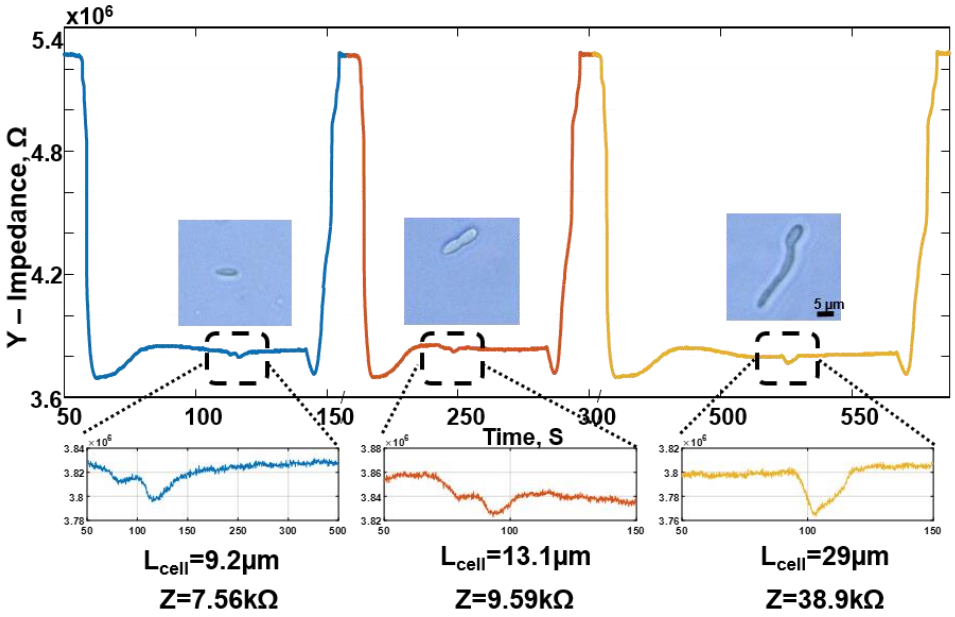

Figure 40. Imaginary part of the impedance signal changed when droplets containing fungal cells in YEPD culture media and surrounded by the carrier oil pass through the detection electrodes. Three different cell lengths (L_{cell}) presented on the graph showed different negative impedance peak height based on the cell size and shape.

As shown in Figure 41, the fungal cell in droplet were successfully detected and analyzed using the developed impedance spectroscopy microsystem. Small length of cultured fungal cells (< 30 µm) encapsulated in droplet were detected and analyzed. However, there were less number of elongated fungal cell of lengths more than 30 µm have been encapsulated and detected due to microfluidic channel dimensions that could not meet the very elongated fungi cell.

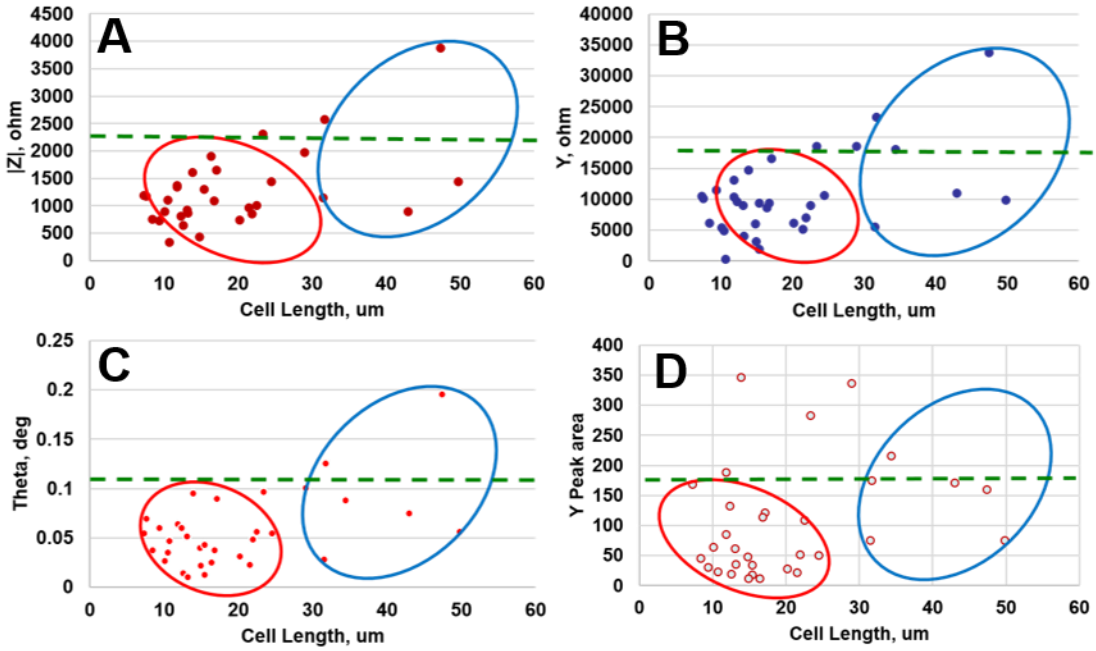

Figure 41. Filamentous fungal cells of different growths were detected and characterized within droplet. Peak amplitude, phase and imaginary electrical impedance signals were analyzed. Also, due to the cell shape, detected peak of the imaginary impedance signal was calculated and identified.

4.6. Conclusion

In this work, a low-cost and label-free impedance spectroscopy-based cell encapsulated in droplet using impedance spectroscopy was developed and successfully demonstrated in detecting and distinguish different cell types within droplet. We have successfully characterized yeast cell encapsulated in droplet using the developed microsystem at height of 15 µm. Yeast cells in droplets have been successfully tested and compared for three different YEPD diluted medium (100, 50, and 10 %). Significant results have been represented when different medium conductivities were used. The results showed that when the detected impedance signals were analyzed using the four

different parameters that mentioned before, the amplitude and real parts of the detected impedance signal shown higher sensitivity and lower standard deviations.

Furthermore we used the developed impedance spectroscopy-based droplet microsystem to discriminate filamentous fungal cells in droplets. Our results demonstrated the distinguishable impedance difference between single fungal spores and cultured filamentous fungal hyphae in droplets. Due to microchannel dimensions, few number of more than 30 μm length of filamentous fungal cells were passed the microfluidic channel. However, wider microchannel dimension can solve this issue. This method can readily be integrated with droplet-based high-throughput screening systems to enable label-free detection of droplet contents.

CHAPTER V

CONCLUSIONS AND FUTURE WORKS

5.1. Conclusions

The high-throughput, label-free, low-cost on-chip impedance spectroscopy based microfluidic technology has proved its capabilities as an emerging technology for characterizing the dielectric properties of mediums, particles, and cellular or sub-cellular contents with respect to the stimulating frequency. Using this technology, invaluable information for many biological and biomedical applications can be successfully achieved, therefore we have developed wide range of different microfluidic based impedance spectroscopy microsystems for cell/particle screening applications that could not only used for characterizing cells and particles but also for integrating and completing other technologies for endless emerging applications that could solve many of limited on-chip technologies.

Therefore different microsystems have been successfully developed by integrating an only single pair of impedance spectroscopy based electrodes. In chapter II, a high-throughput and low-cost impedance spectroscopy-based particle position detection method was developed and successfully demonstrated in determining the transverse positions of particles within a microfluidic channel and achieving a detection rate of more than 400 particles/sec. Even though the presented work used only a single electrode pair, the peak amplitude results of neighboring positions showed significant difference ($p<0.05$) and achieved our goal in discriminating the particle positions without having to

use a two-channel differential measurement. Based on the need, the exact configuration of the presented system can be easily modified for different application scenarios, adding more versatility and flexibility to the presented method. This method offers a simple, fast and low-cost approach for quantification of particle/cell positions inside a microchannel without complex optical setup. Also this method can be readily integrated with most microfluidic systems and impedance spectroscopy systems with minimum effort, greatly enabling the capability of the techniques in which particle position is of interest such as flow cytometry and particle/cell sorting/separation applications.

Another novel label-free and low-cost cells separation and sorting quantification technique has been developed and utilized using a single pair of step-shaped impedance spectroscopy based electrodes that has the capabilities for detecting, discriminating and quantifying the separated/sorted cells that flow through multiple microfluidic outlet channels. Therefore two different pairs of impedance electrodes that have two different five electrode to electrode gaps were successfully designed, tested and compared to detect suspended yeast cells flowed through five different outlet microchannels. To quantify the performance of the cells detection and counting using a single pair of electrodes, three different classification methods were utilized, showing that the lowest overall misclassification error of 1.85% can be successfully achieved when the electrode to electrode gaps in the developed single pair of electrodes were optimized to have 10, 30, 50, 90, and 170 μm electrode to electrode gaps. This developed system promises low-cost and on-chip cells and particles screening quantification module for all available developed sorting and separation techniques.

This third platform presented the achievement of developing a low-cost and label-free impedance spectroscopy-based microfluidic system for detecting and characterizing cells encapsulated in droplet. We have successfully characterized yeast cell encapsulated in droplet using the developed microsystem at height of 15 μm. Significant results have been represented when different medium conductivities were used. The results showed that when the detected impedance signals were analyzed using the four different parameters that mentioned before, the amplitude and real parts of the detected impedance signal shown higher sensitivity and lower standard deviations. Furthermore we used the developed impedance spectroscopy-based droplet microsystem to discriminate filamentous fungal cells in droplets. Our results demonstrated the distinguishable impedance difference between single fungal spores and cultured filamentous fungal hyphae in droplets. This method can readily be integrated with droplet-based high-throughput screening systems to enable label-free detection of droplet contents.

5.2. Future Works

For the cells separation and sorting quantification multioutlet based impedance spectroscopy microsystem, the future work can successfully involves in integrating our cell/particle counting detection scheme to range of passive or active sorting and separation methods, which could overcome the traditional techniques that have been suffered from either cell losses during the collecting and handling process for off-chip cell counting and analysis, unknown markers, or expensive instruments. Furthermore since the largest electrode to electrode gap of 170 μm has been demonstrated a maximum of 16.3×10^3 V

m^{-1} electric field strength and has been successfully utilized for cell detecting and counting, and the minimum electrode to electrode gap of 10 µm showed high electric field strength of 114.08 x 10^3 V m^{-1}, five more other electrode to electrode gaps can be used that could have more than 15 x 10^3 V m^{-1} electric field strength difference, which will allow the sorting and separation microsystems to have up to seven microfluidic outlet channels, enabling successful on-chip cell counting and quantification using a single pair of impedance electrodes.

For cells encapsulated in droplets screening microsystems, the developed impedance spectroscopy based microfluidic platform can play an important role by integrating this detection module to range of high-throughput, label-free, and low-cost screening systems that needs range of different on-chip functions such as single cell encapsulating, incubating, mixing, detection, characterization and sorting.

Therefore integrating a simple pair of impedance spectroscopy based electrodes could enables and solves range of technologies that need high-throughput, label-free and low-cost platforms for successful and significant cells and particles screening applications.

REFERENCES

1. Teh, S.Y., et al., *Droplet microfluidics.* Lab on a Chip, 2008. **8**(2): p. 198-220.

2. Frèohlich, H., *Theory of dielectrics; dielectric constant and dielectric loss.* 1949, Oxford, Clarendon Press.

3. Hasted, J.B., *Aqueous dielectrics*. 1973, London, Chapman and Hall.

4. Barthel, J., et al., *Dielectric Spectra of Some Common Solvents in the Microwave Region - Water and Lower Alcohols.* Chemical Physics Letters, 1990. **165**(4): p. 369-373.

5. Cicmanec, P., *Cavity Perturbation Method for Measurement of Permittivity and Conductivity of Medium Lossy Semiconductors and Dielectrics.* Solid-State Electronics, 1971. **14**(2): p. 153-166.

6. Rouleau, J.F., et al., *Performance of a microwave sensor for the precise measurement of water vapor in gases.* IEEE Transactions on Dielectrics and Electrical Insulation, 2000. **7**(6): p. 825-831.

7. Merchant, S.S., et al., *The Chlamydomonas genome reveals the evolution of key animal and plant functions.* Science, 2007. **318**(5848): p. 245-251.

8. Gawad, S., et al., *Dielectric spectroscopy in a micromachined flow cytometer: theoretical and practical considerations.* Lab on a Chip, 2004. **4**(3): p. 241-251.

9. Morgan, H., et al., *Single cell dielectric spectroscopy.* Journal of Physics D-Applied Physics, 2007. **40**(1): p. 61-70.

10. Sun, T., et al., *Broadband single cell impedance spectroscopy using maximum length sequences: theoretical analysis and practical considerations.* Measurement Science & Technology, 2007. **18**(9): p. 2859-2868.

11. Sun, T., et al., *Analytical electric field and sensitivity analysis for two microfluidic impedance cytometer designs.* IET Nanobiotechnology, 2007. **1**(5): p. 69-79.

12. Sun, T. and Morgan, H., *Single-cell microfluidic impedance cytometry: a review.* Microfluidics and Nanofluidics, 2010. **8**(4): p. 423-443.

13. Cooney, C.G., et al., *Electrowetting droplet microfluidics on a single planar surface.* Microfluidics and Nanofluidics, 2006. **2**(5): p. 435-446.

14. El-Ali, J., et al., *Cells on chips.* Nature, 2006. **442**(7101): p. 403-411.

15. Hansen, C. and Quake, S.R., *Microfluidics in structural biology: smaller, faster... better.* Current Opinion in Structural Biology, 2003. **13**(5): p. 538-544.

16. Sackmann, E.K., et al., *The present and future role of microfluidics in biomedical research.* Nature, 2014. **507**(7491): p. 181-189.

17. Whitesides, G.M., *The origins and the future of microfluidics.* Nature, 2006. **442**(7101): p. 368-373.

18. Yager, P., et al., *Microfluidic diagnostic technologies for global public health.* Nature, 2006. **442**(7101): p. 412-418.

19. Friend, J. and Yeo, L., *Fabrication of microfluidic devices using polydimethylsiloxane.* Biomicrofluidics, 2010. **4**(2): p. 026502.

20. Kim, K., et al., *Rapid replication of polymeric and metallic high aspect ratio microstructures using PDMS and LIGA technology.* Microsystem Technologies, 2002. **9**(1-2): p. 5-10.

21. Tamanaha, C.R., et al., *Hybrid macro–micro fluidics system for a chip-based biosensor.* Journal of Micromechanics and Microengineering, 2002. **12**(2): p. N7-N17.

22. Culbertson, C.T., et al., *Micro Total Analysis Systems: Fundamental Advances and Biological Applications.* Analytical Chemistry, 2014. **86**(1): p. 95-118.

23. Manz, A., et al., *Miniaturized Total Chemical-Analysis Systems - a Novel Concept for Chemical Sensing.* Sensors and Actuators B-Chemical, 1990. **1**(1-6): p. 244-248.

24. Reyes, D.R., et al., *Micro total analysis systems. 1. Introduction, theory, and technology.* Analytical Chemistry, 2002. **74**(12): p. 2623-2636.

25. Jang, L.S. and Wang, M.H., *Microfluidic device for cell capture and impedance measurement.* Biomedical Microdevices, 2007. **9**(5): p. 737-743.

26. Malleo, D., et al., *Continuous differential impedance spectroscopy of single cells.* Microfluidics and Nanofluidics, 2010. **9**(2-3): p. 191-198.

27. Hua, S.Z. and Pennell, T., *A microfluidic chip for real-time studies of the volume of single cells.* Lab on a Chip, 2009. **9**(2): p. 251-256.

28. Cho, Y., et al., *Whole-Cell Impedance Analysis for Highly and Poorly Metastatic Cancer Cells.* Journal of Microelectromechanical Systems, 2009. **18**(4): p. 808-817.

29. Di Carlo, D., et al., *Single-cell enzyme concentrations, kinetics, and inhibition analysis using high-density hydrodynamic cell isolation arrays.* Analytical Chemistry, 2006. **78**(14): p. 4925-4930.

30. Di Carlo, D., et al., *Dynamic single cell culture array.* Lab on a Chip, 2006. **6**(11): p. 1445-1449.

31. Skelley, A.M., et al., *Microfluidic control of cell pairing and fusion.* Nature Methods, 2009. **6**(2): p. 147-152.

32. Benazzi, G., et al., *Discrimination and analysis of phytoplankton using a microfluidic cytometer.* IET Nanobiotechnology, 2007. **1**(6): p. 94-101.

33. Cheung, K.C., et al., *Microfluidic Impedance-Based Flow Cytometry.* Cytometry Part A, 2010. **77A**(7): p. 648-666.

34. Holmes, D., et al., *Leukocyte analysis and differentiation using high speed microfluidic single cell impedance cytometry.* Lab on a Chip, 2009. **9**(20): p. 2881-2889.

35. Gawad, S., et al., *Micromachined impedance spectroscopy flow cytometer for cell analysis and particle sizing.* Lab on a Chip, 2001. **1**(1): p. 76-82.

36. Cheung, K., et al., *Impedance spectroscopy flow cytometry: On-chip label-free cell differentiation.* Cytometry Part A, 2005. **65A**(2): p. 124-132.

37. Wu, Y.F., et al., *Micromachined Coulter counter for dynamic impedance study of time sensitive cells.* Biomedical Microdevices, 2012. **14**(4): p. 739-750.

38. Mernier, G., et al., *Characterization of a novel impedance cytometer design and its integration with lateral focusing by dielectrophoresis.* Lab on a Chip, 2012. **12**(21): p. 4344-4349.

39. Myers, F.B., et al., *Label-free electrophysiological cytometry for stem cell-derived cardiomyocyte clusters.* Lab on a Chip, 2013. **13**(2): p. 220-228.

40. Mernier, G., et al., *Cell viability assessment by flow cytometry using yeast as cell model.* Sensors and Actuators B-Chemical, 2011. **154**(2): p. 160-163.

41. Sun, T., et al., *High speed multi-frequency impedance analysis of single particles in a microfluidic cytometer using maximum length sequences.* Lab on a Chip, 2007. **7**(8): p. 1034-1040.

42. Lanz, T., et al. *Differential impedance spectrometer and vision system for analysis of single cells*. IEEE Solid-State Sensors, Actuators and Microsystems Conference, TRANSDUCERS 2009, 2009. p. 1297-1300.

43. Haandbæk, N.M., et al. *Characterization of Cell Phenotype Using Dynamic Vision Sensor and Impedance Spectroscope*. µTAS 2011. 2011: p. 2-6.

44. Burgel, S.C., et al., *Dynamic and Static Impedance Spectroscopy for Single Particle Characterization in Microfluidic Chips.* 2012 IEEE 25th International Conference on Micro Electro Mechanical Systems (MEMS), 2012: p. 1033-1036.

45. Emaminejad, S., et al., *Microfluidic diagnostic tool for the developing world: contactless impedance flow cytometry.* Lab on a Chip, 2012. **12**(21): p. 4499-4507.

46. Cheung, K., et al., *Microfluidic impedance spectroscopy flow cytometer: Particle size calibration.* Mems 2004: 17th IEEE International Conference on Micro Electro Mechanical Systems (MEMS), 2004: p. 343-346.

47. Chen, J.A., et al., *A microfluidic device for simultaneous electrical and mechanical measurements on single cells.* Biomicrofluidics, 2011. **5**(1): p. 014113.

48. Haandbaek, N., et al., *Characterization of subcellular morphology of single yeast cells using high frequency microfluidic impedance cytometer*. Lab on a Chip, 2014. **14**(2): p. 369-377.

49. Chen, J., et al., *Classification of cell types using a microfluidic device for mechanical and electrical measurement on single cells.* Lab on a Chip, 2011. **11**(18): p. 3174-3181.

50. Tan, Q.Y., et al., *Quantification of the specific membrane capacitance of single cells using a microfluidic device and impedance spectroscopy measurement.* Biomicrofluidics, 2012. **6**(3): p. 034112.

51. Zhao, Y., et al., *A microfluidic system for cell type classification based on cellular size-independent electrical properties.* Lab on a Chip, 2013. **13**(12): p. 2272-2277.

52. Bernabini, C., et al., *Micro-impedance cytometry for detection and analysis of micron-sized particles and bacteria.* Lab on a Chip, 2011. **11**(3): p. 407-412.

53. Evander, M., et al., *Microfluidic impedance cytometer for platelet analysis.* Lab on a Chip, 2013. **13**(4): p. 722-729.

54. Bhagat, A.A.S., et al., *Inertial microfluidics for sheath-less high-throughput flow cytometry.* Biomedical Microdevices, 2010. **12**(2): p. 187-195.

55. Gossett, D.R., et al., *Label-free cell separation and sorting in microfluidic systems.* Anal Bioanal Chem, 2010. **397**(8): p. 3249-67.

56. Lenshof, A. and T. Laurell, *Continuous separation of cells and particles in microfluidic systems.* Chem Soc Rev, 2010. **39**(3): p. 1203-17.

57. Liu, Z., et al., *Effects of fluid medium flow and spatial temperature variation on acoustophoretic motion of microparticles in microfluidic channels.* The Journal of the Acoustical Society of America, 2016. **139**(1): p. 332-49.

58. Sajeesh, P. and A.K. Sen, *Particle separation and sorting in microfluidic devices: a review.* Microfluidics and Nanofluidics, 2014. **17**(1): p. 1-52.

59. Shields, C.W., et al., *Microfluidic cell sorting: a review of the advances in the separation of cells from debulking to rare cell isolation.* Lab on a Chip, 2015. **15**(5): p. 1230-1249.

60. Tia, S. and Herr, A.E., *On-chip technologies for multidimensional separations.* Lab on a Chip, 2009. **9**(17): p. 2524-36.

61. Applegate, R.W., Jr., et al., *Microfluidic sorting system based on optical waveguide integration and diode laser bar trapping.* Lab on a Chip, 2006. **6**(3): p. 422-6.

62. Fei, P., et al., *A compact optofluidic cytometer with integrated liquid-core/PDMS-cladding waveguides.* Lab on a Chip, 2012. **12**(19): p. 3700-3706.

63. Monat, C., et al., *Integrated optofluidics: A new river of light.* Nature Photonics, 2007. **1**(2): p. 106-114.

64. Psaltis, D., et al., *Developing optofluidic technology through the fusion of microfluidics and optics.* Nature, 2006. **442**(7101): p. 381.

65. Schade-Kampmann, G., et al., *On-chip non-invasive and label-free cell discrimination by impedance spectroscopy.* Cell Proliferation, 2008. **41**(5): p. 830-840.

66. Xu, Y., et al., *A review of impedance measurements of whole cells.* Biosensors & Bioelectronics, 2016. **77**: p. 824-836.

67. Gu, W. and Zhao, Y., *Cellular electrical impedance spectroscopy: an emerging technology of microscale biosensors.* Expert Review of Medical Devices, 2010. **7**(6): p. 767-779.

68. Zheng, Y., et al., *Recent advances in microfluidic techniques for single-cell biophysical characterization.* Lab on a Chip, 2013. **13**(13): p. 2464-2483.

69. Lee, W., et al., *Microfluidic Cell Sorting and Separation Technology*, in *Microtechnology for Cell Manipulation and Sorting*. 2017, Springer. p. 1-14.

70. Xi, H.-D., et al., *Active droplet sorting in microfluidics: a review.* Lab on a Chip, 2017. **17**(5): p. 751-771.

71. Ding, X. and Huang, T.J., *Microfluidic manipulation and sorting of particles using tunable standing surface acoustic wave*. U.S. Patent 9,608,547, issued March 28, 2017.

72. Di Carlo, D., et al., *Equilibrium separation and filtration of particles using differential inertial focusing.* Analytical Chemistry, 2008. **80**(6): p. 2204-2211.

73. Huh, D., et al., *Gravity-driven microfluidic particle sorting device with hydrodynamic separation amplification.* Analytical Chemistry, 2007. **79**(4): p. 1369-1376.

74. Shevkoplyas, S.S., et al., *Biomimetic autoseparation of leukocytes from whole blood in a microfluidic device.* Analytical Chemistry, 2005. **77**(3): p. 933-937.

75. Huang, R., et al., *A microfluidics approach for the isolation of nucleated red blood cells (NRBCs) from the peripheral blood of pregnant women.* Prenatal Diagnosis, 2008. **28**(10): p. 892-899.

76. Takagi, J., et al., *Continuous particle separation in a microchannel having asymmetrically arranged multiple branches.* Lab on a Chip, 2005. **5**(7): p. 778-784.

77. Nilsson, A., et al., *Acoustic control of suspended particles in micro fluidic chips.* Lab on a Chip, 2004. **4**(2): p. 131-135.

78. Arata, H.F., et al., *Towards single biomolecule handling and characterization by MEMS.* Analytical and Bioanalytical Chemistry, 2008. **391**(7): p. 2385-2393.

79. McCloskey, K.E., et al., *Magnetic cell separation: characterization of magnetophoretic mobility.* Analytical Chemistry, 2003. **75**(24): p. 6868-6874.

80. Wang, M.M., et al., *Microfluidic sorting of mammalian cells by optical force switching.* Nature Biotechnology, 2005. **23**(1): p. 83.

81. Perroud, T.D., et al., *Microfluidic-based cell sorting of Francisella tularensis infected macrophages using optical forces.* Analytical Chemistry, 2008. **80**(16): p. 6365-6372.

82. Ekpenyong, A.E., et al., *Viscoelastic properties of differentiating blood cells are fate-and function-dependent.* PLoS One, 2012. **7**(9): p. e45237.

83. Guo, Q., et al., *Deformability based Cell Sorting using Microfluidic Ratchets Enabling Phenotypic Separation of Leukocytes Directly from Whole Blood.* Scientific Reports, 2017. **7**: p. 6627.

84. Goda, K., et al., *High-throughput single-microparticle imaging flow analyzer.* Proceedings of the National Academy of Sciences, 2012. **109**(29): p. 11630-11635.

85. Alyassin, M.A., et al., *Rapid automated cell quantification on HIV microfluidic devices.* Lab on a Chip, 2009. **9**(23): p. 3364-3369.

86. Haandbæk, N., et al., *Characterization of single yeast cell phenotypes using microfluidic impedance cytometry and optical imaging.* ACS Sensors, 2016. **1**(8): p. 1020-1027.

87. Edd, J.F., et al., *Controlled encapsulation of single-cells into monodisperse picolitre drops.* Lab on a Chip, 2008. **8**(8): p. 1262-1264.

88. Gunther, P.M., et al., *Formation of monomeric and novolak azo dyes in nanofluid segments by use of a double injector chip reactor.* Chemical Engineering & Technology, 2005. **28**(4): p. 520-527.

89. Boedicker, J.Q., et al., *Detecting bacteria and determining their susceptibility to antibiotics by stochastic confinement in nanoliter droplets using plug-based microfluidics.* Lab on a Chip, 2008. **8**(8): p. 1265-1272.

90. Hwang, D.K., D. Dendukuri, and P.S. Doyle, *Microfluidic-based synthesis of non-spherical magnetic hydrogel microparticles.* Lab on a Chip, 2008. **8**(10): p. 1640-1647.

91. Shestopalov, I., J.D. Tice, and R.F. Ismagilov, *Multi-step synthesis of nanoparticles performed on millisecond time scale in a microfluidic droplet-based system.* Lab on a Chip, 2004. **4**(4): p. 316-321.

92. Brouzes, E., et al., *Droplet microfluidic technology for single-cell high-throughput screening.* Proceedings of the National Academy of Sciences of the United States of America, 2009. **106**(34): p. 14195-14200.

93. Clausell-Tormos, J., et al., *Droplet-based microfluidic platforms for the encapsulation and screening of mammalian cells and multicellular organisms.* Chemistry & Biology, 2008. **15**(5): p. 427-437.

94. Koster, S., et al., *Drop-based microfluidic devices for encapsulation of single cells.* Lab on a Chip, 2008. **8**(7): p. 1110-1115.

95. Song, H., et al., *Reactions in droplets in microflulidic channels.* Angewandte Chemie-International Edition, 2006. **45**(44): p. 7336-7356.

96. Um, E., et al., *Random breakup of microdroplets for single-cell encapsulation.* Applied Physics Letters, 2010. **97**(15): p. 153703.

97. Weltin, A., et al., *Cell culture monitoring for drug screening and cancer research: a transparent, microfluidic, multi-sensor microsystem.* Lab on a Chip, 2014. **14**(1): p. 138-146.

98. Kemna, E.W.M., et al., *Label-free, high-throughput, electrical detection of cells in droplets.* Analyst, 2013. **138**(16): p. 4585-4592.

99. Xia, Y.N. and Whitesides, G.M., *Soft lithography.* Annual Review of Materials Science, 1998. **28**: p. 153-184.

100. Wang, H., N. Sobahi, and A. Han, *Impedance spectroscopy-based cell/particle position detection in microfluidic systems.* Lab on a Chip, 2017. **17**(7): p. 1264-1269.

101. Fisher, R.A., *The use of multiple measurements in taxonomic problems.* Annals of Human Genetics, 1936. **7**(2): p. 179-188.

102. Friedman, J.H., *Regularized discriminant analysis.* Journal of the American Statistical Association, 1989. **84**(405): p. 165-175.

103. Bratchell, N., *Cluster Analysis.* Chemom. Intell. Lab. Syst. , 1987. **6**: p. 105–125.

104. Cheng, X., et al., *Cell detection and counting through cell lysate impedance spectroscopy in microfluidic devices.* Lab on a Chip, 2007. **7**(6): p. 746-755.

105. Xu, J.-R., et al., *The dawn of fungal pathogen genomics.* Annu. Rev. Phytopathol, 2006. **44**: p. 337-366.

106. Baret, J.-C., et al., *Fluorescence-activated droplet sorting (FADS): efficient microfluidic cell sorting based on enzymatic activity.* Lab on a Chip, 2009. **9**(13): p. 1850-1858.

APPENDIX A

MASK DESIGN

A.1. Cell and Particle Position Detection Impedance Spectroscopy-Based Device

Figure A. 1: Cell and particle position detection microfluidic channel. (File name: Particle position detection-microfluidic channel.dwg).

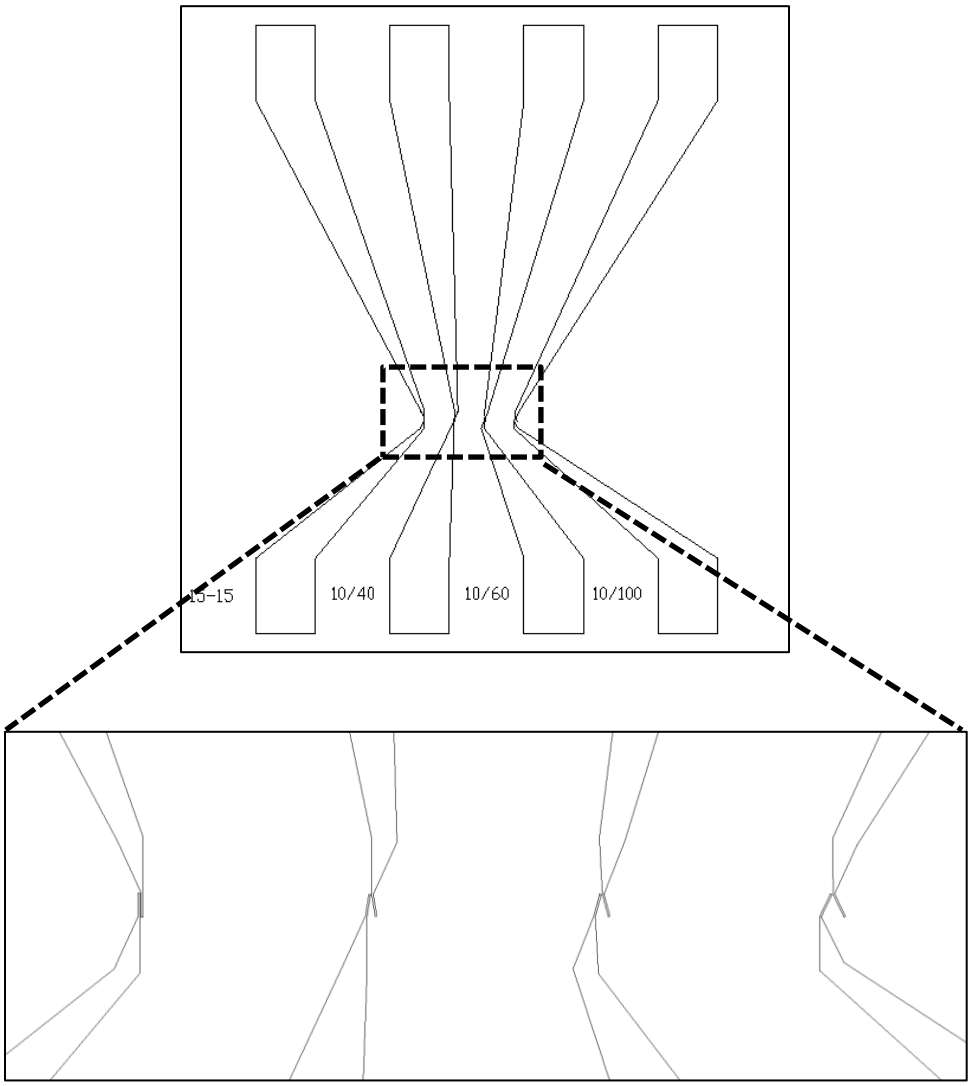

Figure A. 2: Three different tilted single-ended pairs of electrodes with different angles. Also another pair of parallel electrode for cells sizing and quantification. (File name: Particle position detection-detection electrodes.dwg).

A.2. Multioutlet Cell Counting Microsystem Using Impedance Spectroscopy

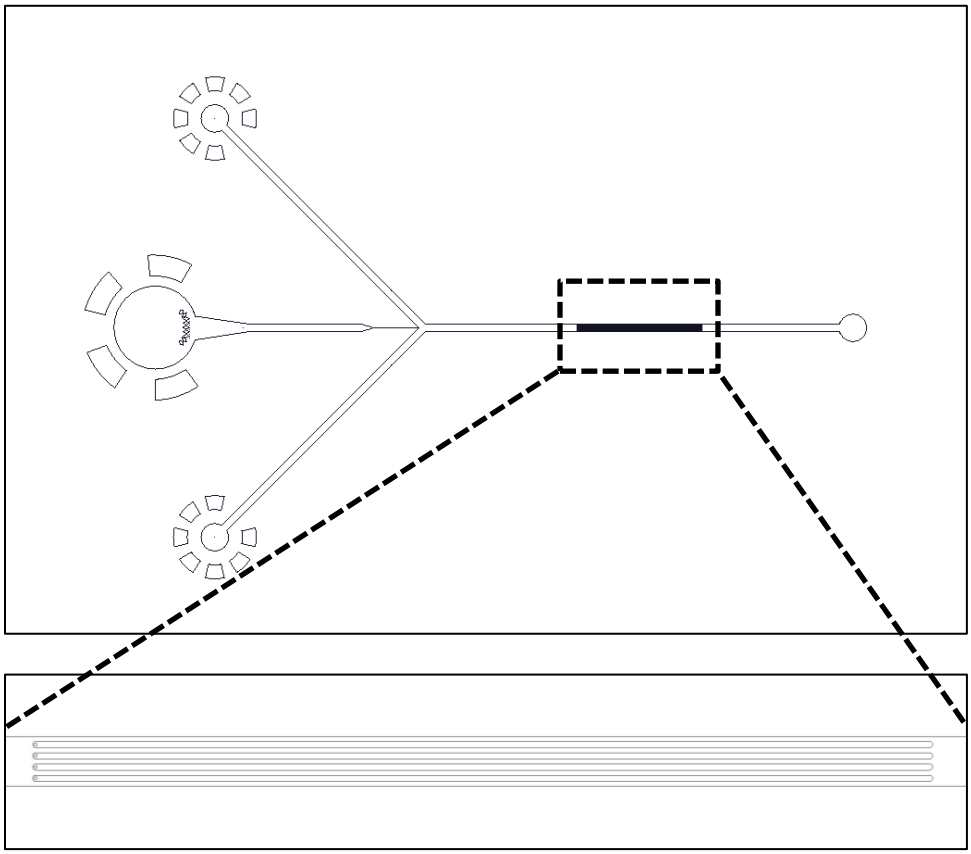

Figure A. 3: Multioutlet microfluidic of 5 parallel channels with flow-focusing. (File name: Multioutlet cell counting-microfluidic channel.dwg).

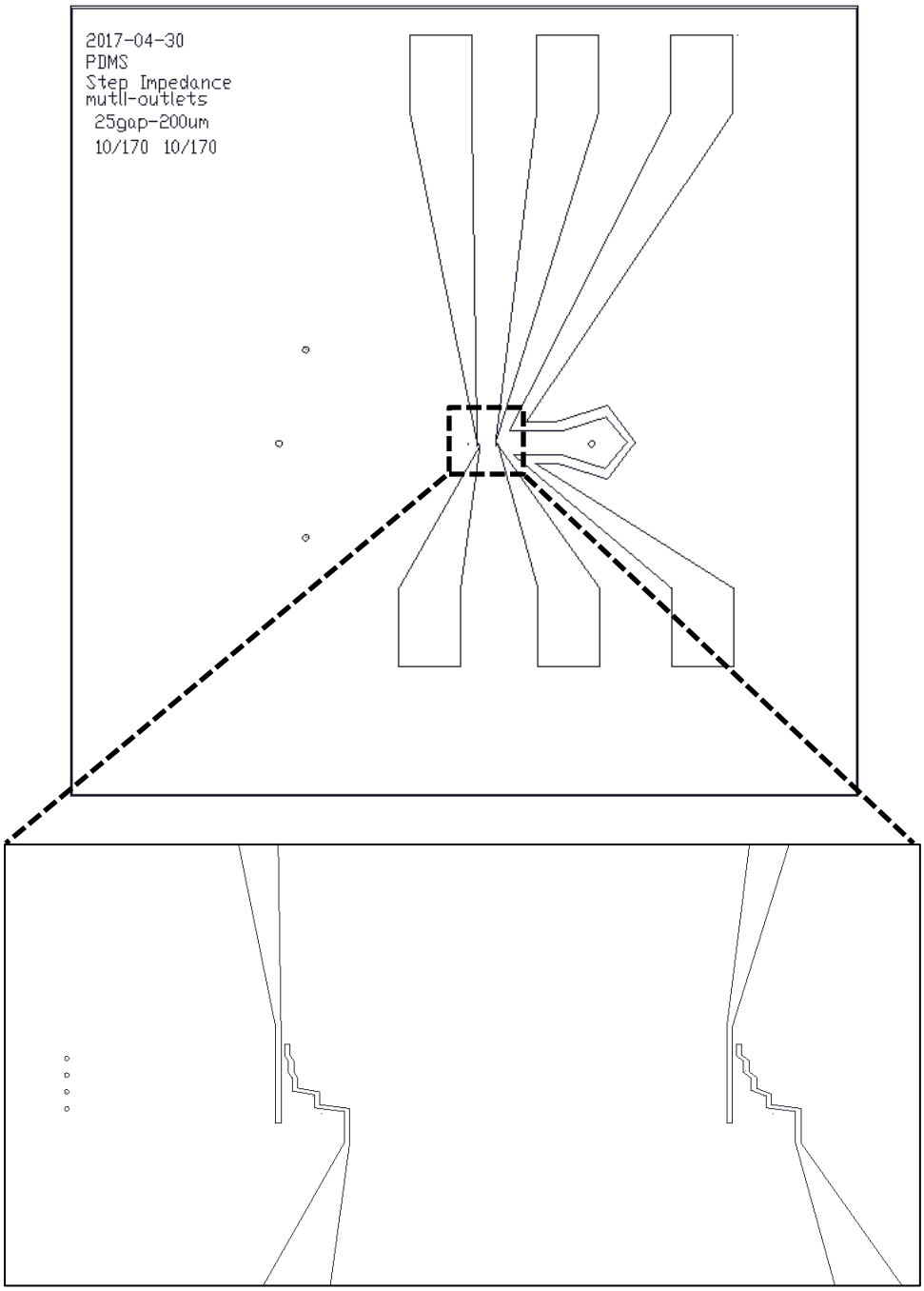

Figure A. 4: Two pairs of step-shaped electrodes that has five different electrode to electrode gaps. The five electrode to electrode gaps in each pair is different. (File name: Multioutlet cell counting-detection electrode.dwg).

A.3. Detection and Characterization of Cells in Droplet Microsystem Using Impedance Spectroscopy

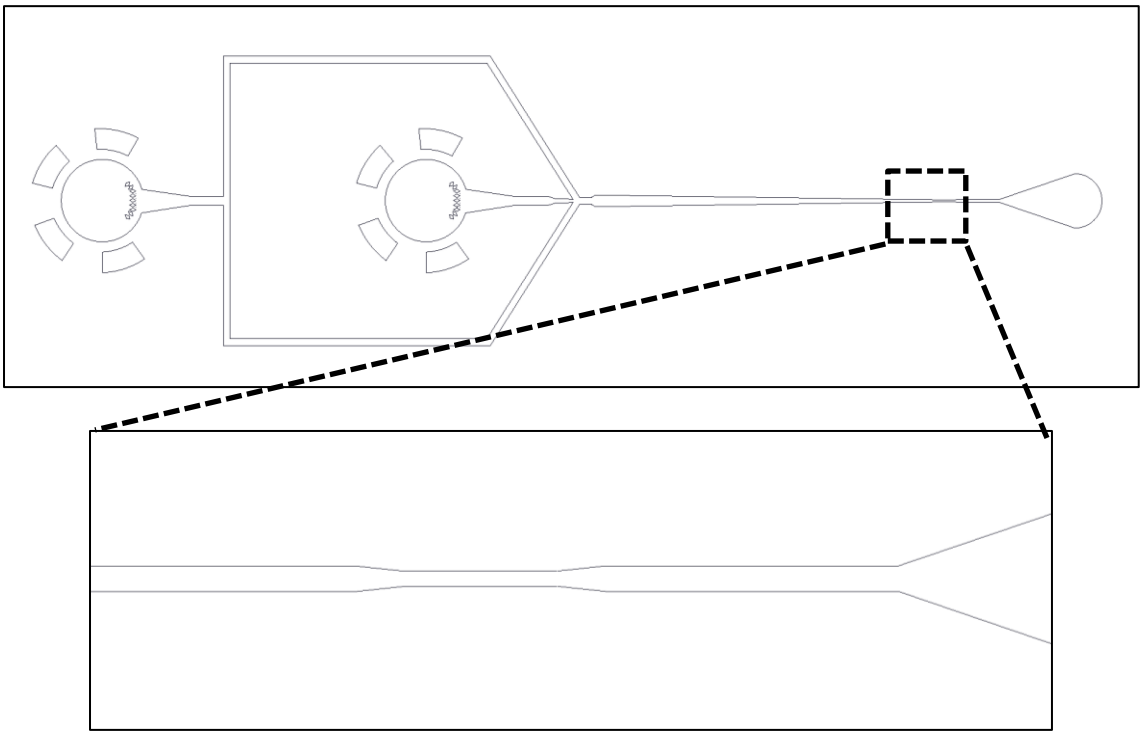

Figure A. 5: Droplet generation and impedance detection microfluidic channels. (File name: Cell in droplet detection and characterization-microfluidic channel.dwg).

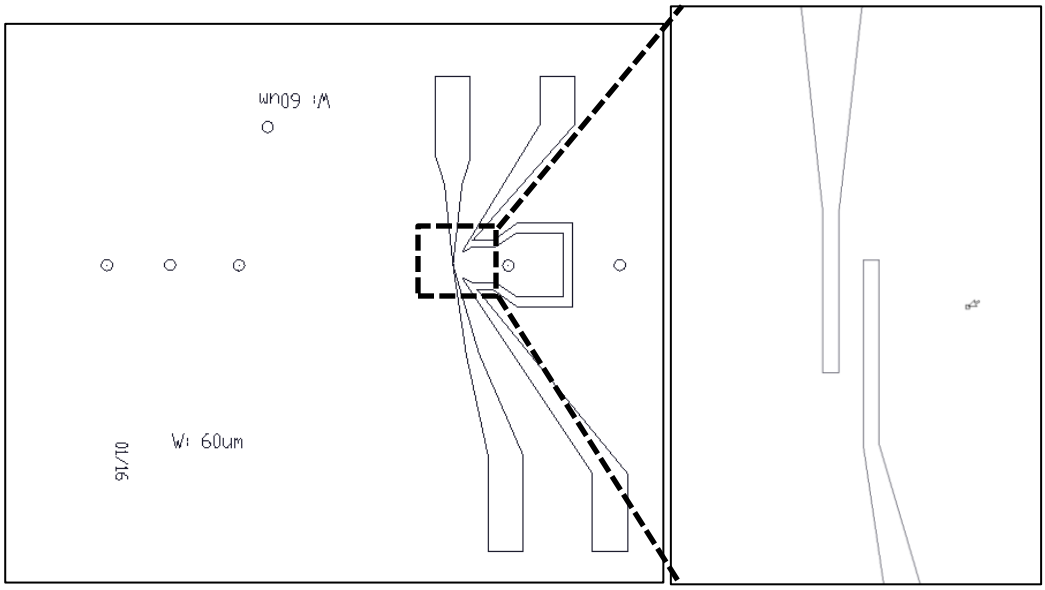

Figure A. 6: Single pair of electrodes that has 15 µm gap and 10 µm electrode width. (File name: Cell in droplet detection and characterization-detection electrode.dwg).

APPENDIX B

MASTER AND ELECTRODE FABRICATION PROCEDURE

B.1. Microfluidic Channel Layer Master Fabrication Procedure

1. Clean a 3 inch wafer by rinsing using acetone, IPA, methanol, DI water, and drying with nitrogen (N_2) gas.
2. Remove remaining solvents by baking at 95 ºC for 10 minutes
3. To get 15 µm height, use the spin machine at two different speeds (500 rpm for 10s using ramp for 5s, then 2800 for 30 s using 5 s ramp) using negative photoresist (SU-8 2015), to uniform the photoresist on the wafer.
4. soft baking using a hotplate for 30 min at 60 ºC then 4 min at 90 ºC.
5. Expose the wafer to UV light (Karl Suss MA6 Mask Aligner) using dark field mask at dosage of 180 mJ/cm^2
6. Hard baking the wafers at 90 ºC for 3 min.
7. Develop the wafer using Thinner type P or equivalent to remove the non-exposed photoresist by immersing the wafer inside the developer until the non-exposed photoresist completely removed
8. Rinse the wafer with IPA and dried with N2 gas gently.
9. Check the pattern height using either Bruker DektakXT Surface Profiler or VEECO WYKO NT9100 Optical Profilometer

B.2. Microelectrodes Pattern Fabrication Procedure

1. Clean 2 x 3/2 x 2 inch glass slides glass slides using the piranha cleaning process.
2. Deposit a uniform of (Au/Ti) layer using E-beam evaporation equipment (Lesker PVD 75 Ebeam Evaporator) of thickness 200/20 nm.
3. Spin coat a positive photoresist, S1818 at 3000 rpm for 30 s onto a gold coated slide. The setting of the spin machine is as follow: 500 rpm for 10 s using 5 s ramp, then 3500 rpm for 30 s using 5 s ramp.
4. Soft bake the glass slides at 110 ºC for 10min (preheated hotplate)
5. Cool down the glass slide before UV exposing.
6. Expose the glass slide to UV light (Karl Suss MA6 Mask Aligner) using clearfiled pattern mask to perform the electrode pattern at 85 mJ/cm^2
7. Develop the slides for 30 s using MF319 (or equivalent) to remove the exposed area.
8. Rinse it by DI water
9. Hard bake the glass slides at 115 ºC for 2~3 min then cool down
10. Immerse the patterned slides in Au etchant (Type TFA, Transene Company Inc.) to remove the exposed area for around 30 s or more (need to shake it all time)
11. Rinse it by DI water
12. Etch the exposed Ti area using Ti etchant (HF:H2O at 1:300, around 2 mL in DI Water of 1.5 L).
13. Rinse it by DI water
14. Remove the remaining photoresist using acetone then water.

15. Clean the pattern gold electrodes using DI water and dry by N2 gas.

16. Coat the patterned electrodes with silicon oxide (50 nm) using PECVD if needed.

APPENDIX C

PDMS DEVICE FABRICATION PROCEDURE

C.1. Microfluidic PDMS Layer Fabrication Procedure

1. Coat the fabricated microfluidic master wafer with tridecafluoro-1,1,2,2-tetrahydroocty-l,1,2,2- tetrahydrooctyl (trichlorosilane, United Chemical Technologies, Inc.) by placing the fabricated wafer inside the desiccator chamber together with 6 ~ 7 drops of trichlorosilane in weight boats
2. Degas the desiccator chamber for 20 min to vaporize the trichlorosilane and coat the fabricated pattern wafer
3. Clean the coated patterned wafer with Isopropyl alcohol (IPA) and dry with N_2 gas
4. Mix 25 g of PDMS prepolymer (Sylgrad 184, Dow Corning, Inc) with the curing agent at 10:1 ratio
5. Degas the PDMS mixture using the desiccator for 15 min or more
6. Place and fix the coated patterned wafer in petri dish using tape
7. Pour the PDMS mixture on the coated patterned wafer
8. Place the petri dish inside the desiccator chamber and degas for 15 min or more
9. Cure at 85 ºC for 2 hr only for optimum results
10. Bond the PDMS immediately to glass slide after the baking stage

C.2. Microfluidic PDMS to Glass Slide Methanol Bonding Procedure

1. Peel off the cured PDMS microfluidic channel layer

2. Punch the inlets and outlets using a needle of gauge 19 or the suitable size for the tubing
3. Use the air pump to push any PDMS residue from bottom to top. (Extra: For clearing, Kapton tape can be used)
4. Place the PDMS microfluidic channel layer and coated gold electrodes glass slide inside the oxygen plasma treatment (100mTorr and 100 W) for 1.5 min. The oxygen plasma use is as follow: place the part inside the chamber, then close the chamber and degas for 2 min, then start to UV and set it to High, followed by adjusting the entering air to 10 mTorr for 1.5 min.
5. Rinse the coated gold electrodes glass slide with methanol
6. Align the microfluidic layer on the coated electrodes
7. Put the assembled device on hotplate:
    a. For hydrophobic devices, put the device on the hotplate for 10 min at 85 ºC , then rise the temperature to 200 ºC and bake for 4 hr maximum
    b. For hydrophilic devices, bake the device for 7-8 hr at 85 ºC

APPENDIX D

IMPEDANCE ANALYZER EXPERIMENTAL PROCEDURE

D.1. Experimental Setup Procedure

1. Solder SMA connectors (Type: CONN SMA JACK STR 50 OHM PCB, J494-ND, ROHS COMP) on the patterned gold pads using a soldering machine of 600 ^{o}K as a maximum temperature. Flux should be used before soldering the connectors.
2. Check the connectivity between the SMA connectors and the patterned gold using a multi-meter.
3. Solder the shielding sheet if needed.
4. Place the fabricated device on an upright microscope.
5. Connect the SMA/BNC cable (CABLE SMA/BNC 6" RG-316, J3606-ND, ROHS COMP) to the input soldered SMA connector
6. Connect the SMA/SMA cable (CABLE SMA/SMA 6" RG-316, J3706-ND, ROHS COMP) to the output soldered SMA connector
7. Connect the another end of the SMA/SMA cable to the current amplifier (HF2TA Current Amplifier, Zurich Instruments AG)
8. Connect the BNC of the SMA/BNC cable to the impedance analyzer (HF2IS Impedance Spectroscopy, Zurich Instruments AG)
9. Connect the current amplifier to the impedance analyzer (ZCtrl connector) using a standard straight-through as opposed to cross-over of single Ethernet cable to power and control signals

10. Connect the impedance analyzer to the PC using USB cable

11. Power on the impedance analyzer and Zeiss microscope.

D.2. Experimental Procedure

1. Start the ziControl software

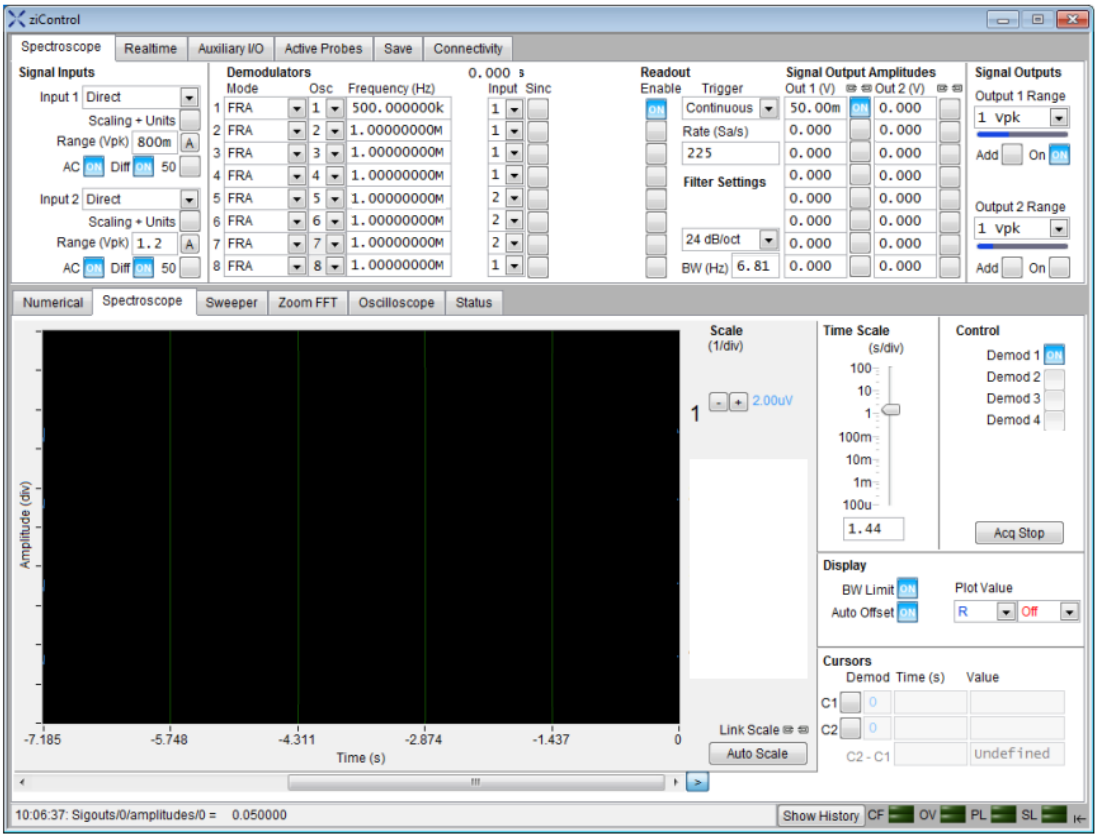

Figure D. 1: ziControl impedance spectroscopy interface.

2. Set the signal output amplitude

3. Set the sampling rate to 7.2 kS s^{-1} or more

4. Select the 8^{th} filter order and the BW (should be more than 2 kHz)

5. Enable the first readout

6. Select 2-Term Z in Mode Demodulators section
7. Set the excitation frequency
8. From the Input Signal section, select the input 1 of the HF2TA current amplifier
9. Disable/enable the Diff button (based on your connection)
10. Select the proper feedback resistor amplifying and select G to 1.0 gain
11. Enable the AC button in the front panel
12. Enable the On button from the Signal Input section
13. Press the A button of the range
14. From the bottom menu of the interface, enable the Demo 1 under the Spectroscope tab

APPENDIX E

YEAST CELL AND YEPD MEDIUM PREPARATION

E.1. YEPD Medium Preparation

1. For 1 L YEPD medium, mix:
    a. 3 g of yeast extract
    b. 10 g of peptone
    c. 20 g of Dextrose
2. Add all the components to 1 L of purified water, mix then very well using magnetic mixer
3. Autoclave the mixture for 15 minutes at 15 psi at 121 °C.

E.2. Yeast Cells Culturing

1. Add small amount of yeast cell from the agar plate (agar plate is the yeast banking) to YEPD medium

2. Incubate the yeast cells at 37^{o} C for 1 day before the experiment